CONTRACT REPORT

Naval Facilities Engineering Service Center, Port Hueneme, CA 93043-4328

CR 94.001-SHR

March 1994

DEVELOPMENT OF A PLASTICITY BOND MODEL FOR REINFORCED CONCRETE -
Preliminary Calibration and Cyclic Applications

An Investigation Conducted by:

Leonard R. Herrmann, University of California, Davis
James V. Cox, Naval Facilities Engineering Service Center

Sponsored by

Office of Naval Research
Arlington, VA

Abstract A bond model is developed to describe the inelastic behavior of the bond between reinforcing bars and concrete. The bond model is applicable to both monotonic and cyclic loading conditions. It is based on classical non-associative, elasticity-plasticity theory. The model is calibrated by considering available experimental bond studies for short embedment length bond tests. There is good quantitative agreement between the predictions of the bond model and the results of several published bond pull-out tests with steel bars. The tests vary significantly in specimen configuration, concrete strength, and bar rib geometry.

METRIC CONVERSION FACTORS

Approximate Conversions to Metric Measures

Symbol	When You Know	Multiply by	To Find	Symbol
		LENGTH		
in	inches	*2.5	centimeters	cm
ft	feet	30	centimeters	cm
yd	yards	0.9	meters	m
mi	miles	1.6	kilometers	km
		AREA		
in^2	square inches	6.5	square centimeters	cm^2
ft^2	square feet	0.09	square meters	m^2
yd^2	square yards	0.8	square meters	m^2
mi^2	square miles	2.6	square kilometers	km^2
	acres	0.4	hectares	ha
		MASS (weight)		
oz	ounces	28	grams	g
lb	pounds	0.45	kilograms	kg
	short tons (2,000 lb)	0.9	tonnes	t
		VOLUME		
tsp	teaspoons	5	milliliters	ml
Tbsp	tablespoons	15	milliliters	ml
fl oz	fluid ounces	30	milliliters	ml
c	cups	0.24	liters	l
pt	pints	0.47	liters	l
qt	quarts	0.95	liters	l
gal	gallons	3.8	liters	l
ft^3	cubic feet	0.03	cubic meters	m^3
yd^3	cubic yards	0.76	cubic meters	m^3
		TEMPERATURE (exact)		
°F	Fahrenheit temperature	5/9 (after subtracting 32)	Celsius temperature	°C

*1 in = 2.54 (exactly). For other exact conversions and more detailed tables, see NBS Misc. Publ. 286, Units of Weights and Measures, Price $2.25, SD Catalog No. C13.10:286.

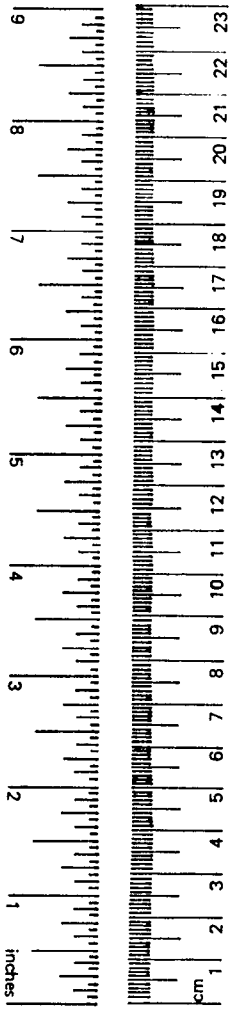

Approximate Conversions from Metric Measures

Symbol	When You Know	Multiply by	To Find	Symbol
		LENGTH		
mm	millimeters	0.04	inches	in
cm	centimeters	0.4	inches	in
m	meters	3.3	feet	ft
m	meters	1.1	yards	yd
km	kilometers	0.6	miles	mi
		AREA		
cm^2	square centimeters	0.16	square inches	in^2
m^2	square meters	1.2	square yards	yd^2
km^2	square kilometers	0.4	square miles	mi^2
ha	hectares (10,000 m^2)	2.5	acres	
		MASS (weight)		
g	grams	0.035	ounces	oz
kg	kilograms	2.2	pounds	lb
t	tonnes (1,000 kg)	1.1	short tons	
		VOLUME		
ml	milliliters	0.03	fluid ounces	fl oz
l	liters	2.1	pints	pt
l	liters	1.06	quarts	qt
l	liters	0.26	gallons	gal
m^3	cubic meters	35	cubic feet	ft^3
m^3	cubic meters	1.3	cubic yards	yd^3
		TEMPERATURE (exact)		
°C	Celsius temperature	9/5 (then add 32)	Fahrenheit temperature	°F

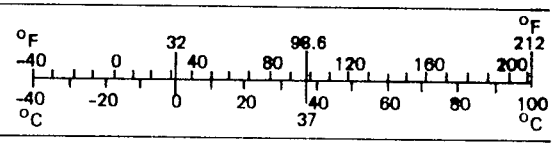

PREFACE

On 1 October 1993, the Naval Civil Engineering Laboratory (NCEL) and the Naval Energy and Environmental Support Activity (NEESA) were consolidated with four other Naval Facilities Engineering Command (NAVFAC) components into the Naval Facilities Engineering Service Center (NFESC). Due to publishing timeframes, this document may have references to NEESA or NCEL instead of NFESC.

REPORT DOCUMENTATION PAGE

Form Approved
OMB No. 0704-0188

1. AGENCY USE ONLY (Leave blank)	2. REPORT DATE	3. REPORT TYPE AND DATES COVERED
	March 1994	Final; Sep 1989 - Sep 1992

4. TITLE AND SUBTITLE

DEVELOPMENT OF A PLASTICITY BOND MODEL FOR REINFORCED CONCRETE - PRELIMINARY CALIBRATION AND CYCLIC APPLICATONS

5. FUNDING NUMBERS

PE - 61153N
C-N47408-89-C-1056
WU - DN666342

6. AUTHOR(S)

7. PERFORMING ORGANIZATION NAME(S) AND ADDRESS(ES)

Leonard R. Herrmann, University of California, Davis
James V. Cox, Naval Facilities Engineering Service Center

8. PERFORMING ORGANIZATION REPORT NUMBER

CR 94.001

9. SPONSORING/MONITORING AGENCY NAME(S) AND ADDRESS(ES)

Office of Naval Research
Arlington, Virginia 22217-5000

10. SPONSORING/MONITORING AGENCY REPORT NUMBER

11. SUPPLEMENTARY NOTES

12a. DISTRIBUTION/AVAILABILITY STATEMENT

Approved for public release; distribution is unlimited.

12b. DISTRIBUTION CODE

13. ABSTRACT (Maximum 200 words)

A bond model is developed to describe the inelastic behavior of the bond between reinforcing bars and concrete. The bond model is applicable to both monotonic and cyclic loading conditions. It is based on classical non-associative, elasticity-plasticity theory. The model is calibrated by considering available experimental bond studies for short embedment length bond tests. There is good quantitative agreement between the predictions of the bond model and the results of several published bond pull-out tests with steel bars. The tests vary significantly in specimen configuration, concrete strength, and bar rib geometry.

14. SUBJECT TERMS

Reinforced concrete, bond model, plasticity, cyclic loading, monotonic loading, constitutive model, finite elements

15. NUMBER OF PAGES
120

16. PRICE CODE

17. SECURITY CLASSIFICATION OF REPORT	18. SECURITY CLASSIFICATION OF THIS PAGE	19. SECURITY CLASSIFICATION OF ABSTRACT	20. LIMITATION OF ABSTRACT
Unclassified	Unclassified	Unclassified	

Contents

1. SCOPE

The overall research project consisted of studies carried out by the principal investigator and three graduate students. In order to keep this report to a reasonable length, wherever possible, duplication of contents between this report and the doctoral dissertation of Dr. James Cox (Cox 1994), and the M.S. theses of Mr. Ko-Tao Chang (Chang 1992) and Mr. Larry McMichael (McMichael 1993) has been avoided. The information contained in their theses will be referenced as appropriate.

2. INTRODUCTION

A survey of the literature on the bond between concrete and reinforcement, and the modeling of bond behavior is reported by Cox (1994); those items directly needed for the description of the work reported here will be referenced as needed.

The finite element analysis of reinforced concrete structures requires mathematical models for the properties of concrete (including behavior due to cracking), properties of the reinforcement and of the bond between the concrete and reinforcement. The modeling of the elastic-plastic properties of steel is fairly well established. Considerable research effort has been expended and progress has been made in the development of inelastic characterizations of concrete; still much work remains to be done on the modeling of crack initiation and propagation, and aggregate interlock across partially open cracks. It is widely agreed, however, that the area in which the least is known is in the modeling of the bond between the reinforcement and concrete.

Numerous experiments have been conducted to try and measure the bond behavior between reinforcement and concrete. Many of the investigators have attempted to fit analytical expressions to their experimental data with the hope that the results could be used to predict bond behavior for analysis purposes. Unfortunately these bond models have been less than successful in predicting bond behavior for conditions markedly different than what was used in the test set-up.

What is needed is a *universal bond model*, i.e., one that can not only reproduce the experimental data base on which it is built but also predict, with acceptable accuracy, the response of a wide range

of tests and actual structures. Such broad predictive capabilities should not depend on any recalibration of the model when the conditions of the test or field structure differ markedly from conditions previously considered (other than using the proper physical parameters such as concrete strength, bar diameter, etc.).

The objective of the research described in this report was the development, calibration and verification of a more comprehensive model to describe the interaction between reinforcing bars and the surrounding concrete for reinforced concrete. Both monotonic and cyclic loading conditions were considered. The model relates the bond stresses to the deformations that occur in the bond layer. The scale of the model is macroscopic, i.e., the stresses are averages, of the microscopic stresses, over one lug spacing (a *unit cell*) of the bar. Hence no distinction is made between the local bond stresses that exist at a lug and the bond stresses occurring between lugs. Both elastic and inelastic deformations are considered.

3. EXPERIMENTAL EVIDENCE

3.1. Available Experimental Data

In most situations, physical models are motivated, calibrated and verified using experimental data for the system in question. Because this study does not contain an experimental component it relies on available experimental evidence. The first step is to briefly review the most pertinent evidence available.

There are several different levels of investigation at which experimental evidence is needed. The first is to define the general problem and to suggest a broad framework for its solution. Nearly all experimental evidence related to the subject is valuable for this phase of the investigation, including experimental studies which are not sufficiently well documented to be of value in quantitatively establishing a physical model. A comprehensive review of available experimental evidence for concrete-reinforcement bond is given by Cox (1994).

For experimental evidence to be of value in quantitatively establishing a physical model it must be thoroughly documented; unfortunately, many of the past bond studies do not meet this criterion. For bond studies the required documentation should

include: (a) all physical dimensions of the reinforced concrete sample, (b) the properties of the concrete and the reinforcement including lug characteristics, (c) a description of the loading rate, the type of control used for the independent variables and the instrumentation used to measure the dependent variables and finally (d) some indication of experimental scatter. In addition the test specimen must be sufficiently simple so that it can be easily analyzed.

Few of the studies reported in the literature meet the above criteria to a sufficient degree to be of quantitative value. The studies that were found to be useful for detailed analysis include the ones reported by Rehm (1979), Eligehausen (1983), Gambarova (1989) and Malvar (1991).

3.2. Scatter in Experimental Data Base and Modeling Uncertainties

When developing a physical model it is absolutely imperative that information be available concerning the degree of scatter present in the experimental data. Without such evidence a great deal of time may be wasted in attempting to describe apparent physical phenomena which are in fact only the result of experimental anomalies.

Local failure takes place in the vicinity of the lugs very early in the response of reinforced concrete bond (most likely even before the peak stress is reached). Because failure is inherently a random process one should expect a great deal of scatter in bond behavior.

Eligehausen (1983), performed, with a great deal of care, a total of 125 tests on pullout specimens designed to simulate beam-column joints. For a given test series he normally performed only one repetition unless the results varied significantly from the original test in which case he performed a third test. He found significantly more scatter when the specimens were cast from different batches of concrete rather than a single batch. In Figs. 1 and 2, the results (bond shear vs. bond slip) of three tests for samples taken from a single batch are shown. Figure 3 compares results when the samples were cast from different batches of concrete.

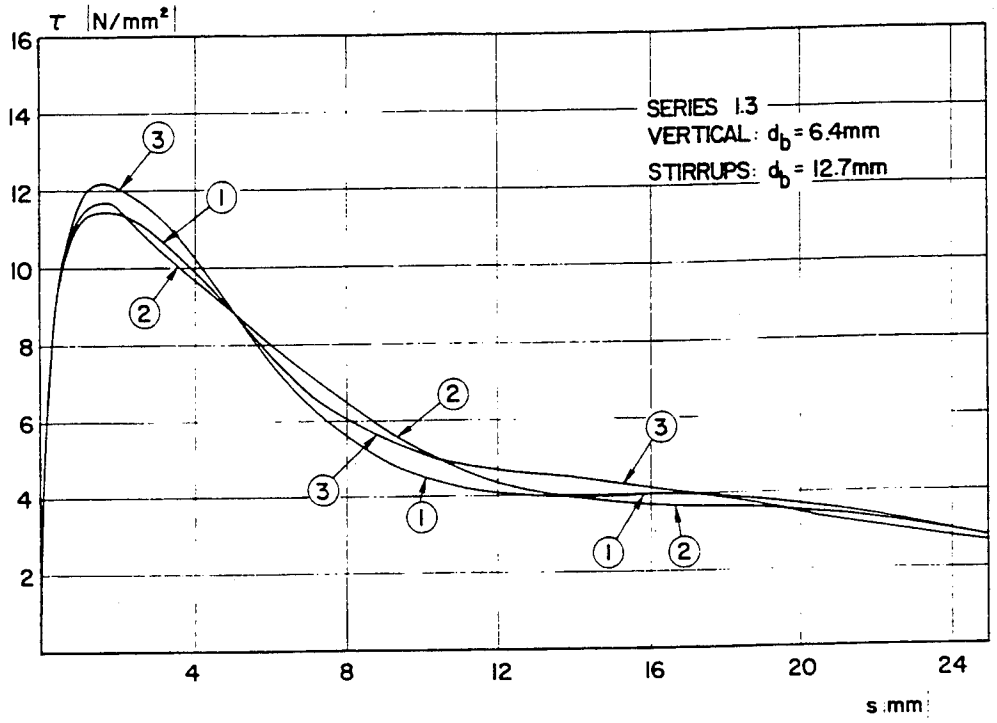

Figure 1. Example of Experimental Scatter (taken from Fig. 4.5 of Eligehausen 1983).

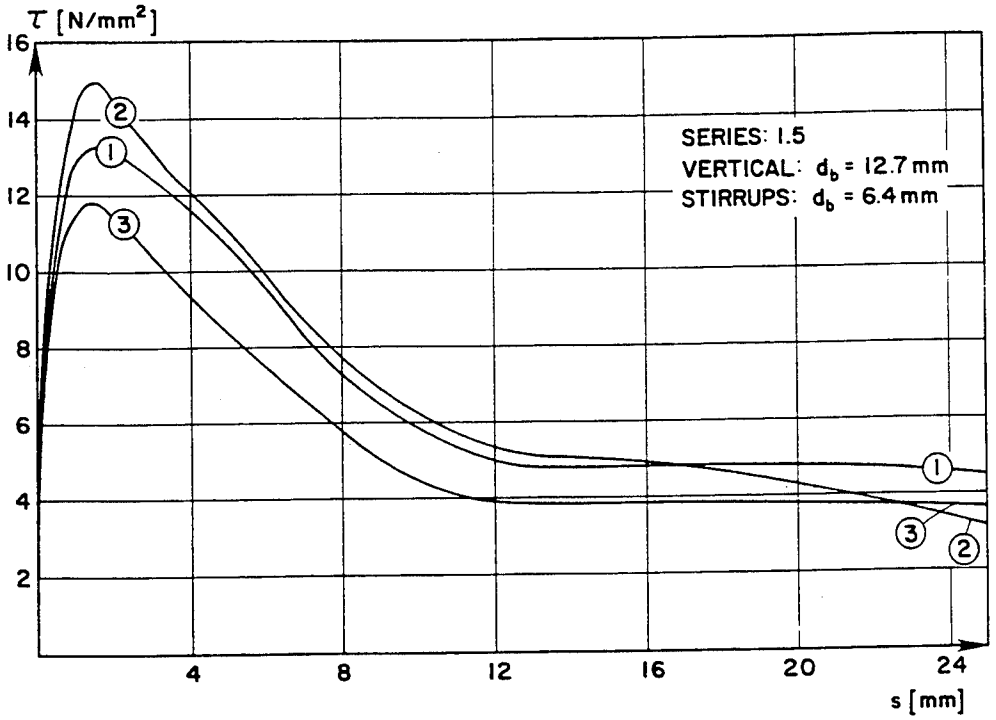

Figure 2. Example of Experimental Scatter
(taken from Fig. 4.7 of Eligehausen 1983)

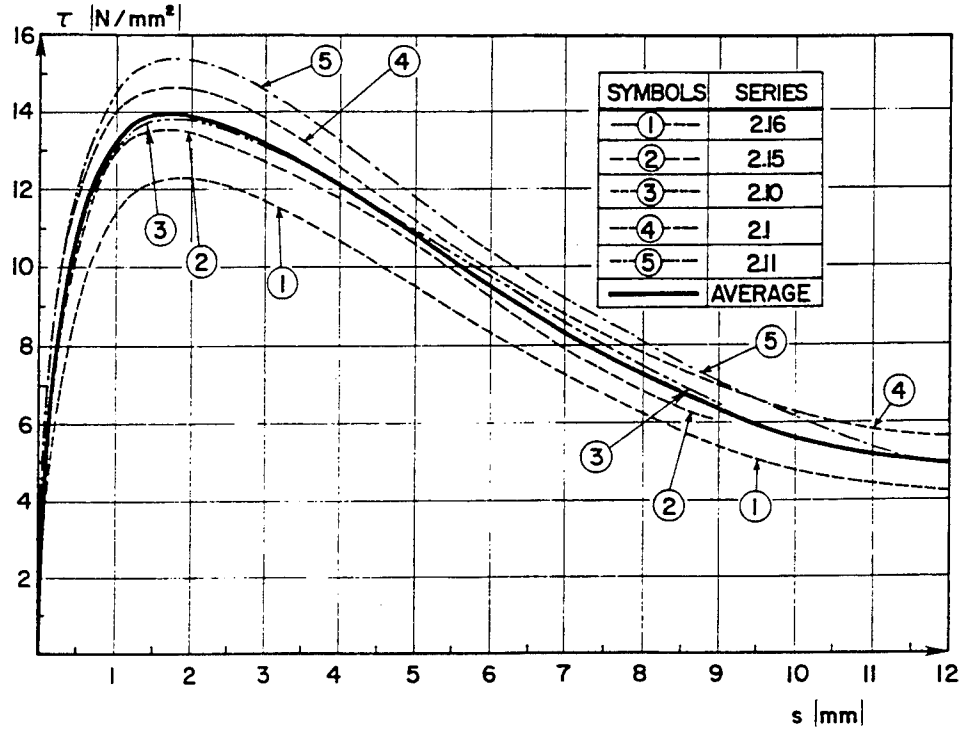

Figure 3. Inter-batch Experimental Scatter
(taken from Fig. 4.8 of Eligehausen 1983)

Edwards and Yannopoulos (1978) carried out a series of bond tests for the expressed purpose of studying the experimental scatter in bond test data. For each of eight basic test series they reported a minimum of five different tests results. Two of the reported figures are shown in Figs. 4 and 5. Figure 4 has the least amount of scatter of any of their plots while Fig. 5 has nearly the most. The scatter reflected in Fig. 5 is more representative of most of their results.

The above two sited studies reported average bond stress versus bar end slip (embedment lengths of 9.5 lug spacings in the first case and 4 in the second). Even greater scatter is to be expected when measurements of a more local nature are made. The variation in scatter has two sources. First, the results given in Figs. 1-5 are all averages over the embedded length, a process that tends to reduce scatter. Second, reported local measurements of bond quantities are usually made by placing strain gages along the length of the bar to determine the axial strain distribution, the local bond shear stress is then found by numerically differentiating the results and using equilibrium considerations (see Appendix A). Numerical differentiation, of course, is well known for magnifying experimental scatter. Some appreciation of the problem can be obtained from noting the irregularities of the curve given in Fig. 6 which was taken from the report by Cowell (1982).

A second major source of uncertainty in this study arises because of the difficulty of interpreting the experimental results. The quantities of interest are the bond stresses and deformations; unfortunately, no test has been devised which unambiguously measures these quantities. Instead certain related quantities are measured, e.g., surface forces and displacements, strains in the reinforcement bar, etc. Then an analysis must be used to try and relate these quantities to the items of interest. Unfortunately this is far from a straight forward task. The problem is two fold. Firstly, the development and break down of bond involves local failure of concrete. The ability to analyze the behavior of concrete under failure conditions is severely restricted because of our very incomplete understanding of the multi-axial stress-strain behavior of concrete out to and including failure, and our limited ability to perform analyses which include localizations such as crack initiation and propagation. Secondly, many of the devised bond tests are exceedingly complicated in nature, e.g., see Morita (1979) and Eligehausen (1983).

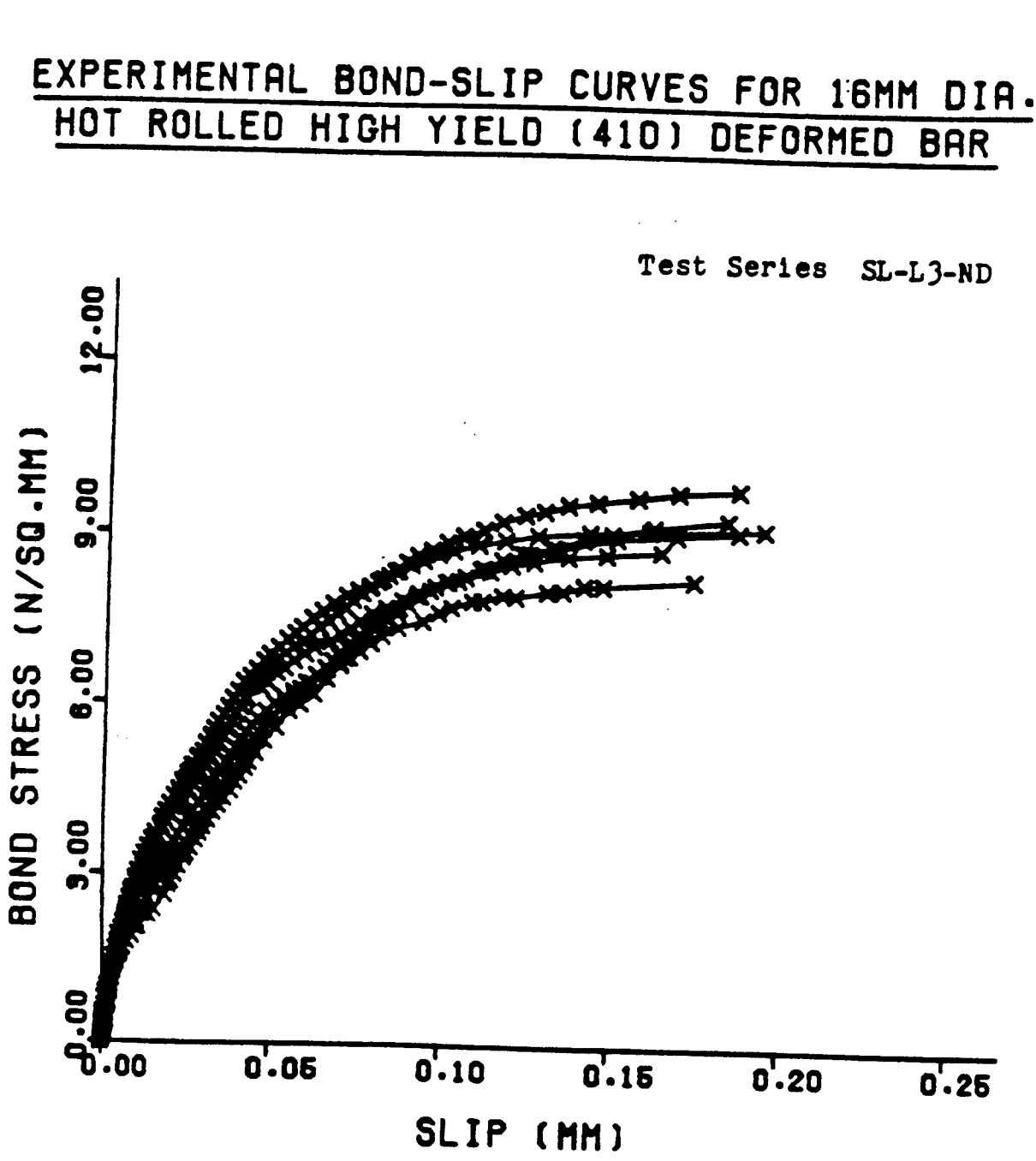

Figure 4. Example of Experimental Scatter
(taken from Fig. 6.10 of Edwards and Yannopoulas 1978)

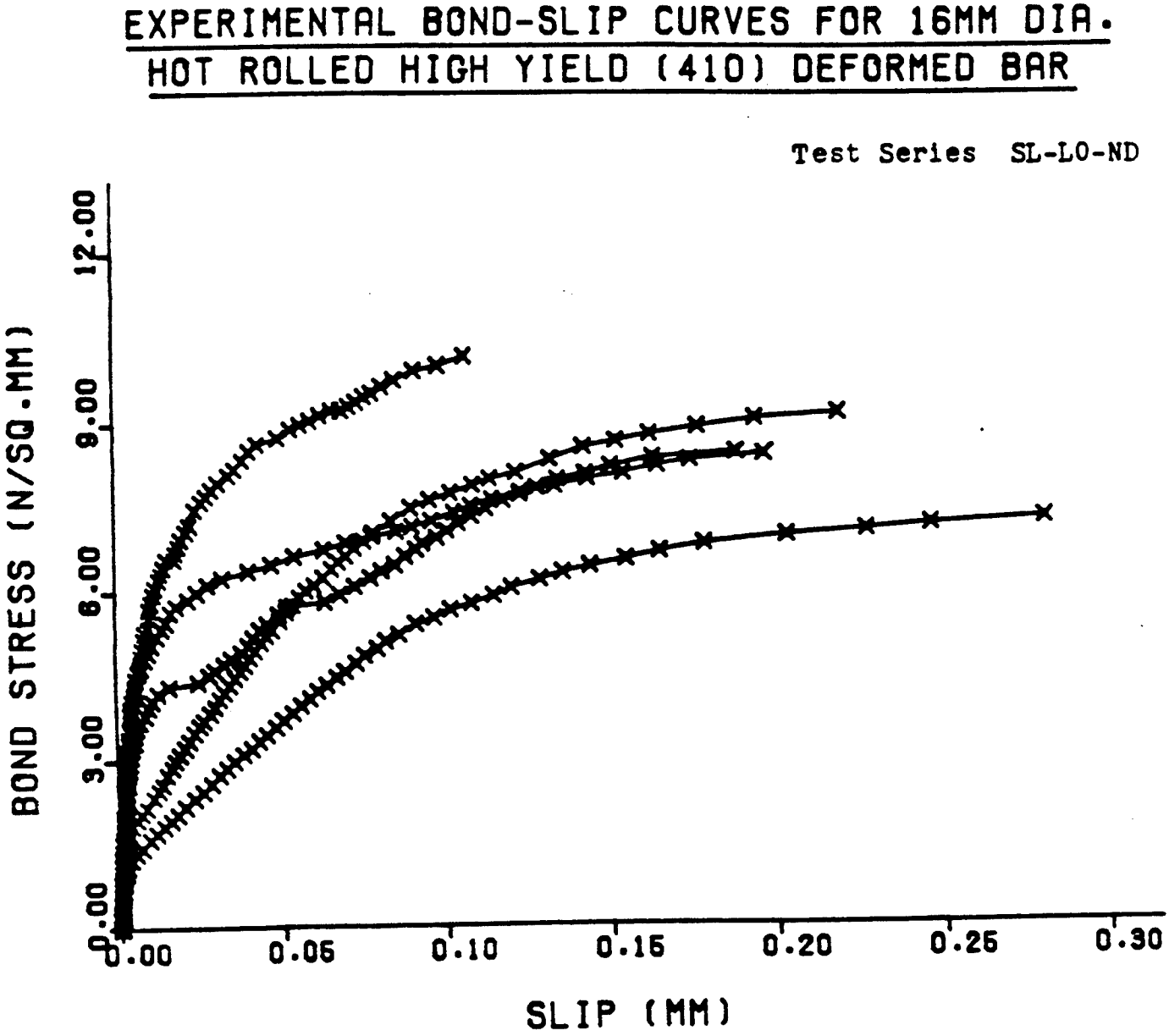

Figure 5. Example of Experimental Scatter
(taken from Fig. 6.7 of Edwards and Yannopoulas 1978)

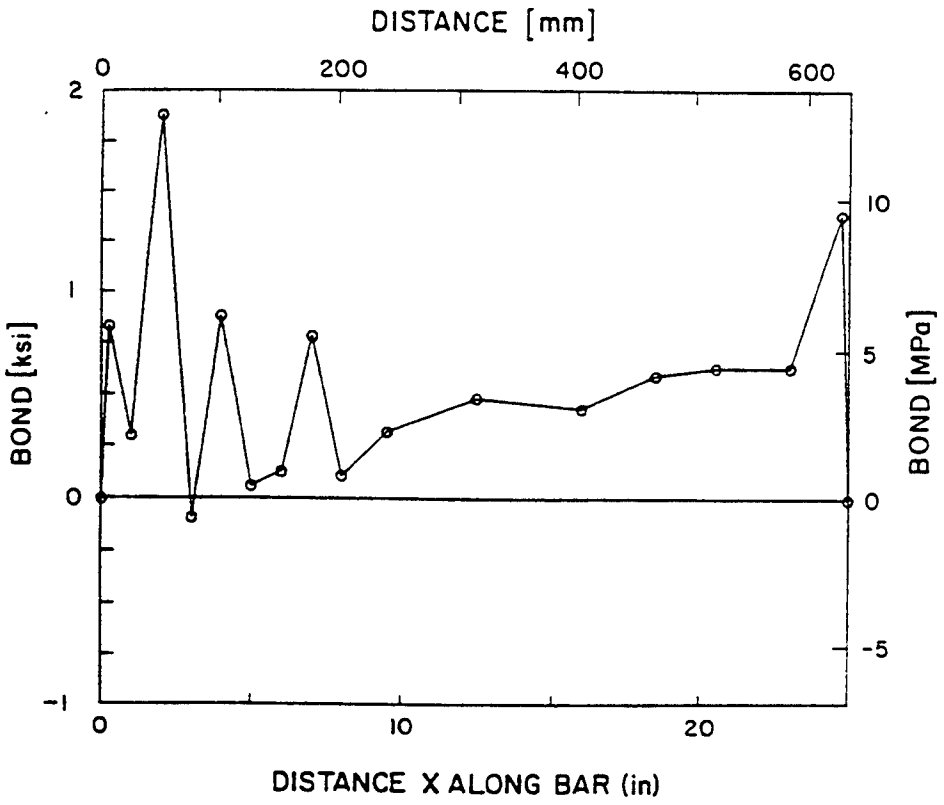

Figure 6. Bond-Stress Distribution - No Smoothing (taken from Fig. 4.2 of Cowell 1982)

In many ways it is a "catch 22" situation. The more one attempts to reduce uncertainty by realistically modeling the geometry of the tests, the more one is required to include poorly understood phenomena such as multi-axial stress-strain behavior of concrete, crack propagation, etc.

Thus, when assessing the confidence level for the developed bond model both the uncertainties of the underlying experimental data base and the uncertainties of interpretation of individual test results must be considered.

4. FRAMEWORK FOR GENERAL MODEL

The scale of interest for this development is phenomenological, i.e., large with respect to the size of the aggregates in the concrete and the spacing of the lugs on the reinforcing bar. The concrete-reinforcement interface is idealized as shown in Fig. 7. The "bond zone" consists of the interface between the concrete and the reinforcement and possibly a layer of concrete immediately surrounding the reinforcing bar in which severe local deformations occur due to the bond stresses.

The physical thickness of the bond zone will change during the course of the loading process. However, there appears to be little experimental evidence concerning the evolution of this quantity. In addition, it would seem that for most situations the bond zone thickness will be very small compared to the dimensions of the finite elements used to model the surrounding concrete. Thus, in this study, the bond zone will effectively be taken to have zero thickness. The local deformations of the bond zone will still be included in the bond behavior by concentrating them at the zero thickness interface. The approximation of zero thickness is consistent with the common modeling idealization of treating reinforcing bars as lines. The zero thickness idealization will most likely have adverse effects in some special cases such as the modeling of a lap splice of two bars. For a more detailed investigation of the bond zone thickness question the reader is referred to Cox (1994).

The bond stresses consist of the normal component σ_n, the longitudinal shear stress τ_{nz} (often just referred to as "the bond stress") and the circumferential shear stress $\tau_{n\theta}$. The bond stresses

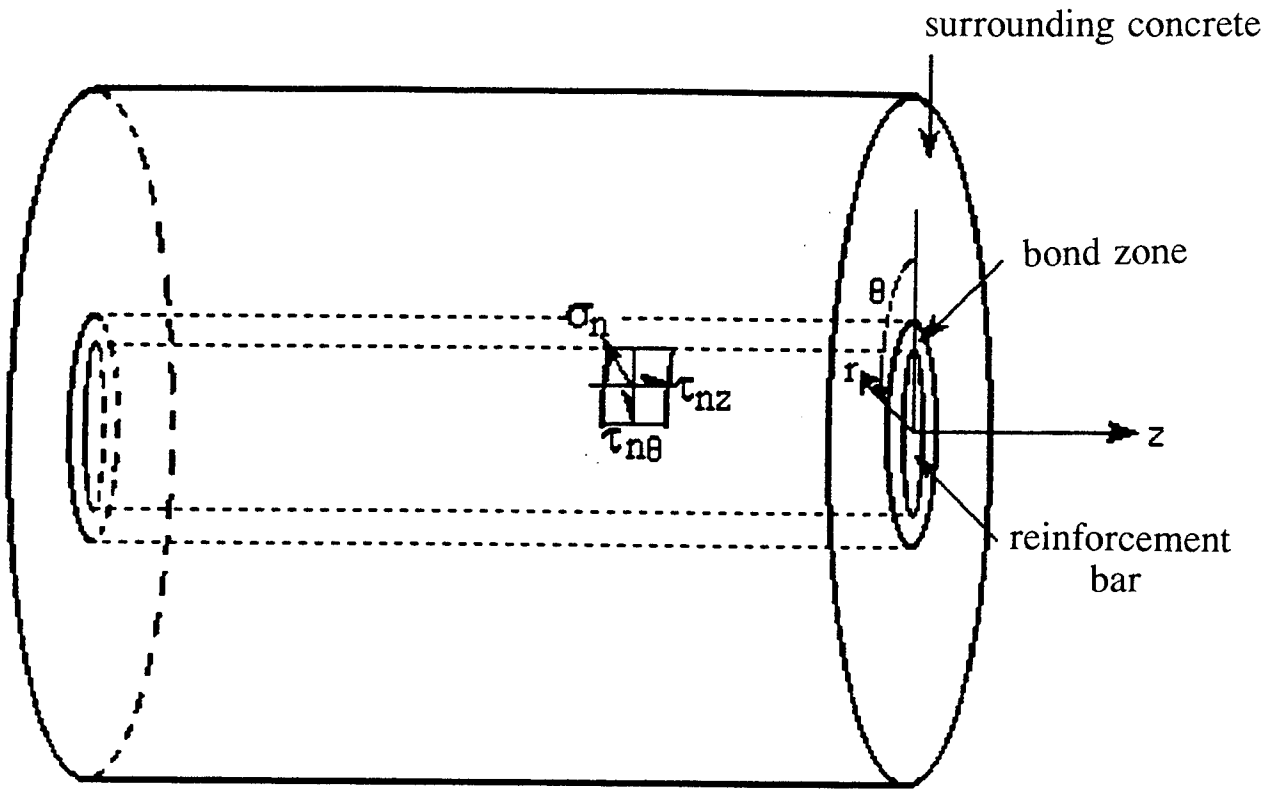

Figure 7. Bond Zone and Bond Stresses

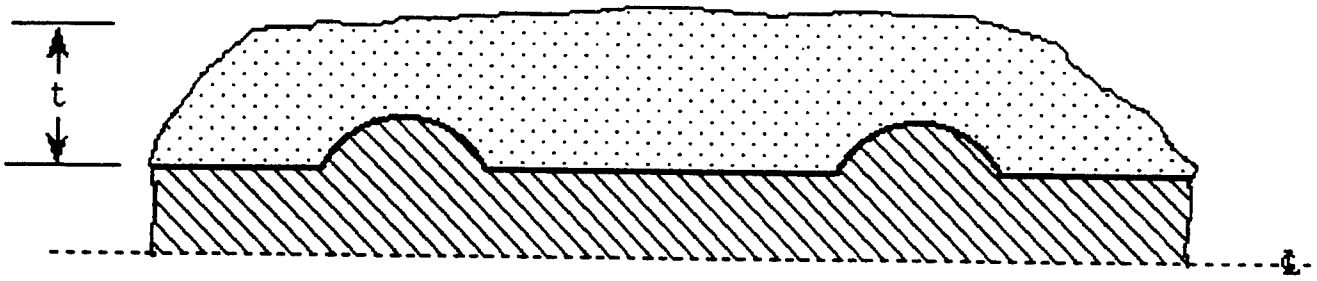

a) underformed bond zone

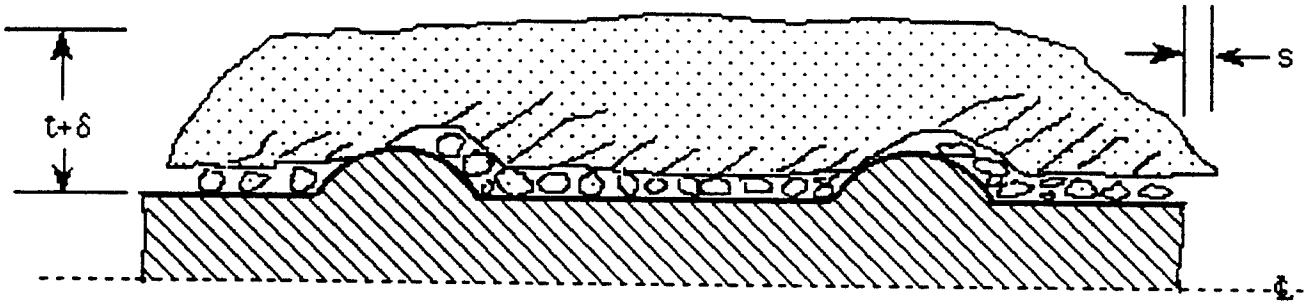

b) Deformed bond zone

Figure 8. Deformation of Bond Zone

will be given the generalized notation $\{Q\}$, i.e., $Q_1 = \tau_{nz}$, $Q_2 = \sigma_n$, and $Q_3 = \tau_{n\theta}$ (when a thick bond zone is considered it may be desirable to include the other three stress components σ_θ, σ_z and $\tau_{\theta z}$ to describe the internal forces). A tensile, normal, bond stress is defined to be positive.

The corresponding deformation quantities will be denoted as $\{q\}$. Where q_2 is the dilation of the bond layer (due to cracking and crushing of the concrete in the bond layer and the overriding of the lugs by the surrounding concrete as it slips by; see the quantity δ in Fig. 8). The shear deformation quantities are denoted as q_1 and q_3. The quantity q_1 is made up of the axial slip of the reinforcement relative to the concrete (see Fig. 8) and the local shear deformation (γ_{rz}) that takes place in the bond layer. Because slip will dominate this deformation quantity, it will be referred to simply as "slip". In the circumferential direction a similar interpretation is given to q_3.

In order that s and δ of Fig. 8 should have the units of deformation they must be divided by a characteristic length quantity. While the thickness of the bond zone might appear to be a logical choice there are two arguments against it. Because the dilation is distributed throughout the bond zone, dividing δ by the bond zone thickness gives a meaningful average strain quantity. However, the interface slip component of s is concentrated at the interface and thus normalizing s with respect to the bond zone thickness is less rational. The main reason, however, for not choosing the bond zone thickness is the fact that it is not explicitly determined.

If the behavior of a single bar embedded in a very large mass of concrete is considered, the only length scales present are those associated with the reinforcing bar (assuming the concrete is treated as homogeneous so that a length scale related to aggregate size is not present). The three bar scales are the bar diameter (D_b), the lug height and the lug spacing. If the ratios of these three quantities remain nearly the same for a series of bars then there is only one scale and any one of the three can be selected. For these ideal conditions, bond behavior will be independent of bar size if s and δ are non-dimensionalized with respect to D_b. Shima (1987) reported that he experimentally observed this to be true. However, Eligehausen (1983) suggests that this is not the case. The difference in the two observations may be due to the fact that Eligehausen's test

apparently introduces multiple scales due to the nature of the test specimen (e.g., proximity of the column reinforcement). For some applications (e.g. those having a characteristic element size greater than the bond zone size) other length scales (such as spacings between adjacent bars, cover depth, etc.) may exist; in these cases relying on only D_b may not be sufficient.

Following the convention adopted by Shima (1987) and others, s and δ are normalized with respect to the bar diameter, e.g. $q_1 = s/D_b$, etc. Under some circumstances the bond zone thickness would be expected to be correlated to the bar diameter (assuming that the lug height and spacing are correlated to bar diameter) and, thus, the defined deformations will be directly related to the average strains that would be obtained if one normalized with respect to bond zone thickness.

The goal of this research is the development of a comprehensive constitutive model for the relationship between {Q} and {q}. A consideration of the inelastic nature of deformation in concrete, the permanence of the local failures that takes place in the concrete in the vicinity of the lugs, the frictional component of bond behavior and experimental observations, leads to the conclusion that the behavior is elastic-plastic with a yield surface that evolves with "damage." For example, the cyclic bond tests reported in Fig. 9 clearly show classic elastic-plastic behavior and the yield states plotted in Fig. 10 indicate a strong dependency on damage. The several components of elastic-plastic theory must now be identified for reinforcement-concrete bond.

It is becoming increasingly accepted that the behavior of concrete can be described by constitutive law where the elastic moduli are damage dependent (elasto-plastic coupling); hence, it would seem reasonable to include this behavior in an elasto-plastic bond law. Unfortunately, bond tests to date have not been conducted with the goal or necessary precision to isolate the elasto-plastic coupling behavior. In addition this refinement would seem not to have a significant impact on bond behavior, hence, it will not be considered at this time. Instead the elastic component of the deformation $\{q\}_e$ is simply expressed in terms of {Q} by an assumed linear elastic law

$$\{q\}_e = [A]\ \{Q\} \tag{1}$$

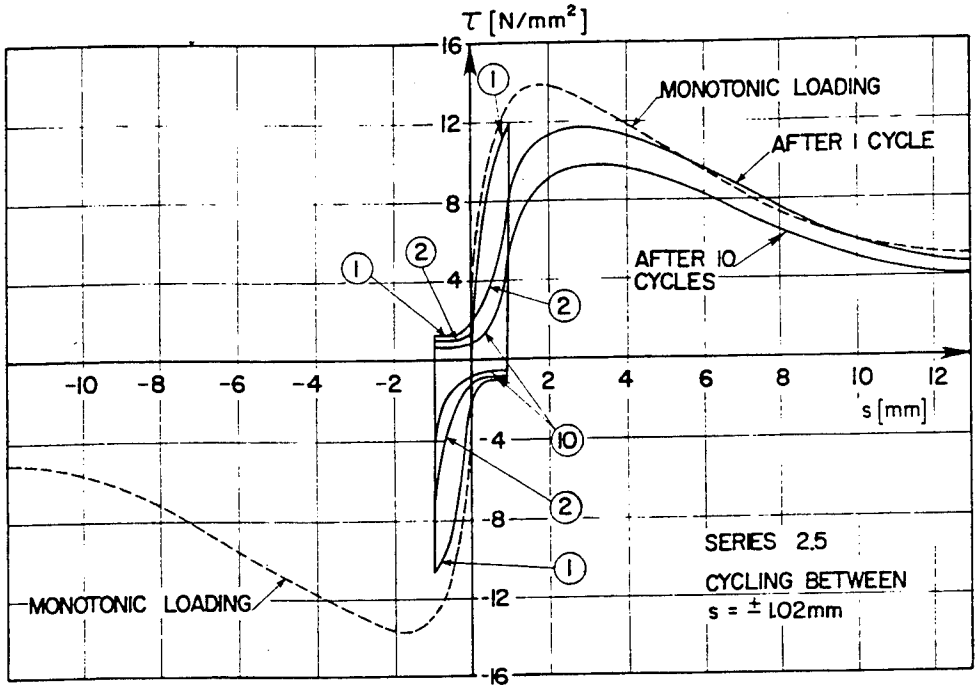

Figure 9. Bond Stress-Slip Relationship for Cyclic Loading (taken from Fig. 4.26 of Eligehausen 1983)

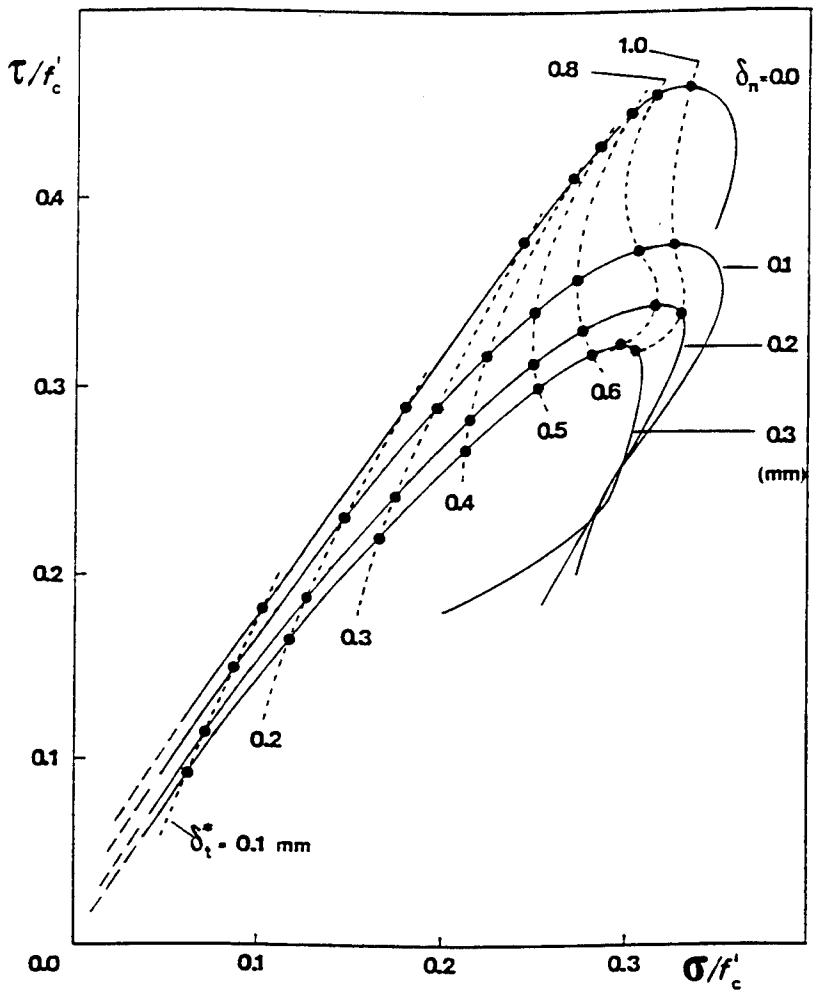

Figure 10. Bond Shear Stress - Bond Normal Stress Envelopes (taken from Fig. 12 of Gambarova 1989)

where the total deformation has been additively decomposed into elastic and plastic components:

$$\{q\} = \{q\}_e + \{q\}_p \tag{2}$$

The coefficients of the compliance matrix [A] are taken to be constants.

The yield function is written in the form

$$\Phi(Q_i, D_k) = 0 \tag{3}$$

where D_k are internal variables whose values determine the instantaneous position of the yield surface in stress space. The D_k will be called "damage measures" even though they may initially lead to a hardening of the yield surface. The damage measures will be functions of the plastic deformation:

$$D_k = D_k(q_{jp}) \tag{4}$$

Because friction is an important component of interface behavior it is expected that the plastic flow will be "non-associative":

$$\{q\}_p = \lambda^* \{\text{grad } \Psi\} \tag{5}$$

The potential function is denoted as Ψ.

The determination of the desired elastic-plastic model requires the identification of the quantities [A], Φ, D_k and Ψ.

The above discussion has been in terms of three bond stress and three deformation components, however, currently there does not appear to be enough evidence to permit this degree of generality and in fact such a model would probably find little use in analysis at present. For the remainder of this work the theory will be limited to the case where $q_3 = Q_3 = 0$. This situation occurs exactly for axisymmetric conditions. For non-axisymmetric conditions q_1, q_2, Q_1, and Q_2 will be circumferential averages of the corresponding θ dependent quantities.

The determination of [A], Φ, D_k and Ψ for the restricted condition of axisymmetry still is a formidable task. Before this

calibration process is undertaken, the necessity of numerically implementing the model must be addressed in preparation for interpreting the experimental data base.

5. SPECIMEN MODEL IMPLEMENTATION

5.1. Ideal Test

The numerical modeling of each test specimen will vary, however, certain common features do exist. The analysis of an *ideal* test that incorporates these common features will be considered first followed by applications to specific tests in the data base.

The *ideal* test is defined as a homogeneous, axisymmetric test in which q_1 (slip) is specified and an external constraint, dependent on Q_1 and Q_2, is placed on the dilation q_2, i.e.,

$$q_1 = \text{given} \tag{6}$$

$$q_2 = H(Q_i). \tag{7}$$

It will be assumed for now that q_1 is an ever increasing function (monotonic conditions) which results first in elastic response followed by continuous plastic behavior. The nature of H will depend upon the type of test and will be addressed when specific tests are considered. The assumption of homogeneous response (along the length of the bar) is rigorously met if the embedment length of the bar is of the order of one lug spacing (one unit cell). Cox (1994) investigated variations in the response along the lengths of longer bars.

First consider the magnitude of q_1 required to reach first yielding, denote it by q_{1y}, etc. Eqs. (1), (3), and (7) give:

$$\{q\}_y = [A]\ \{Q\}_y \tag{8}$$

$$\Phi(Q_{iy},0) = 0 \tag{9}$$

$$q_{2y} = H(Q_{iy}) \tag{10}$$

Equations (8), (9) and (10) constitute a set of 4 simultaneous nonlinear equations in four unknowns q_{1y}, q_{2y}, Q_{1y} and Q_{2y}. This set

of equations can be solved by any number of standard nonlinear equation solving methods, the simplest being successive substitution.

For monotonic conditions, beyond the yield point it is expected that the stress state will continuously remain on the yield surface. This will require for each solution step that $\Delta\Phi = 0$ (for simplicity $\Delta\Phi_N$ of step N has been written as $\Delta\Phi$). For purposes of evaluating test results computational efficiency is not important, however, accuracy and simplicity are, thus, a simple midpoint method with very small time steps is used to enforce consistency. This results in the following approximation for $\Delta\Phi$:

$$\Delta\Phi = \sum_{i=1}^{2} \left.\frac{\partial\Phi}{\partial Q_i}\right|_c \Delta Q_i + \sum_{j=1}^{J} \left.\frac{\partial\Phi}{\partial D_j}\right|_c \Delta D_j = 0 \tag{11}$$

The c indicates that the derivatives are evaluated at the midpoint of the step, also $Q_{1c} = Q_{1_{N-1}} + \Delta Q_1/2$, etc. In Eq. (11) it has been assumed that there are J damage variables.

Similar approximations are used for the constraint Eq. (7)

$$\Delta q_2 = \sum_{i=1}^{2} \left.\frac{\partial H}{\partial Q_i}\right|_c \Delta Q_i \tag{12}$$

and for the evaluation of Eq. (4):

$$\Delta D_j = \sum_{i=1}^{2} \left.\frac{\partial D}{\partial q_{p_i}}\right|_c \Delta q_{p_i} \tag{13}$$

The incremental forms of Eqs. (1) and (2) are:

$$\{\Delta q\}_e = [A]\{\Delta Q\} \tag{14}$$

$$\{\Delta q\} = \{\Delta q\}_e + \{\Delta q\}_p \tag{15}$$

The incremental form of Eq. (6) is simply:

$$\Delta q_1 = \text{given} \tag{16}$$

Finally an incremental form of Eq. (5) is needed; with only two unknowns it is convenient to write it in the form

$$\Delta q_{1p} = \lambda \tag{17}$$

$$\Delta q_{2p} = \lambda \, g_c \tag{18}$$

where g is a function of the state of the material (i.e., a function of the quantities Q_i and D_k) and the c denotes its value at the increment's midpoint. (The quantity λ is just the value of Δq_{1p}, while g is the ratio of Δq_{2p} to Δq_{1p} for non-associative flow.)

Now Eqs. (11) through (18) constitute a set of 9+J simultaneous equations in the 9+J unknowns, Δq_1, Δq_2, Δq_{1e}, Δq_{2e}, Δq_{1p} , Δq_{2p}, ΔQ_1, ΔQ_2, ΔD_1... ΔD_J and λ. These nonlinear equations can be solved using a standard nonlinear solver. In the actual solution of these equations a number of the quantities can be eliminated analytically before a numerical analysis scheme is applied.

5.2. Eligehausen's Test

Eligehausen's (1983) test specimen and setup are shown in Fig. 11. Because no local measurements were made along the length of the bar it is necessary to assume that the bonded length (5 bar diameters = 9.5 lug spacings) is sufficiently short that the behavior can be approximated as homogeneous over the embedded length; for additional discussion on response gradient effects in short specimens see Cox (1994). The test configuration is not axisymmetric about the center line of the bar, hence, it is assumed that the model applies (approximately) to circumferential averages of Q_1, Q_2, q_1 and q_2 as well as to true axisymmetric conditions.

The measurement of the axial slip of the bar relative to the concrete ($s = q_1 * D_b$) was made at the unloaded end. It is assumed that this value is approximately equal to the average value over the embedded length of the bar. Because the strains in the bar and concrete are small, it is expected that this is a reasonable approximation, see Cox (1994). The bond shear stress reported by

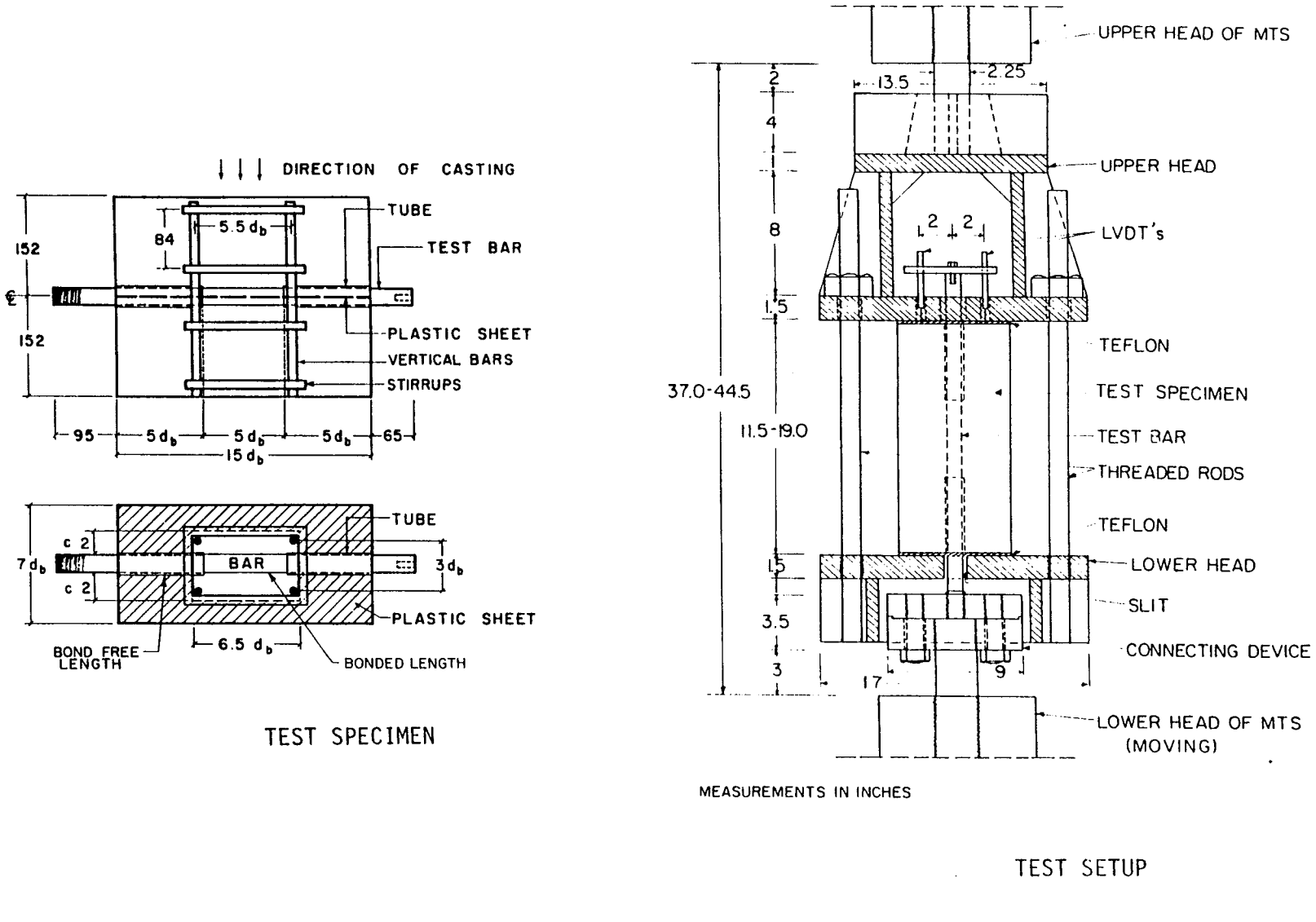

Figure 11. Details of Eligehausen's Test
(taken from Figs. 3.5 and 3.6 of Eligehausen 1983)

Eligehausen was found by dividing the total force applied to the bar by the circumferential contact area thus giving an average value.

Making the above assumptions, Eligehausen's test fits the specification of the *ideal* test provided that the constraint to the bond zone dilation can be expressed in the form of Eq. (7). The specimen was designed so that very early in the test a splitting crack would form. Figure 12 shows an idealized free body of the transverse forces acting on the lower portion of the concrete column stub assuming that the splitting crack has formed and no external forces are applied to the column (only a very small part of the normal bond stress $Q_2 = \sigma_n$ is shown). The quantity F_v denotes the average force, at the crack level, in the vertical steel. The bonded length of the horizontal bar is $L = 5D_b$. Equilibrium gives:

$$- D_b \, L \, Q_2 = 4 \, F_v \tag{19}$$

or

$$F_v = -1.25 \, D_b^2 \, Q_2 \tag{20}$$

Each vertical bar will be modeled as a semi-infinite reinforcing bar embedded in a large piece of concrete. The force F_v applied to this steel will cause it to pull some distance δ_{c1} out of the concrete. In Appendix B an empirical relationship, based on experimental data taken from Shima (1987), between δ_{c1} and F_v is found (combining Eqs. B-5 and B-12):

$$\frac{\delta_{c1}}{D_b} = \frac{D_{bv}}{D_b} \left[\eta \left(\frac{F_{v_{max}}}{\frac{\pi}{4} D_{bv}^2 \, E_r} \right)^{1.62} - \frac{(F_{v_{max}} - F_v)}{E_{un}} \right] \tag{21}$$

where E_r is the modulus of the vertical reinforcement; D_{bv} is its diameter; η and E_{un} are defined in the Appendix, and $F_{v_{max}}$ is the maximum value of F_v experienced in the test to the point in question.

The increase in the size of the cavity due to the splitting crack is shown in Fig. 13. The average radial enlargement of the cavity can be found from the integral:

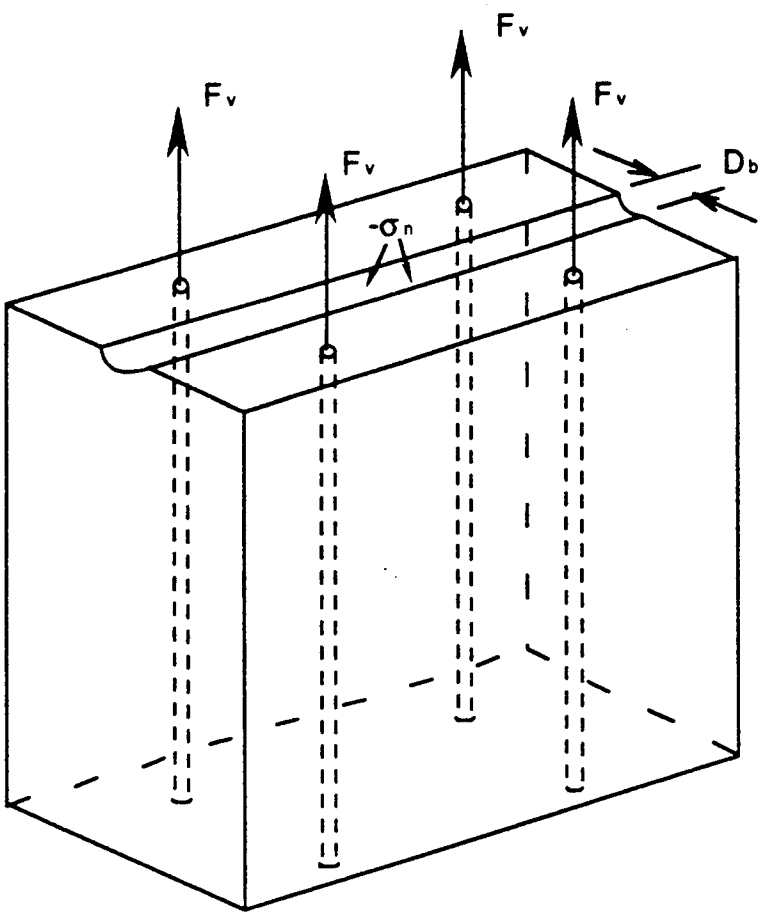

Figure 12. Idealized Free Body of Lower Half of Eligehausen's Concrete Sample

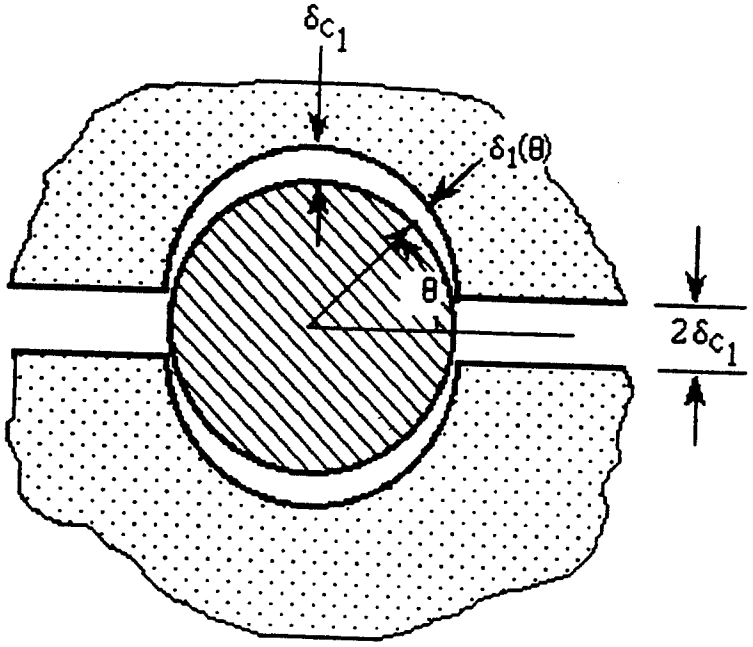

Figure 13. Dilation of Bond Layer due to a Splitting Crack

$$\frac{\bar{\delta}_{c1}}{D_b} = \frac{2}{\pi D_b} \int_0^{\pi/2} \delta_1(\theta)\, d\theta = \frac{2}{\pi D_b} \int_0^{\pi/2} \delta_{c1} \sin\theta\, d\theta \simeq .64 \frac{\delta_{c1}}{D_b} \qquad (22)$$

In addition to the above, there is local deformation of the concrete that immediately surrounds the reinforcing bar. This concrete will be approximately modeled as a thick walled-cylinder of outer radius equal to the distance to the center-line of the vertical bars, i.e., $b = 3a = 3(D_b/2)$. For the purpose of calculating the additional deformation contributed by the thick-walled cylinder, the displacement is taken to be zero at its outer surface. Using the elastic, thick-walled, cylinder solution for the case of plane stress (e.g., see Timoshenko 1987), it is easy to show that the radial deformation at the inner surface of the cylinder of concrete can be written in the form:

$$\delta_{c2}/D_b = (\xi/E_c)\, \sigma_n \qquad (23)$$

If no cracking is assumed:

$$\xi = \frac{\frac{1}{2}\left[\left(\frac{b}{a}\right)^2 - 1\right]}{\left[\frac{1}{1-\nu_c} + \left(\frac{b}{a}\right)^2 \frac{1}{1+\nu_c}\right]} \qquad (24)$$

For a Poisson's ratio of concrete of 0.17 and b/a = 3: $\xi = 0.45$. If instead complete cracking of the cylinder is assumed then

$$\xi = .5\, \ln(b/a) \qquad (25)$$

which gives $\xi = 0.55$. Because the value of ξ varies over such a small range, a constant value of $\xi = 0.55$ is used.

Due to the axial stress σ_z, and the radial and hoop stresses $\sigma_r = \sigma_\theta = \sigma_n = Q_2$ in the reinforcement, the diameter of the bar changes by (for linear, isotropic, elastic behavior):

$$\frac{\delta_b}{D_b} = \frac{1}{2E_r} [(1 - \nu_r)Q_2 - \nu_r \sigma_z] \qquad (26)$$

Poisson's ratio of the bar is denoted as ν_r. The axial stress in the bar is required to balance the shear bond stress Q_1. Recalling that Q_1 is taken here to be the average bond stress, the axial stress in the bar at the center of the embedment is approximately:

$$\sigma_z = 2LQ_1/D_b \tag{27}$$

Substituting into Eq. (26) gives:

$$\frac{\delta_b}{D_b} = \frac{1}{2E_r}\left[(1 - \nu_r)Q_2 - \frac{2\nu_r L}{D_b}Q_1\right] \tag{28}$$

The quantity q_2 is the dilation of the bond layer (normalized by the bar diameter). Compatibility requires that this dilation be accommodated by a combination of a decrease in bar diameter and an increase in the diameter of the cavity in the concrete. The decrease in bar diameter is $-\delta_b$ while the increase in the cavity size is $\overline{\delta}_{c1} + \delta_{c2}$. Thus compatibility gives:

$$q_2 = (-\delta_b + .64\ \delta_{c1} + \delta_{c2})/D_b \tag{29}$$

Comparing this expression to Eq. (7) yields

$$H(Q_i) = (-\delta_b + .64\ \delta_{c1} + \delta_{c2})/D_b \tag{30}$$

where δ_b/D_b, δ_{c1}/D_b and δ_{c2}/D_b are given by Eq. (28), Eq. (21), and Eq. (23).

Having an expression for H now permits the analysis of Eligehausen's test as an *ideal* test. The principal approximations in this analysis are: (1) the slip measured at the free end of the bar is approximately the average of q_1, (2) the averages of the stress and deformation quantities satisfy the point plasticity model (i.e., assuming homogeneous conditions over the embedded length), and (3) the expression used for H.

The expression given in Eq. (30) is obviously quite approximate and, thus, the analysis of Eligehausen's tests must be considered as less than exact.

The analysis of Eligehausen's cyclic tests requires only a slight extension of the solution procedure outlined for the *ideal* test under monotonic conditions. Between each plastic segment of a cyclic test there is an elastic phase whose extent is determined by a process similar to that described for the initial elastic behavior; see the description of the *ideal* test. For these subsequent elastic phases, the damage variables are not zero but equal to the values found at the end of the preceding plastic segment.

5.3. Gambarova's Test

The details of the test performed by Gambarova (1989) are shown in Figs. 14 and 15. The length of the bar embedment is 3 bar diameters = 5 lug spacings. The concrete specimen is pre-cracked (splitting crack) with a prescribed crack opening (width). The normal force N required to maintain the selected crack opening (as observed on the surface of the specimen) is measured during the course of the pull-out test.

The sample is not axisymmetric and, thus, again one must deal with circumferential averages of the stresses and deformations. An idealized free body of the transverse forces and stresses acting on one quarter of the cross-section of the sample is shown in Fig. 16 (the shear stress $\tau_{n\theta}$ is assumed to be negligible). Because no information is available concerning the distribution of σ_n, it is approximated as a constant. Equilibrium gives:

$$Q_2 = \sigma_n = -N/(D_b L) \tag{31}$$

Gambarova used the following formula to define a generalized normal stress quantity (for distinction, in this report it will be called σ_{gam}):

$$\sigma_{gam} = (2N)/(\pi D_b L) \tag{32}$$

Comparing these two expressions it is seen that:

$$Q_2 = -\pi\, \sigma_{gam}/2 \tag{33}$$

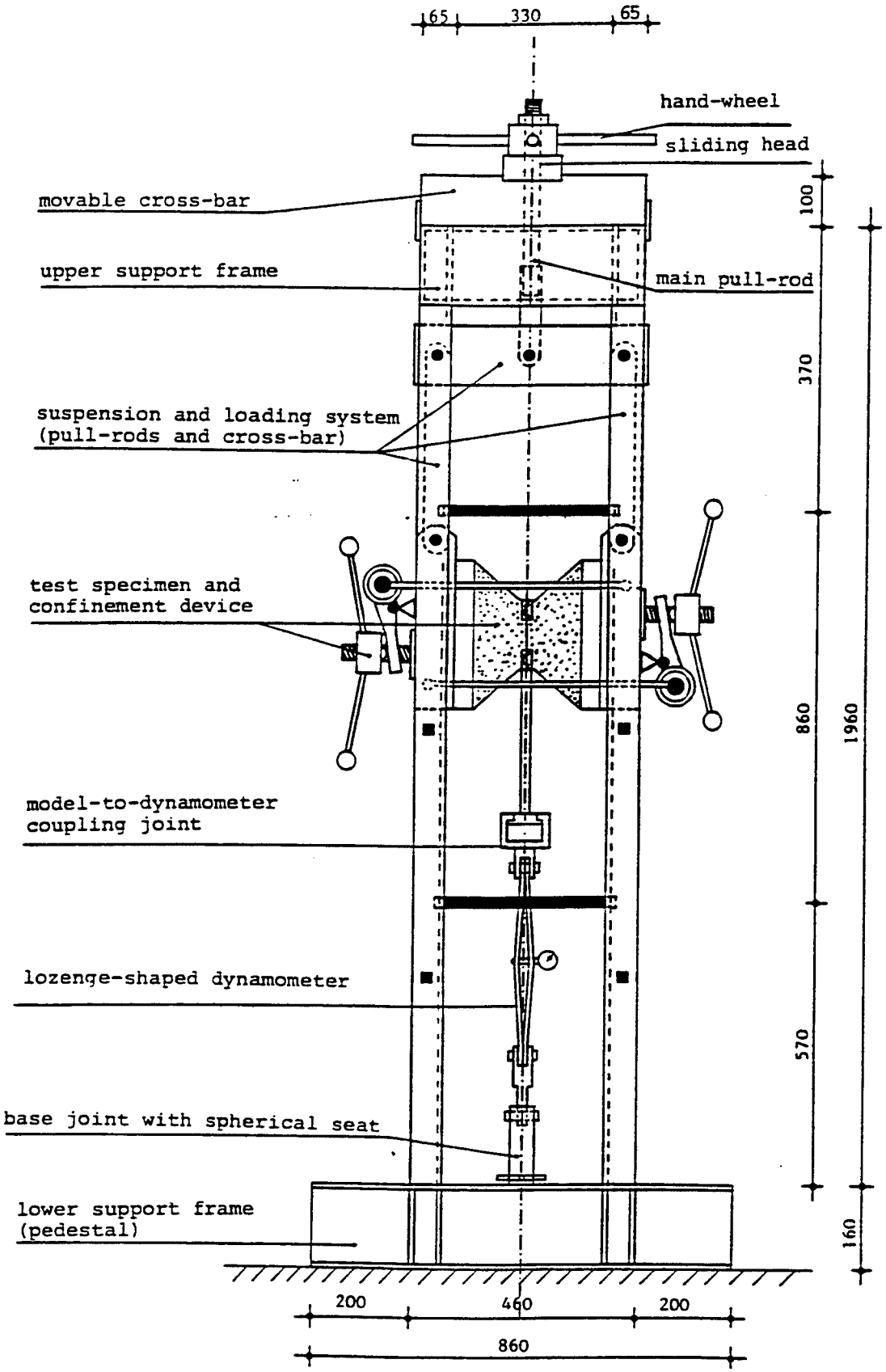

Figure 14. Details of the Testing Machine used by Gambarova (taken from Fig. 8 of Gambarova 1989)

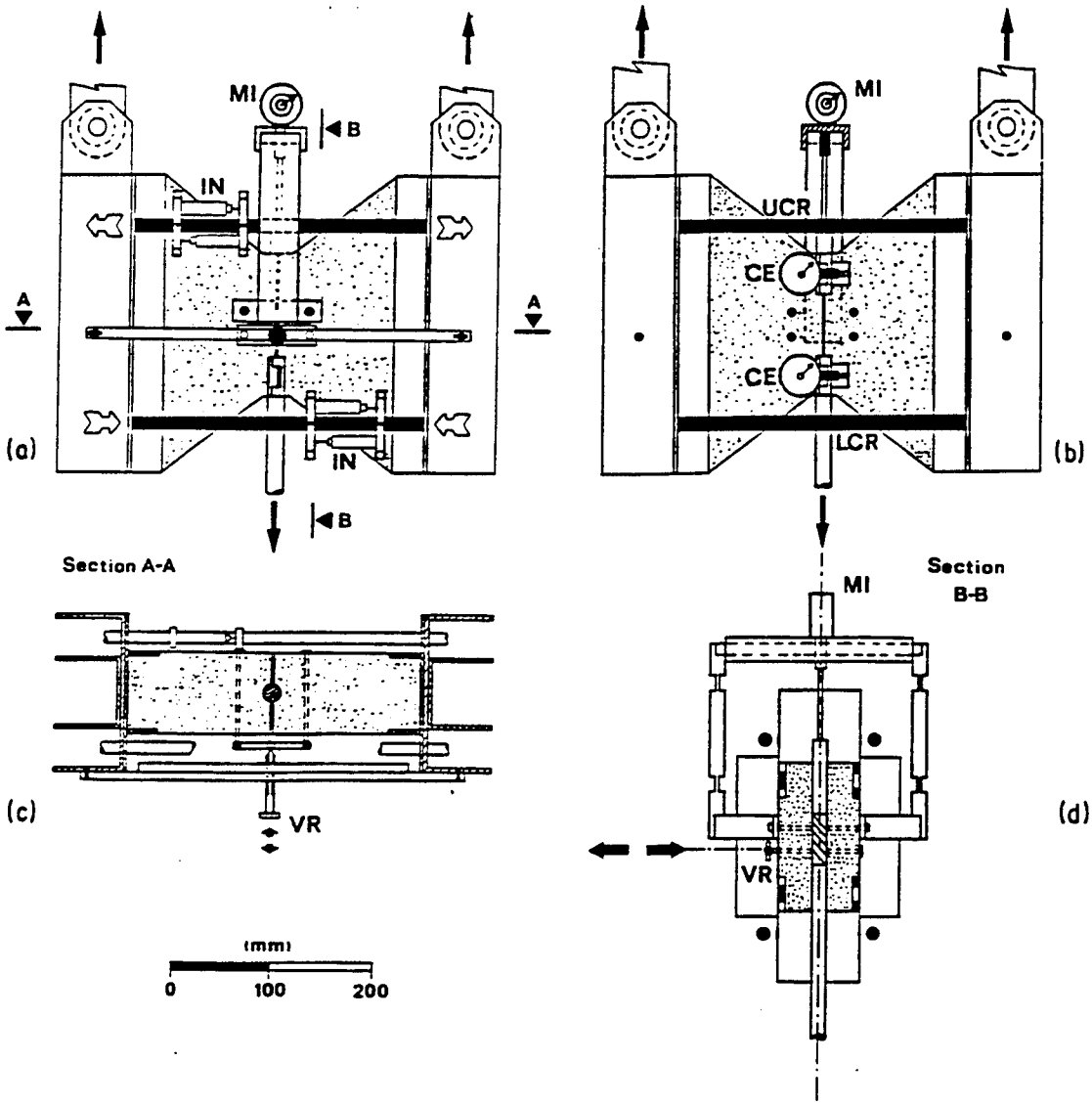

Figure 15. Details of Concrete Sample used by Gambarova (taken from Fig. 9 of Gambarova 1989)

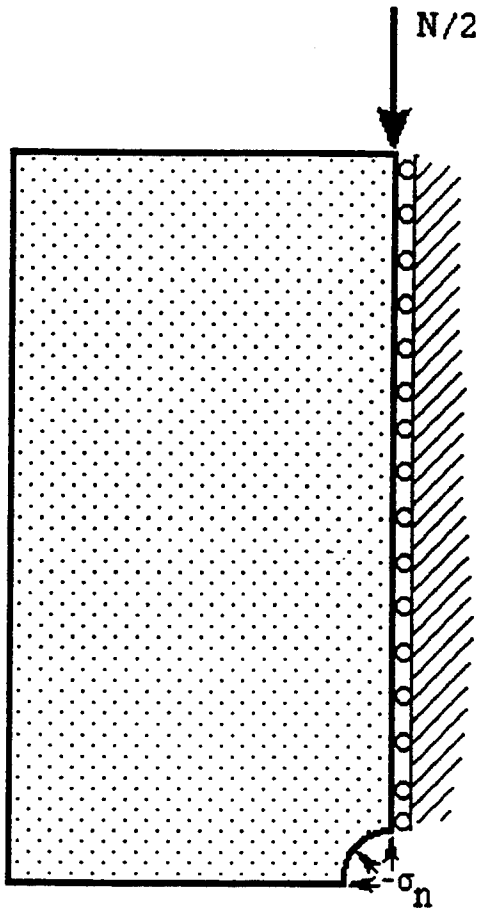

Figure 16. Idealized Free Body of Gambarova's Test Specimen

Again the relative slip between the bar and the concrete was measured at the free end of the bar; this value is taken to be the average value of q_1.

The dilation of the bond zone q_2 is accommodated by the prescribed splitting crack (δ_o), the decrease in diameter of the bar (-δ_b of Eq. 28), and local deformation of the concrete in the vicinity of the bar (δ_{con}). A two-dimensional (plane stress) finite element analysis of one quarter of the cross-section of the concrete (see Fig. 16) was performed. The distribution of the normal bond stress was taken to be a constant, and the concrete was treated as linear elastic ($\nu_c = 0.17$). The average radial growth (δ_{con}) of the cavity was calculated and correlated to the bond stress Q_2 as:

$$\delta_{con} = -.59\ Q_2/E_c \tag{34}$$

The constraint H of Eq. (7) is found by combining all the above effects as:

$$H(Q_i) = (-\delta_b + \delta_{con} + .64\ \delta_o/2)/D_b \tag{35}$$

where δ_b is given by Eq. (28), δ_{con} by Eq. (34) and δ_o is the specified opening of the splitting crack. (Eq. 22 is used in determining the average dilation due to the spitting crack.)

With the exception of Eq. (9), Gambarova's test can now be analyzed as an *ideal* test. Depending upon the nature of the expressions for the damage measures D_i, they may have some initial values D_{i_o} due to the introduction of the splitting crack prior to the beginning of the pull-out test; this will be discussed in more detail.

Finally it is noted that in comparing the model predictions for normal bond stress to the reported values by Gambarova that Eq. (33) is used.

5.4. Rehm's Test

The test specimen is shown in Fig. 17 (see Rehm 1979). For the test of interest here the embedded length was 3 bar diameters = 5 lug spacings. The configuration is initially axisymmetric and will be

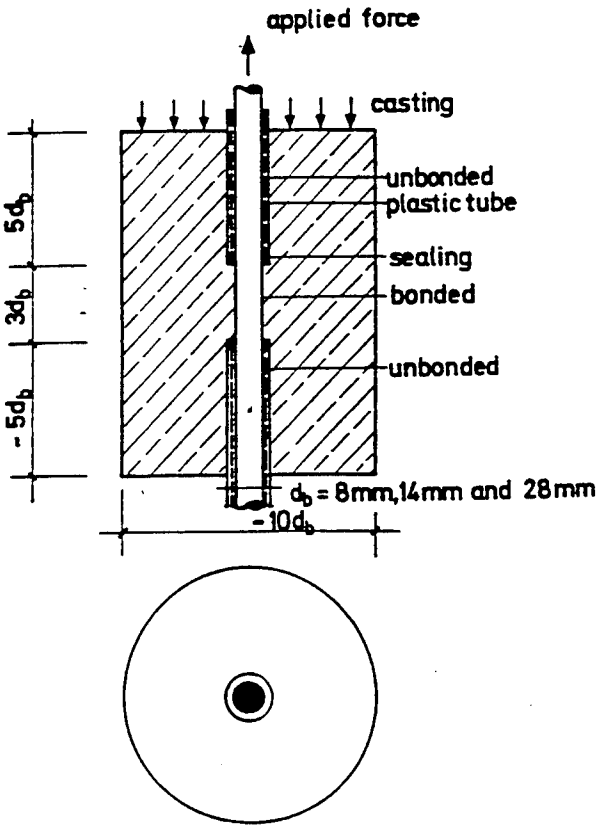

Figure 17. Test Specimen for Rehm's Test
(taken from Fig. 1 of Rehm 1979)

assumed to remain so during the course of the test. (Strictly speaking this would require infinitely many radial cracks to form which only differed in their orientation (θ); the best one can hope for is that a reasonable number form at equal intervals around the circumference.) Thus, the forces and deformations need only be averaged in the length direction. Again the slip is measured at the free end of the configuration.

The identification of the constraint function H, see Eq. (7), requires the determination of the stiffness of the concrete cylinder surrounding the bar. There are two difficulties. Firstly the cylinder is considerably longer than the embedded length of the bar and secondly the cylinder develops radial cracks.

How much of the total length of the cylinder is actually effective in resisting the normal bond stress Q_2 is a question for which no easy answer is available. Before cracking begins, one might perform a simple linear elastic finite element analysis to determine the effective length, however, this is not a straight forward matter once cracking is initiated. Because of the other modeling assumptions used in the consideration of the *ideal* test, it is felt that such a refinement is not justified at this time. Instead it is assumed that the entire length L^* of the concrete cylinder is effective; for a 2-D analysis of this specimen see Cox (1994).

To determine the constraint offered by the concrete an idealized thick walled cylinder of concrete subjected to an internal pressure $\sigma_i = -(L/L^*)Q_2$ is considered, see Fig. 18. The extent of cracking at a given stage of the test is denoted by $X = D_{cr}/D_{cyl}$. The concrete will be treated as an idealized linear elastic material (E_c,ν_c) which cracks when the maximum principal stress reaches the tensile strength (f_t) of concrete. For later use an external pressure (zero for Rehm's test) σ_o will be included in the analysis of the cylinder. The analysis is similar to that developed by Tepfers (1979). The values of E_c and f_t for concrete are correlated with the compressive strength f_c' (see Appendix C).

For the present, considerations are limited to the case where σ_o is a constant and σ_i is an ever increasing function. From manipulation of the classical thick-walled cylinder solution of elasticity, e.g., see Timoshenko (1987), several important results can be easily found.

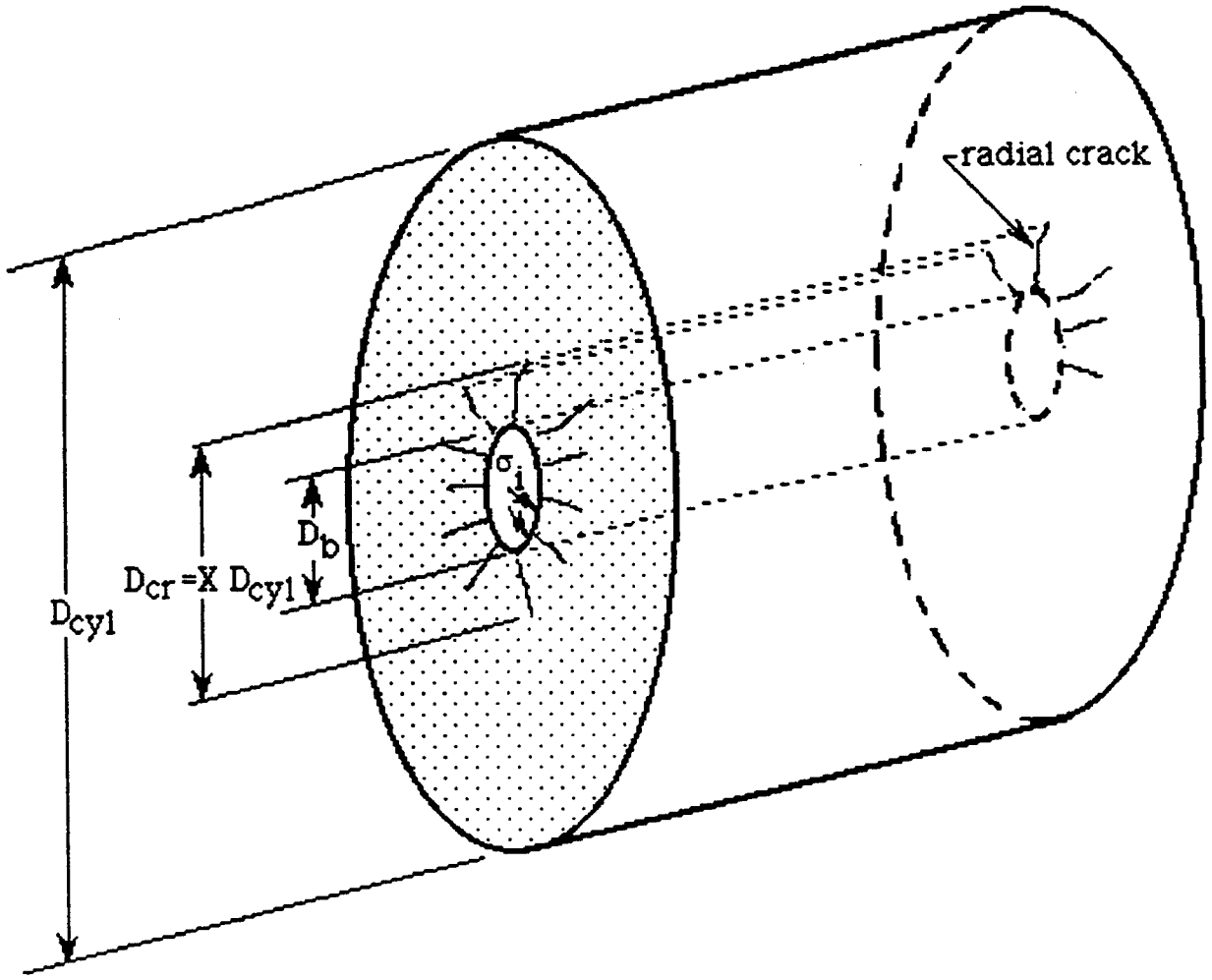

Figure 18. Idealized Thick-Walled Cylinder of Concrete Surrounding the Reinforcing Bar in Rehm's Test

The first cracking of the cylinder occurs when the internal pressure reaches a value σ_i^*, and when the cracking progresses to X^{**} (caused by an internal pressure σ_i^{**}) the situation becomes unstable and cracking proceeds through the wall thickness without any further increase in the internal pressure:

$$\sigma_i^* = f_t \left[\frac{1 - \alpha^2 + 2\beta}{1 + \alpha^2} \right] \tag{36}$$

where

$$\alpha = \frac{D_b}{D_{cyl}} \tag{37}$$

$$\beta = \frac{\sigma_o}{f_t} \tag{38}$$

and

$$X^{**} = \sqrt{-2 - \beta + \sqrt{5 + 6\beta + \beta^2}} \tag{39}$$

$$\sigma_i^{**} = \frac{f_t X^{**}}{\alpha} \left[\frac{1 - X^{**2} + 2\beta}{1 + X^{**2}} \right] \tag{40}$$

For values of σ_i between σ_i^* and σ_i^{**}, the corresponding values of X (extent of cracking) can be found by solving the following equation:

$$\alpha \sigma_i - f_t X \left[\frac{1 - X^2 + 2\beta}{1 + X^2} \right] = 0 \tag{41}$$

The radial displacements of the inner and outer surfaces of the cylinder are denoted by δ_c and δ_{c_o} (note: for σ_i less than σ_i^*, $X = \alpha$):

$$\frac{\delta_c}{D_b} = \frac{1}{2E_c} \left\{ \sigma_i \ln(X/\alpha) + \frac{[(1 - \nu_c)X^2 + (1 + \nu_c)]\sigma_i - 2(X/\alpha)\sigma_o]}{(1 - X^2)} \right\} \tag{42}$$

$$\frac{\delta_{c_o}}{D_b} = \frac{1}{2\alpha E_c} \left\{ \frac{2X^2\sigma_i - [(1 - \nu_c) + (1 + \nu_c)X^2]\sigma_o}{(1 - X^2)} \right\} \tag{43}$$

The first term in the expression for δ_c is due to the radial deformation of the concrete in the cracked zone; this term is derived by requiring that the hoop stress σ_θ be zero in that zone and integrating the equations of elasticity.

The dilation of the bond layer q_2 is accommodated by a change in the bar diameter ($-\delta_b$, see Eq. (28)), and the expansion of the cavity in the concrete (δ_c); hence the constraint is given by:

$$H(Q_i) = (-\delta_b + \delta_c)/D_b \qquad (44)$$

Rehm's test (the external pressure σ_o is zero) now can be treated as an *ideal* test. In actual application it was found convenient to break the analysis into two behavioral regimes, i.e., "pre-crack initiation" and "post-crack initiation". In addition, Q_2 was treated as the specified quantity instead of q_1. In the "pre-crack initiation" regime Q_2 was incremented from 0 to $-\sigma_i^*$, while in the "post-crack initiation" regime it was incremented from $-\sigma_i^*$ to $-\sigma_i^{**}$. A failure to converge in the second regime indicated that $-Q_2$ had reached a maximum value of less than σ_i^{**} and as a result complete cracking of the cylinder did not take place.

5.5. Malvar's Test

Malvar's (1991) test specimen consisted of a reinforcing bar surrounded by a cylinder of concrete. The embedded length is 3.5 bar diameters = 5 lug spacings. The ratio (L^*/L) of the total cylinder length to the embedded length is 1.5 and the diameter of the cylinder of concrete is 3.8 times that of the bar. Unlike Rehm's test an external pressure σ_o is applied to the cylinder.

Malvar's test has two phases. In the first phase an external pressure σ_{o1} is applied and the bar is pulled until the cylinder is split completely through by one or more cracks. At this point the bar is unloaded. A residual slip s_o remains. In the second phase the external pressure is changed to σ_{o2} and the bar is then reloaded and pulled out of the concrete.

The analysis of the first phase follows that given for Rehm's test. It is assumed that the unloading is entirely linear elastic. For the second phase it is assumed that: (1) there is no longer any

constraint on the dilation and (2) the value of the normal bond stress is given by:

$$Q_2 = Q_{2_0} = -\left(\frac{D_{cyl}\, L^*}{D_b\, L}\right) \sigma_{o2} \qquad (45)$$

Eq. (45) takes the place of Eq. (7) and $\Delta Q_2 = 0$ takes the place of Eq. (12).

In the numerical analysis of Malvar's test (the results will be discussed later) two problems arise. The first problem stems from the use of the simple cracking criterion of $\sigma_\theta = f_t$. This criterion does not account for the stress concentration introduced by the longitudinal lug that runs the length of the bar, nor the stress concentration at the tip of an existing crack, nor the inherent scatter in the failure process. Thus, the analysis does not always predict cracking of the concrete cylinder at the proper time. In an attempt to overcoming this problem, in the analysis of the first phase of Malvar's test, when the predicted plastic slip exceeds the measured residual slip value (s_o), the end of the phase is assumed. The second difficulty arises for the higher values of σ_{o2}; during the course of the analysis of the second phase, closure of the splitting crack is predicted. When this occurs a third phase is instigated in which the constraint condition (Eq. 44) is again used, however, f_t is now taken to be zero in recognition of the fact that the cylinder is fully cracked.

6. MODEL IDENTIFICATION AND CALIBRATION

The identification of the two degree of freedom, elastic-plastic model for the bond in reinforced concrete requires determination of [A], Φ, D_k, and g, see Eqs. (1), (3), (4), and (18).

The development of the model was carried out in two steps. Initially only monotonic conditions were considered and then later the model was extended to cyclic situations. The extension of the model to cyclic conditions involved only very minor modification of what had been previously developed for the monotonic case, followed by the addition of certain features unique to cyclic conditions.

In the first of the following two sub-sections the development of the monotonic model will be discussed. The identification of a

given model component (e.g., the yield function) was an evolving process involving may intermediate steps; for the sake of brevity only the final forms of the expressions are reported here (some steps in the development of a slightly more general version of the model are given in detail in Cox 1994). In the second sub-section the extensions necessary for cyclic conditions are described.

6.1. Monotonic Model

6.1.1. Elastic properties

Because the elastic behavior of the bond depends for the most part upon local elastic deformations in the concrete of the bond zone, it is expected that the components of the compliance matrix [A] will be proportional to the reciprocal of the concrete modulus E_c:

$$[A] = [a]/E_c \tag{46}$$

In Malvar's test once the concrete cylinder had cracked the sample was unloaded and then reloaded with the external pressure being held constant (i.e. Q_2 remaining a constant and Q_1 varying). From Eq. (1) the elastic changes in deformation during the reloading process are $\Delta q_1 = (a_{11}/E_c)\,\Delta Q_1$ and $\Delta q_2 = (a_{21}/E_c)\,\Delta Q_1$. Comparing these expressions to Malvar's experimental results gave $a_{11} \approx 25$ and $a_{21} \approx 0.8$, see Cox (1994).

For the unloading portion of Eligehausen's cyclic tests a reasonable value is assumed for ΔQ_2, i.e., $\Delta Q_2 \approx -0.5\,\Delta Q_1$. Using this assumption the unloading curves (Q_1 vs. q_1) reported by Eligehausen gave $a_{11} \approx 7.8 + 0.5\,a_{12}$.

In Gambarova's test the initial splitting crack is held at a constant width, if this is assumed to be the major contribution to q_2, Δq_2 will be zero during the initial portion of the pull-out test. This assumption gives $\Delta Q_1 \approx E_c a_{22}/|a|\,\Delta q_1$ and $\Delta Q_2 \approx -E_c a_{21}/|a|\,\Delta q_1$. Using these expressions to interpret the initial slopes of Gambarova's curves gave $a_{21}/|a| \approx 0.025$ and $a_{22}/|a| \approx 0.05$ (where $|a|$ denotes the determinant of [a]). Combining these two expressions yields $a_{21} \approx 0.5a_{22}$ and $a_{11} \approx 20 + 0.5a_{12}$.

In Appendix D an idealist theoretical argument is given which suggests that:

$$a_{12} = a_{21} \quad \text{and} \quad a_{11} \simeq a_{22} \tag{47}$$

The considerable differences (scatter) in the above experimental and theoretical observations are at least partially due to difficulties in making accurate measurements when the deformations are small (as they are in the elastic range). It is also likely that neglecting of the damage dependency of the elastic properties also contributes to the scatter.

For the remainder of this study it is assumed that [A] is symmetric, $a_{12} = a_{21}$. To begin the calibration process, compliance values of $a_{11} = 10$, $a_{12} = a_{21} = 1$ and $a_{22} = 4.5$ were selected from the range of observed values discussed above. These values were refined as comparisons of model predictions were made with the experimental data base. (It is interesting to note that an unweighted least squared error fit to the above experimental and theoretical observations gives $a_{11} = 19.7$, $a_{12} = 7.7$, $a_{21} = 5.9$ and $a_{22} = 18.1$; if symmetry is enforced $a_{11} = 19.0$, $a_{12} = a_{21} = 5.9$ and $a_{22} = 17.6$).

6.1.2. Yield function

In determining the yield function, ideally as a first step one would like to establish the shape of the initial yield surface by picking yield points from various virgin loading curves and plotting these points in stress space. Unfortunately, for bond between concrete and reinforcement there are two obstacles to this step. The first is the relative scarcity of reinforced concrete bond test data for which the complete bond stress state is known. An even more severe problem is the experimental scatter in the data which renders recognition of the yield point very difficult. The determination of the shape of the evolving yield surface from similar observations for reloading curves is equally difficult. Making simplifying assumptions about the evolution of the yield surface, Cox (1994) analyzed the data of Malvar (1991) establishing the general form of the yield surface presented here. An alternative procedure (which considers the data of Gambarova's tests) to establish bounds on the yield surface is presented in the following.

For Gambarova's test, once the yield surface is reached, it is expected that each remaining stress state (pair of values of Q_1, Q_2) will lie on the evolving yield surface. Of course it is not the initial yield surface as some damage has occurred. Thus, if all such points

are plotted in stress space they must lie within the region swept by the yield surface as it evolves from its initial shape to a shape corresponding to complete damage, see Fig. 19.

For Malvar's tests once the concrete cylinder is completely split the value of Q_2 is known (see Eq. 45), and points (Q_1,Q_2) can be added to the plot of the previous paragraph.

In Fig. 19 the first four curves are Gambarova's data with the numbers in parenthesis giving the openings of the prescribed splitting crack (units of mm). For Malvar's tests (the remaining experimental curves) the first number indicates, once splitting has occurred, the normal bond stress (psi) while the second number indicates the test series.

For the moment the stress values have been normalized with respect to the compressive strength of the concrete f_c' (more will be said on this matter later).

The plotted stress states are a subset of all the stress states which occur on the yield surface during its evolution. The assumed boundaries to this set of points (i.e., two bounding curves) are shown on the graph. The equation of the upper curve is $Q_1/f_c' = \alpha_3(Q_2/f_c')^{\alpha_1}$ where $\alpha_1 = 0.26$ and the equation of the lower curve is $Q_1/f_c' = \alpha_4[1-\exp(-\alpha_2(Q_2/f_c'))]$ where $\alpha_2 = 3$. These bounds suggest the writing of a yield function in the form:

$$|Q_1/f_s| = C(D_k)\{[1-h(D_k)]\,\alpha_3(-Q_2/f_s)^{\alpha_1} + h(D_k)[1-e^{(-\alpha_2(-Q_2/f_s))}]\} \qquad (48)$$

where the normalizing factor f_s will be selected below and the reason for the absolute value signs will be discussed in a following section. In Cox (1994) a more general form that includes "kinematic softening" (i.e., the yield surface translates to the right) is presented.

The blending function $h(D_k)$ is zero for zero damage and reaches a value of one for some large value of damage; the following form (see Fig. 20) was found to yield good results:

$$h(D_1) = \begin{cases} 0 & D_1 < D_{1s} \\ 3[f(D_1)]^2 - 2[f(D_1)]^3 & D_{1s} < D_1 < D_{1e} \\ 1 & D_{1e} < D_1 \end{cases} \qquad (49)$$

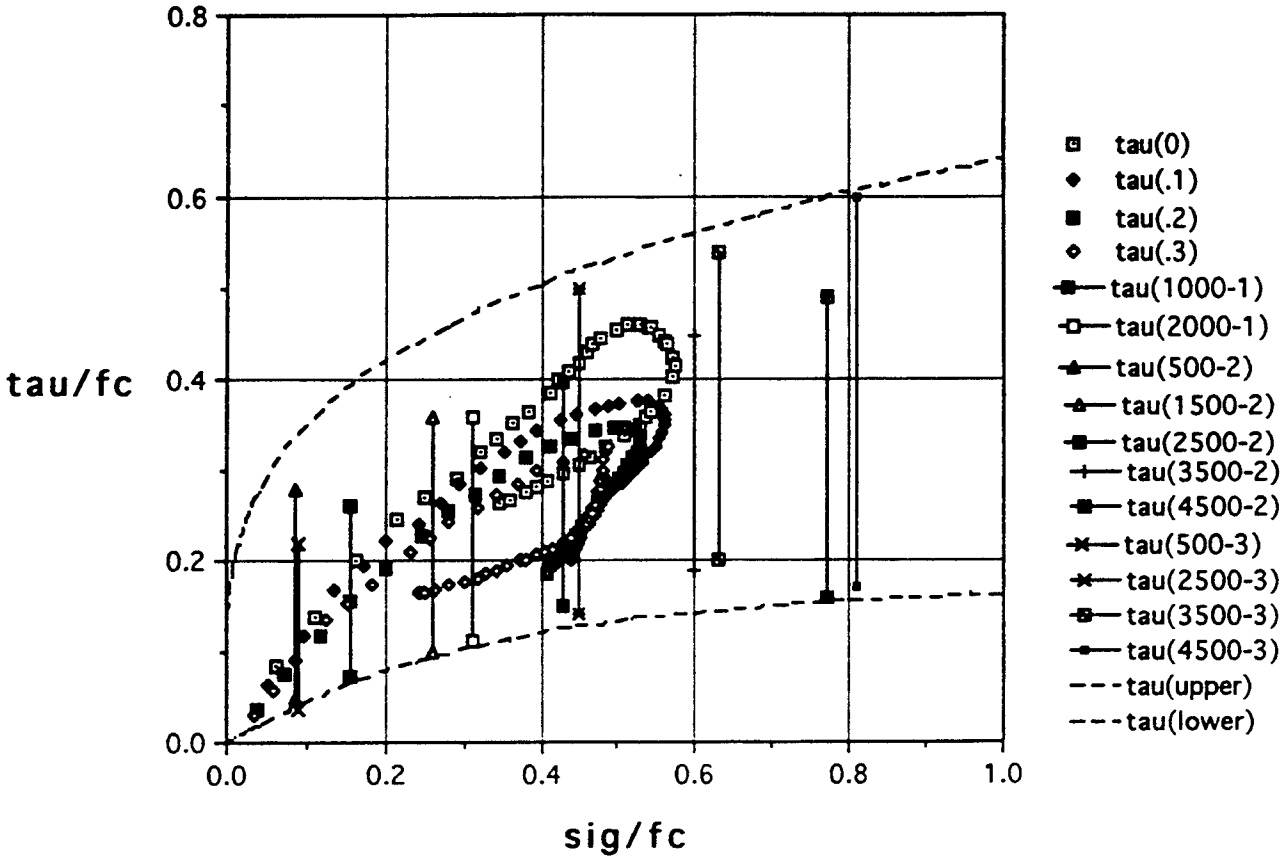

Figure 19. Yield Space

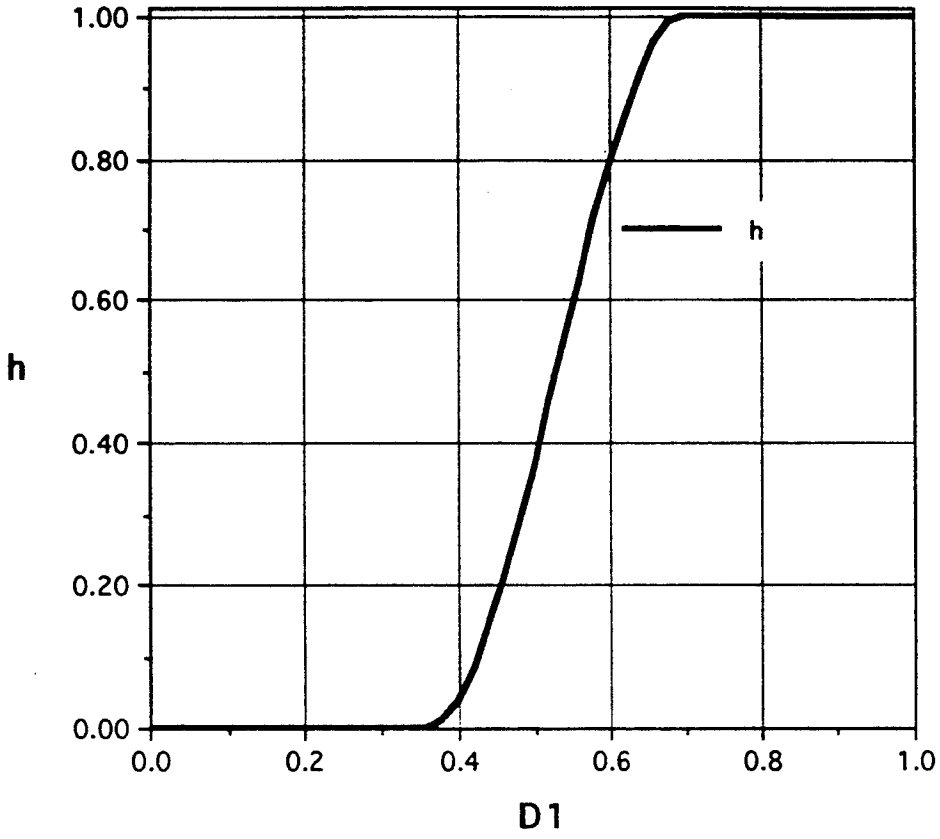

Figure 20. Blending Function for Yield Function

where

$$f(D_1) = (D_1 - D_{1s})/(D_{1e} - D_{1s}). \quad (50)$$

The transition from the power law to the exponential law can perhaps be explained as a transition from yielding by local cracking of the concrete in the bond zone to one of generalized friction (including local crushing as the stress approaches the compressive strength of the concrete).

The damage measure D_1 in Eq. (49) remains to be defined. Eligehausen (1983) used a damage measure based on inelastic work. He, however, points out that such a measure will not be acceptable when a large number of cycles are involved. The present authors were not able to achieve success with his damage measure even for monotonic loading conditions. Eligehausen (1983) also observed that when the slip is equal to one lug spacing that the bond will be completely failed, i.e., the concrete key occupying the space between two successive lugs will have been completely sheared off, thus, effectively providing a free pathway for further sliding inhibited only by frictional behavior. This observation suggests a measure of damage equal to the plastic slip divided by the lug spacing. The best overall results were found if instead of using the lug spacing as measured along the length of the bar, the spacing perpendicular to the lug was used, see Fig. 21:

$$D_1 = (q_{1p}\, D_b)/s_L^* = (q_{1p}\, D_b)/(s_L \cos \phi) \quad (51)$$

The use of s_L^* in place of s_L would suggest that the distance that cracks must propagate in a direction perpendicular to the face of the lug, to reach the next lug, is of fundamental importance.

Returning to a discussion of the yield function (Eq. 48), at a first glance it might appear to be more appropriate to use a simple frictional law $Q_1 = -\mu\, Q_2$ for the yield surface at complete damage rather than the exponential law. However, as the ratio of the normal stress Q_2 to the compressive strength of the concrete f_c' approaches one, something more complicated than simple friction should be expected. An explanation of how local crushing effects the final shape of the yield surface is presented by Cox (1994).

One would like the yield function to be valid for all concrete strengths. When dealing with bond data, there is not complete

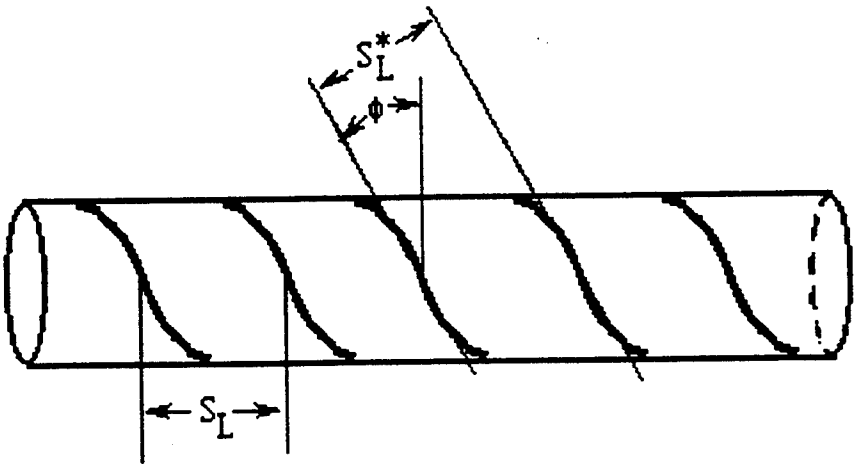

Figure 21. Lug Spacing and Angle

agreement in the literature whether the stresses should be normalized with respect to the compressive strength of concrete f_c' (e.g., see Rehm 1979) or some power of the quantity (e.g., see Menzel 1941, Eligehausen 1983, Shima 1987). Eligehausen (1983) uses $f_c'^{1/2}$ while Shima (1987) uses $f_c'^{2/3}$ for small values of slip and $f_c'^{1/2}$ for large values. An alternative is to use the tensile strength f_t. The tensile strength would seem to be appropriate because bond behavior is thought to be heavily influenced by the formation of cracks in the concrete in the bond zone. In this study, normalization of the stresses in the yield function with respect to f_c', $f_c'^{1/2}$ and f_t were investigated; the value of f_t was found to be the most appropriate. Thus, in Eq. (48) f_s is taken to be f_t. (If f_t is correlated to $f_c'^{2/3}$, as it is in Appendix C, the net effect is to normalize by $f_c'^{2/3}$). When f_t, instead of f_c', is used for f_s the value of α_2 in Eq. (48) becomes 0.26.

The function $C(D_k)$ in Eq. (48) controls the hardening and softening of the yield function as damage progresses. It was found that: (1) C is a function of the damage measure D_1 of Eq. (51) and (2) a dependency on q_2 is also necessary to model the behavior exhibited in Gambarova's tests. Gambarova, in his test series C, performed 4 tests (one repetition each) with different widths (openings) of the prescribed splitting crack. If it is assumed that: (1) C is only a function of D_1, and (2) the plastic slip can be approximated by the total slip, then using Eqs. (33) and (48)-(51) C can be found from Gambarova's experimental data as a function of D_1 (see Fig. 22). The four distinct curves are labeled by the widths δ_o (in mm) of the splitting crack. If C were only a function of D_1 a single curve would have been found. It is obvious that C is also a function of the dilation q_2 (resulting from the presence of the splitting crack). A number of different functional forms for describing the dependence of C on damage and dilation were investigated, the most successful was (an alternative form is given by Chang 1992):

$$C(0) = \alpha_{12} \tag{52}$$

$$dC = [\alpha_4(C_{ub} - C)e^{-\alpha_5 D_1'} - \alpha_6(C - \alpha_{12})e^{-\alpha_7 D_1'}]\, dD_1 \tag{53}$$

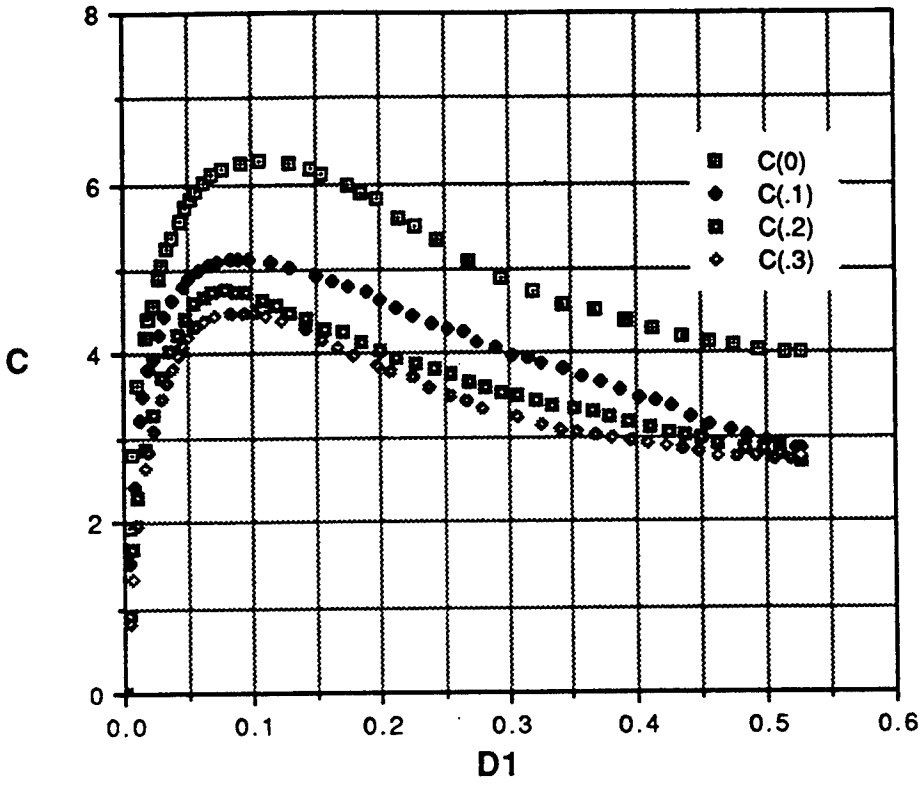

Figure 22. Calculation of C from Gambarova's Data Assuming that it is only a Function of D1

where

$$D_1' = \begin{cases} \dfrac{D_1}{(1 - D_1)} & D_1 < 1 \\ \infty & D_1 \geq 1 \end{cases} \tag{54}$$

$$C_{ub} = \alpha_8 \, [1 + \alpha_9 \, \min(e^{-\alpha_{10} \, q_2}, \alpha_{11})]. \tag{55}$$

Values for the parameters α_4, etc. were initially determine by seeking a reasonable fit to the experimental data of Gambarova (1989); they then were slightly modified by considering the experimental results of Eligehausen (1983): $\alpha_4 = 20$, $\alpha_5 = 4.7$ $\alpha_6 = 5.4$, $\alpha_7 = 0.3$, $\alpha_8 = 4.45$, $\alpha_9 = 0.93$, $\alpha_{10} = 340$, $\alpha_{11} = 0.94$ and $\alpha_{12} = 2.2$. With these coefficients (and the additional assumption that the dominant component of q_2, in Gambarova's test, is the opening of the splitting crack, see Eq. 22) the model was used to predict values of C for Gambarova's tests. The results are compared in Fig. 23 to the values found directly from his experimental data (see the discussion leading to Fig. 22). While the predictions are not perfect they would certainly appear to fall within the range of expected experimental scatter. Because of the several assumptions used in interpreting the experimental results (see description above), at this point no attempt was made to improve the correlation between model and experimental results. Note that some of the experimental data for small values of D_1 may represent pre-yield states and should be ignored.

6.1.3. Non-associative flow rule

The flow rule requires a determination of the function g of Eq. (18). Using Eqs. (1), (2), (7), (33) and (35) and Gambarova's experimental data the function g is calculated and plotted as a function of D_1 in Fig. 24 (the numbers in parentheses are the widths of the prescribed splitting cracks). While a definite trend is shown by the data of Fig. 24, the scatter is very large. This is not unexpected because the determination of g requires taking a derivative (i.e., of q_{2p} with respect to q_{1p}) of the experimental data, an operation which greatly magnifies experimental scatter. The first functional form selected to model the data of Fig. 24 was found to be inadequate to describe the experimental results found by Malvar (1991). Cox (1994) carefully analyzed Malvar's data and proposed an alternative description for g which included a dependence on the confining stress Q_2 (in addition to D_1). A slightly modified form (to

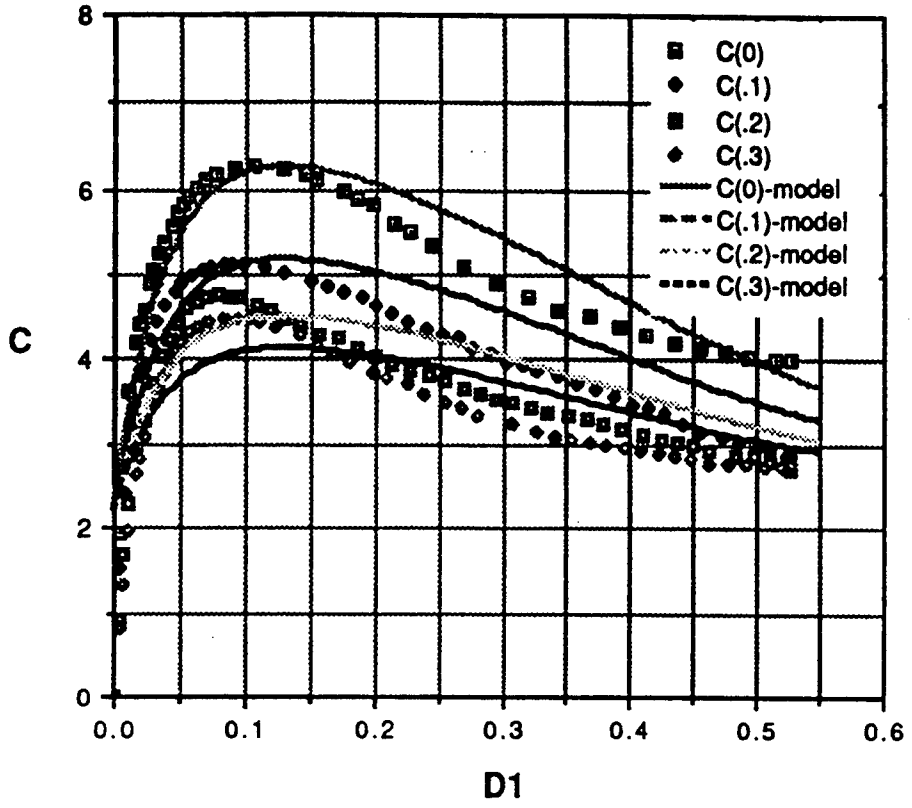

Figure 23. Inclusion of Dilation Effects in Calculation of C, Model vs. Gambarova's Data

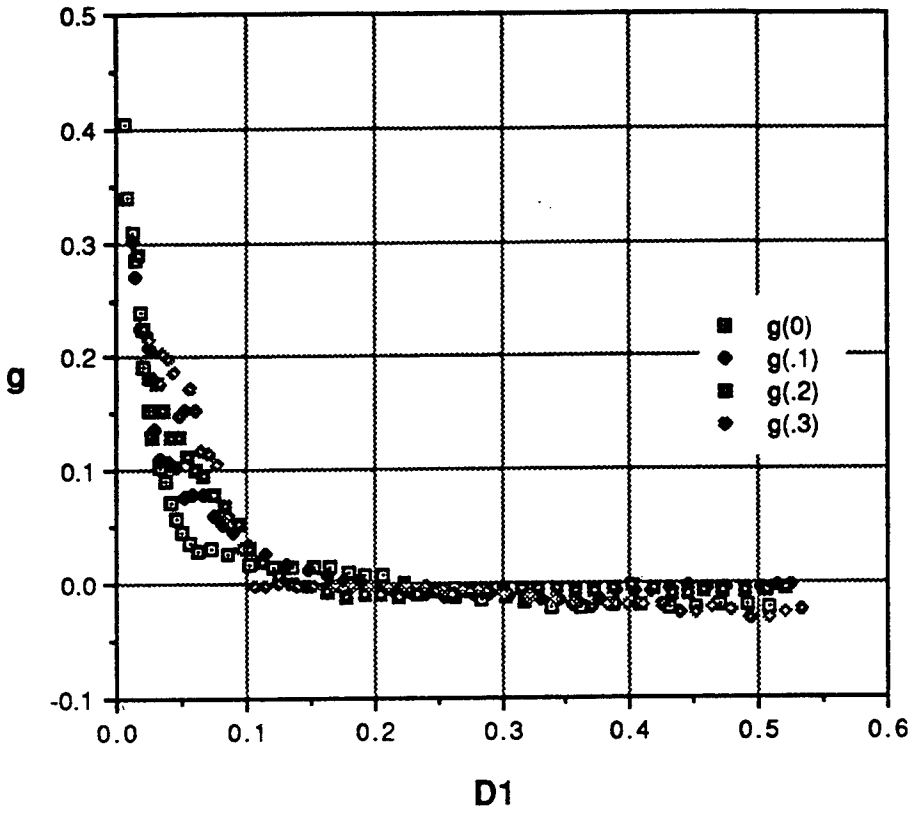

Figure 24. Values of g Derived from Gambarova's Experimental Data

make it more suited for extension to cyclic behavior) of his expression is given below:

$$g = g_o - g_1 + \begin{cases} g_{max} \dfrac{D_1}{d_{max}} & D_1 < d_{max} \\ \dfrac{\beta_1}{v_s} \left(\dfrac{1}{1+\beta_2 D_1 h_s} - \dfrac{1}{1+\beta_2\beta_3} \right) & d_{max} \le D_1 \le \beta_3/h_s \\ 0 & D_1 > \beta_3/h_s \end{cases} \tag{56}$$

where

$$g_1 = \begin{cases} 0 & -Q_2 \le 0 \\ \beta_4 (-Q_2)^{\beta_5} \, | q_{2p} - \beta_6 | & -Q_2 > 0 \end{cases} \tag{57}$$

$$d_{max} = \max \left(\beta_7 - \beta_8 \frac{Q_2}{f_t} , 0 \right) \tag{58}$$

$$h_s = \beta_9 - \beta_{10} \frac{Q_2}{f_t} \tag{59}$$

$$v_s = \beta_{11} - \beta_{12} \frac{Q_2}{f_t} \tag{60}$$

$$g_{max} = \frac{\beta_1}{v_s} \left(\frac{1}{1 + \beta_2 d_{max} h_s} - \frac{1}{1 + \beta_2\beta_3} \right) \tag{61}$$

$$g_o = \begin{cases} \beta_{14} & D_1 < \beta_3/h_s \\ \beta_{14} e^{-\left(\beta_{13} \frac{D_1 - \beta_3 h_s}{1 - \beta_3/h_s} \right)} & \beta_3/h_s \le D_1 \le 1 \\ 0 & D_1 > 1 \end{cases} \tag{62}$$

Using values of $\beta_1 = 0.91$, $\beta_2 = 45$, $\beta_3 = 0.35$, $\beta_4 = 0.5$, $\beta_5 = 0.5$, $\beta_6 = 0.0001$, $\beta_7 = -0.0033$, $\beta_8 = 0.0046$, $\beta_9 = 0.73$, $\beta_{10} = 0.24$, $\beta_{11} = 0.9$, $\beta_{12} = 0.081$, $\beta_{13} = 4$ and $\beta_{14} = 0.019$ values of g were predicted (assuming that the plastic slip can be approximated by the total slip) for Gambarova's tests, two of the curves are shown in Fig. 25.

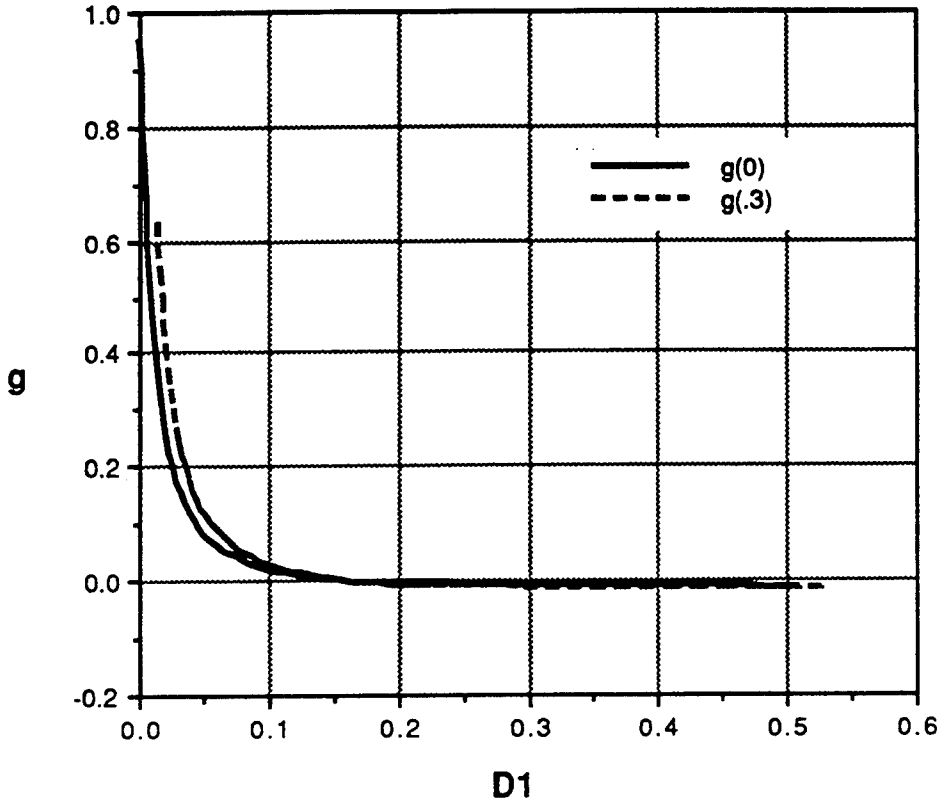

Figure 25. Model for Flow-Rule (Function g) for Gambarova's Test

6.2. Cyclic Behavior

6.2.1. Cyclic elastic properties

Retaining the assumption that the elastic behavior can be approximated as damage independent, only one modification of the monotonic law is required for cyclic conditions. The elastic behavior resulting from the wedging of a lug against the neighboring concrete produces a compression of the bond zone regardless of the direction of the axial movement (q_1) of the reinforcing rod from its initially cast position. The direction of q_1 resulting from a compressive normal bond stress depends upon the sign of the present value of q_1. Both of these phenomena require that the off diagonal terms in the compliance matrix [A] of Eq. (14) to be multiplied by the sign of q_1. When the slip is zero their values are taken to be zero. (Smoother transitions across this discontinuity were investigated, see Cox 1994, however, they did not produce any significant advantages).

6.2.2. Cyclic measure of damage

It is a simple matter to extend the definition of the measure of damage of Eq. (51) to cyclic conditions. The quantity q_{1p} is replaced by the total range of plastic slip experienced in the deformation history:

$$D_1 = (S_{pmax} - S_{pmin})/(s_L \cos \phi) \tag{63}$$

where the extreme values of plastic slip experienced in past positive and negative slip cycles are respectively denoted by S_{pmax} and S_{pmin}. The damage variable D_1 measures the total proportion of the concrete key between neighboring lugs that has been damaged.

6.2.3. Cyclic yield function

For the general case where a combination of loading, unloading, reverse loading and cyclic loading occurs a slight generalization of the monotonic yield function is required. This involves recognizing that the yield function really has two branches, one for positive shear stress (and positive slip) and the other for negative shear stress (and negative slip), i.e., one above the horizontal axis and the other below it, see Fig. 26. The absolute value signs in Eq. (48) were in anticipation of this fact.

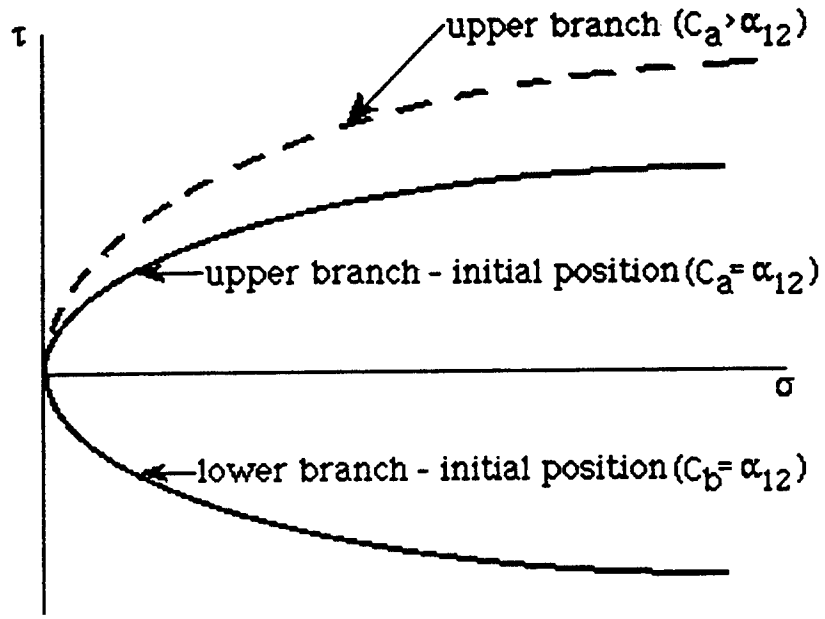

Figure 26. Yield Surface Branches

If the reinforcing bar is horizontal during the casting of the concrete, in the virgin state these two branches will be symmetrically placed about the horizontal axis, however, as plastic deformation occurs they will be permitted to evolve separately, see Fig. 26. When the bar is not horizontal during the casting process, there is experimental evidence (e.g., see Eligehausen 1983 and Mehlhorn 1985) indicating that the two branches would initially not be located symmetrically. Only the case of initial symmetry will be investigated at this time. The values of the hardening functions for the upper (**a**bove) and lower (**b**elow) branches are denoted as C_a and C_b, respectively.

6.2.4. Cyclic hardening function

For monotonic conditions all yielding takes place on one branch of the yield surface; thus, only the corresponding hardening function C evolves. However, when unloading, reverse loading and reloading occur then both branches evolve (i.e., the magnitudes of both C_a and C_b change).

For a virgin bond zone, the initial values of the hardening functions are denoted as $C_a(0) = C_b(0) = \alpha_{12}$ (where the argument of zero denotes zero damage, i.e., the virgin state). It was found, with reasonable accuracy, that the values of the hardening functions for a completely damaged bond can conveniently be taken to be equal to the initial value, i.e., $C_a(\infty) = C_b(\infty) = \alpha_{12}$ (there does not appear to be any rational justification for this condition and with minor modifications to the model it can be relaxed if future evidence should indicate otherwise). The case of complete damage corresponds to the situation when the key of concrete between adjacent lugs has been striped away and frictional behavior is all that remains.

Starting from the virgin state, after some positive plastic slip (a similar argument holds for initial negative plastic slip) has taken place, the value of C_a will have "hardened" to some value greater than α_{12}, see Figs. 26 and 27a. Upon unloading and some small amount of reverse loading, the rib will no longer be bearing against intact concrete but instead will be sliding in the "key-way" that has been plowed through the concrete, see Fig. 27b. This plastic behavior (on the lower branch of the yield surface since the sign of the bond shear stress has reversed) corresponds to frictional behavior, and it is assumed that the value of C_b at this point is α_{12}. In addition, the unloading will have relieved the wedging action which had occurred as positive yielding took place and which had caused the hardening

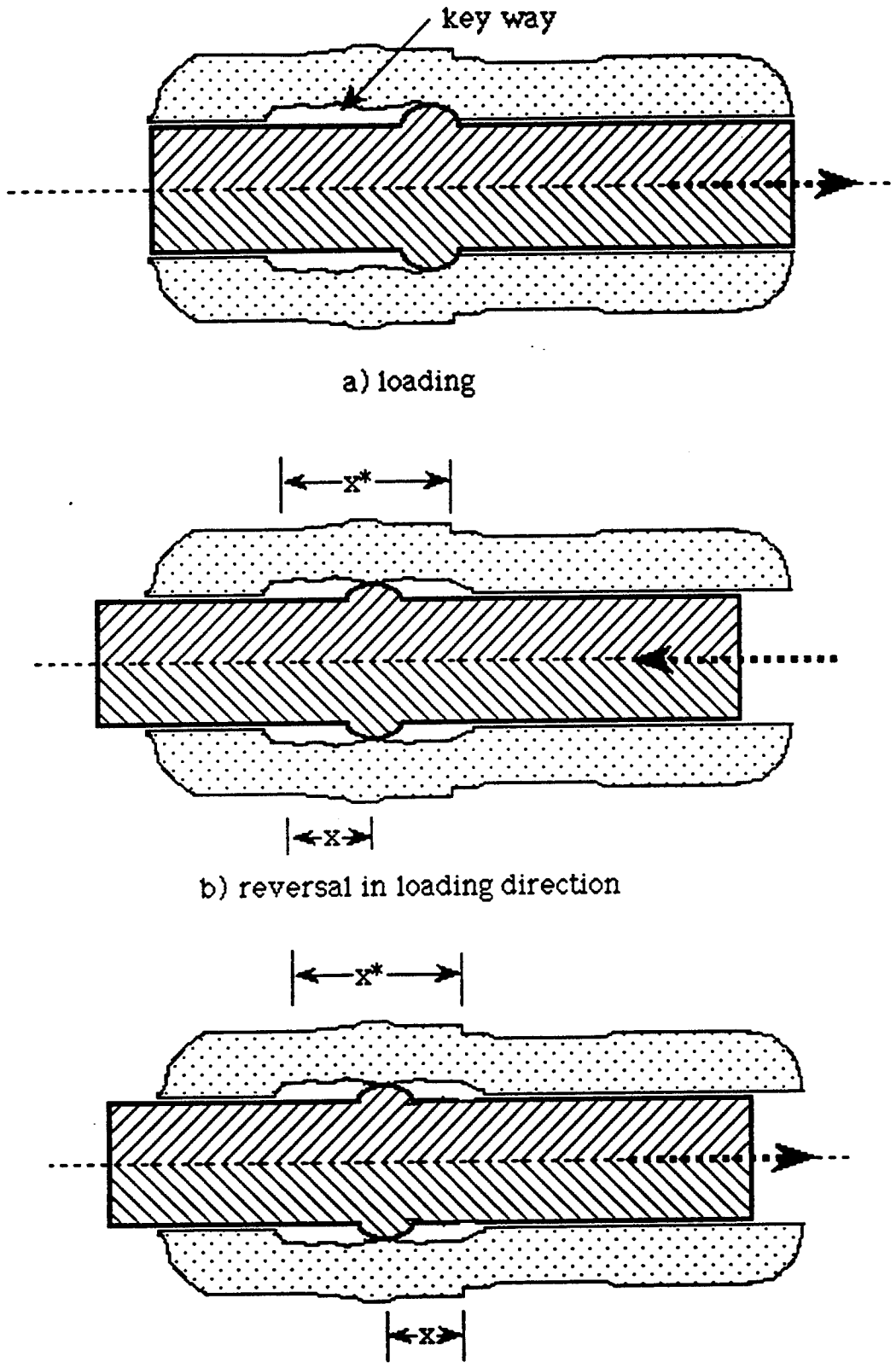

Figure 27. Position of Lug During Loading and Load Reversal

of C_a; so during reverse loading C_a is assumed to very rapidly reduce to the frictional value of α_{12}. Thus, it is assumed that whenever reverse loading is initiated that both C_a and C_b return to the frictional value of α_{12}.

If a second load reversal occurs while the lug is in the key-way, (Fig. 27c) the lug will return to the intact face of concrete that it had previously left. If the cyclic loading excursion away from this face has been small then the lug wedging against this face should very quickly return to its previous configuration, and C_a should rapidly return to almost its previous value. However, if the excursion has been large then particles of concrete from the partially broken concrete key will have lodged between the lug and the concrete face and a more gradual recovery of the hardening of C_a will take place. The behavior suggested by the above physical arguments can be qualitatively observed in the experiments reported by Eligehausen (1983); see for example Figs. 4.26, 4.27a, 4.28, 4.30 and 4.34 of his report (three of these figures are reproduced in Figs. 45, 46 and 47 of this report).

The above qualitative description of the hardening and softening of C_a and C_b are quantitatively described by the following equations (recall that $C_a(0) = \alpha_{12}$ and $C_b(0) = \alpha_{12}$).

a) Complete damage - $(S_{pmax} - S_{pmin}) \geq S_L \cos\phi$, i.e., $D_1 \geq 1$:

$$dC_a = 0 \tag{64}$$

$$dC_b = 0 \tag{65}$$

b) Loading - $(S_{pmax} - S_{pmin}) < S_L \cos\phi$

and (Fig. 27a) $\dot{S}_{pmax} > 0$:

$$dC_a = dC \text{ (Eq. 53 - with } C = C_a) \tag{66}$$

$$dC_b = 0 \tag{67}$$

and $\dot{S}_{pmin} < 0$:

$$dC_a = 0 \tag{68}$$

$$dC_b = dC \quad \text{(Eq. 53 - with } C = C_b\text{)} \tag{69}$$

c) Sliding within the "key-way" (e.g., see Figs. 27b and 27c) which occurs when (i) $S_{pmax} < S_p < S_{pmin}$ or (ii) $S_p = S_{pmax}$, $\dot{S}_p < 0$ or (iii) $S_p = S_{pmin}$, $\dot{S}_p > 0$. Define the following:

$$x^* = S_{pmax} - S_{pmin} \tag{70}$$

$$x = \begin{cases} S_p - S_{pmin} & \dot{S}_p < 0 \quad \text{(Fig. 27b)} \\ S_{pmax} - S_p & \dot{S}_p > 0 \quad \text{(Fig. 27c)} \end{cases} \tag{71}$$

$C_{a_{last}}$ = last value of C_a experienced in positive virgin yield
$C_{b_{last}}$ = last value of C_b experienced in negative virgin yield
Σx_a = the total frictional slip since the last update of $C_{a_{last}}$
Σx_b = the total frictional slip since the last update of $C_{b_{last}}$

$$C^* = \alpha_{12} + (C_{last} - \alpha_{12})e^{-\left(\alpha_{13} \frac{\Sigma x}{S_L \cos\phi}\right)} \tag{72}$$

$$dC = (C^* - C)\left(\frac{1 - e^{-\left(\alpha_{14} \frac{0.5x^* - x}{S_L \cos\phi}\right)}}{1 - e^{-\left(\alpha_{14} \frac{0.5\, x^*}{S_L \cos\phi}\right)}}\right)\left(\frac{|dS_p|}{x}\right) \tag{73}$$

when $\frac{x}{x^*} > 0.5$:

$$C_a = C_b = \alpha_{12} \tag{74}$$

when $\frac{x}{x^*} \leq -0.5$ and $\dot{S}_p < 0$:

$$C_a = \alpha_{12} \tag{75}$$

$$dC_b = dC \text{ (in Eq. 72, } C_{last} = C_{b_{last}} \text{ and } \Sigma x = \Sigma x_b\text{; in Eq. 73, } C = C_b\text{)} \tag{76}$$

when $\frac{x}{x^*} \leq -0.5$ and $\dot{S}_p > 0$:

$$dC_a = dC \text{ (in Eq. 72, } C_{last} = C_{a_{last}}, \text{ etc.)} \tag{77}$$

$$C_b = \alpha_{12} \tag{78}$$

Values of $\alpha_{13} = 3$ and $\alpha_{14} = 100$ were found to yield acceptable results. For $\dot{S}_p > 0$ the ratio $C^*/C_{a_{last}}$ is the proportion of the last value of C_a, in virgin yielding, that will be reached upon reloading. The second and third terms in Eq. (73) both go to 1 as $x \rightarrow 0$ (initiation of reloading) giving $dC = C^* - C$, thus, resulting in $C \rightarrow C^*$. The growth of C_a from α_{12} (the value assigned upon unloading, see Eq. (74)) to C^* upon reloading in the positive direction gives the behavior indicated in Fig. 28 (for example, compare this behavior to Fig. 4.34 in Eligehausen, which is Fig. 45 of this report).

6.2.5. Cyclic flow rule

For general loading conditions the monotonic flow rule must be extended to include the behavior when the lug is sliding within the "key-way" formed by previous damage, i.e., when $S_{pmax} < S_p < S_{pmin}$ (Figs. 27b and 27c). The plastic flow in this region has two components.

One part relates to generalized friction. Generalized friction also occurs for monotonic conditions when the key of concrete between adjacent lugs has been completely damaged, i.e. $D_1 > 1$. From Eq. (56) it is seen that for this situation $g = -g_1$. The form selected for g_1 accounts for the grinding of large particles into fine ones and the gradual approach to a limit dilation of β_6. Assuming that the frictional behavior is the same for both monotonic and cyclic conditions, one component of g, in the "key-way", will be $-g_1$.

A second component relates to the loss of wedging action as the lug backs away from an intact face of concrete ($S_p = S_{pmax}$ and $\dot{S}_p < 0$ or $S_p = S_{pmin}$ and $\dot{S}_p > 0$) and the regaining of it as the lug approaches an intact face of concrete ($S_p \rightarrow S_{pmin}$ or $S_p \rightarrow S_{pmax}$). For the first case the wedging action is lost very abruptly and the existing plastic dilation $q_{2p_{last}}$ is very rapidly reduced to some residual value q^*_{2p} (in

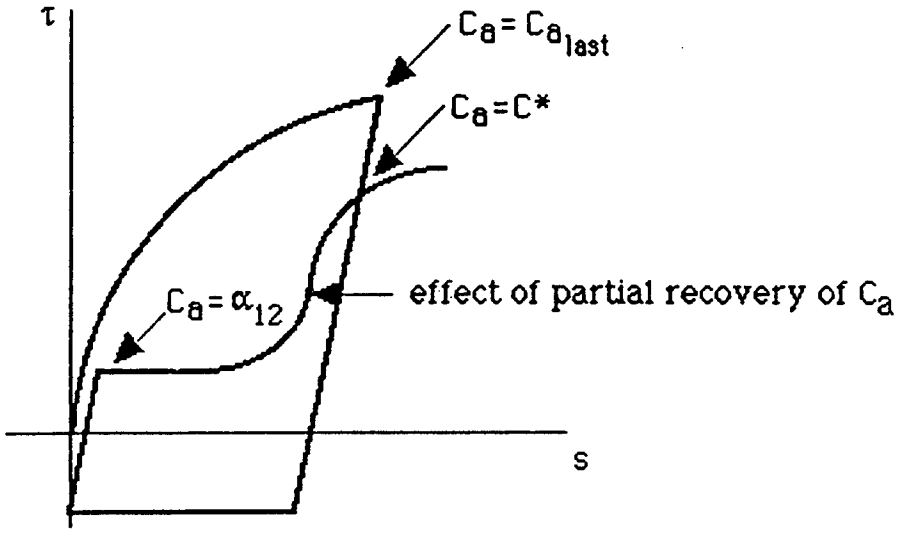

Figure 28. Model Behavior for Reloading

practice it is found to be convenient to spread this process over one solution increment). From Eligehausen's (1983) cyclic data the following expression was found for the residual plastic dilation ($q_{2p_{last}}$ is the plastic dilation just prior to unloading):

$$q^*_{2p} = [\beta_{15} + (1 - \beta_{15})\, e^{-\beta_{16} D_1}]\, q_{2p_{last}} \tag{79}$$

Appropriate values of $\beta_{15} = 0.55$ and $\beta_{16} = 7.3$ were found. As sliding occurs in the "key-way" not only is q_{2p} affected by the grinding action as described by g_1 but so is q^*_{2p}; this is modeled by modifying $q_{2p_{last}}$. Thus, for any given increment of dq_{1p} in the "key-way"

$$dq_{2p_{last}} = -g_1 |dq_{1p}| \tag{80}$$

As the lug approaches an intact face of concrete the wedging action is recovered. This recovery is accomplished by adding to the frictional component of g (i.e., g_1) the following quantity (x and x^* are defined in Fig. 27 and $\beta_{17} = 4$):

$$g^* = \frac{(q_{2p_{last}} - q_{2p})\,(1 - \frac{x}{x^*})^{\beta_{17}}}{(x/D_b)} \tag{81}$$

Note that as $x \to 0$, $(1 - \frac{x}{x^*})^{\beta_{17}} \to 1$, $\frac{dq_{1p}}{x/D_b} \to 1$, therefore $dq_{2p} = g^* dq_{1p} \to q_{2p_{last}} - q_{2p}$ and $q_{2p} + dq_{2p} \to q_{2p_{last}}$ (with the modification of Eq. 80 included).

6.2.6. Determination of model parameters

Most of the analytical functions used to represent the various phenomena associated with the elastic-plastic behavior of reinforced-concrete bond were selected so as to accurately reflect the experimental data. For many of the functions, it is likely that alternative forms can be found that would provide an equally good fit of the experimental data and, thus, should have little effect on the behavior of the model for the range of applications of interest. Two exceptions are the exponential functions used in Eq. (72) and (79). These expressions require that their functional parts have the property that $f(\Delta_1+\Delta_2+\Delta_3+...) = f(\Delta_1)f(\Delta_2)f(\Delta_3)...$, a property that

dictates the use of exponential functions. This condition arises from the requirement that the predicted behaviors for the members of a family of nearly identical cyclic tests should yield essentially identical results. Examples of the two such hypothetical tests are (i) cycling between fixed limits of slip where at the extremes of each cycle the value of specified slip is precisely controlled so as to fall just "ε" short of reaching a virgin yield state and (ii) cycling between fixed limits of slip where in each cycle the extreme values of specified slip are precisely controlled so the bond response does just reach virgin yield. In the first test the values of Σx and q_{2plast} are not reset each cycle while in the second test they are. For the predicted model behavior be essentially the same for these two tests the above indicated property of the exponential function is required.

The model, see Eqs. (46) to (81), would seem to have an excessive number of model parameters (a_{11}, a_{12},...,β_{17}). However, it is anticipated that their values can be calibrated once and for all so all that will remain, for a given application, is to specify the compressive strength of the concrete f_c' (the modulus and tensile strength would be calculated from the correlations of Appendix C, or by using alternative equations available in the literature), the bar diameter D_b, the lug spacing s_L and the lug angle ϕ.

The calibration reported here is for normal weight concrete and standard lug designs on steel bars; the process may have to be repeated for light weight concrete and other unique situations.

The monotonic model first was used (see Section 5: Model Implementation) to analyze the tests of Gambarova (1989) and Malvar (1991) and in the process the preliminary values of the model parameters were revised to produce the best overall fit of their experimental data. The model was then used to analyze the monotonic experiments of Eligehausen (1983), the comparisons were on the whole very good; only slight modifications were made to a couple of the coefficients as a result of these comparisons. The parameters describing the cyclic features of the model were selected solely on the basis of Eligehausen's cyclic test data.

Parameter	Value	Reference Equation	Parameter	Value	Reference Equation
a_{11}	10.0	46	D_{1_s}	0.40	49
a_{12}	0.43	46	D_{1_e}	0.67	49
a_{21}	0.43	46	β_1	0.80	56
a_{22}	14.3	46	β_2	45.0	56
α_1	0.26	48	β_3	0.35	56
α_2	0.26	48	β_4	0.50	57
α_3	0.53	48	β_5	0.50	57
α_4	30.0	53	β_6	0.0001	57
α_5	4.0	53	β_7	-0.0033	58
α_6	9.3	53	β_8	0.0046	58
α_7	0.50	53	β_9	0.73	59
α_8	4.5	55	β_{10}	0.24	59
α_9	0.93	55	β_{11}	0.90	60
α_{10}	200.0	55	β_{12}	0.081	60
α_{11}	0.94	55	β_{13}	4.0	62
α_{12}	2.2	52	β_{14}	0.0186	62
α_{13}	3.0	72	β_{15}	0.55	79
α_{14}	100.0	73	β_{16}	14.0	79
			β_{17}	4.0	81

Table 1. Model Parameters for Normal Weight Concrete and Standard Steel Bar Designs

Table 1 gives the final results for the model parameters as determined from the calibration process. The values of some parameters, such as α_2, have changed by an order of magnitude from the values first used because f_t not f_c' is now used for f_s in Eq. 48). All results reported in the following sections were obtained using these values.

7. COMPARISONS TO EXPERIMENTAL DATA

In this section comparisons are made between model predictions and the experimental results of several investigators. Where possible an indication of the scatter in the experimental data is given. For those cases where no data concerning scatter is available, the reader is referred to the general comments concerning uncertainties in Section 3.2.

As noted in the last section, the model parameters were determined from an analysis of the results of Gambarova (1989) and Malvar (1991) with some consideration given to the data of Eligehausen (1983). Thus, most of the comparisons given in this section can not be taken as true validation tests but rather serve as a demonstration of the ability of the model to capture the salient features of bond behavior between concrete and reinforcement under a wide variety of test conditions.

In the figures which follow, experimental results are given by discrete points and model predictions by curves.

7.1. Gambarova's Data

The bond model was used in the prediction of the results of Gambarova's (1989) tests; the analysis is described in Section 5.3. To that description must be added an account of how the prescribed splitting crack was modeled.

The induced splitting crack slightly separates the concrete from the bar and, thus, when the bar is initially pulled some time elapses before any bond stresses are generated. This behavior is treated as yielding at a zero stress state, see Fig. 19. Using Eqs. (17), (18) and (56) the initial value of q_{1p} which corresponds to the q_{2p} resulting from the splitting crack (see Eq. 22) is found. This process initializes the values of D_1 and C (see Eqs. 51, 52 and 53). The analysis then proceeds as described in Section 5.3.

Figures 29 and 30 compare the model predictions (curves) to the digitized data taken from Gambarova (1989) for his series C tests. The numbers in parenthesis refer to the width (in mm) of the prescribed splitting crack. Gambarova's normal bond stress has been scaled using Eq. (33) so that it could be directly compared to the predictions of the model. The predicted data has been shifted to the

left as did Gambarova in constructing his graphs, i.e., shifted by the amount of slip that preceded the development of any appreciable bond stress.

In light of the expected uncertainties in both the experimental data and the predicted results (due to modeling Gambarova's test as an "ideal" test), the agreement is satisfactory particularly for the case where the value of the splitting crack is zero. The disagreement in the region of small slips, for the case of an initially open splitting crack, may be due to the use of constant elastic properties instead of damage dependent ones. The disagreement is not judged to be a significant problem because the existence of an open splitting crack prior to loading is relatively rare in practice.

In the plateau region of the normal stress curves, the experimental data variations do not appear to follow a consistent pattern. Gambarova recognized this problem, and his model - like ours - showed: (1) "smooth" softening behavior, and (2) decreased normal stress with increased splitting crack width.

7.2. Malvar's Data

Figures 31 through 35 compare the model predictions (based on the analysis of Section 5.5) of bond stress vs. slip to experimental results. The discrete points are taken from experimental data provided by Malvar (1991), and the solid and dashed curves are the model predictions. The numbers reported in parentheses are the pressures at the bar level assuming that none of the external pressure is carried by hoop stress (i.e., assuming the cylinder is completely cracked and the cracks are open). The actual magnitudes of the applied external pressure are $(D_b/D_{cyl})(L/L^*)$ times the reported numbers; where D_b is the bar diameter, D_{cyl} is the external diameter of the test cylinder, L^* is the length of the test cylinder, and L is the bonded length of the bar.

Each figure with the exception of Fig. 32 reports two sets of results, series #2 and #3 (excluding the series #3 test at1500). The two series differ slightly in concrete strength (f'_{c_2} = 40.2 N/mm^2 and f'_{c_3} = 38.7 N/mm^2) and significantly in lug characteristics ($\phi_2 = 22^o$, $\phi_3 = 0^o$). In addition, for the 2500, 3500 and 4500 psi tests of series #3, the initial pressure was 500 psi; once the cylinder cracked it was unloaded and then the external pressure was increased until the desired level was reached. The model's bond-slip behavior is not

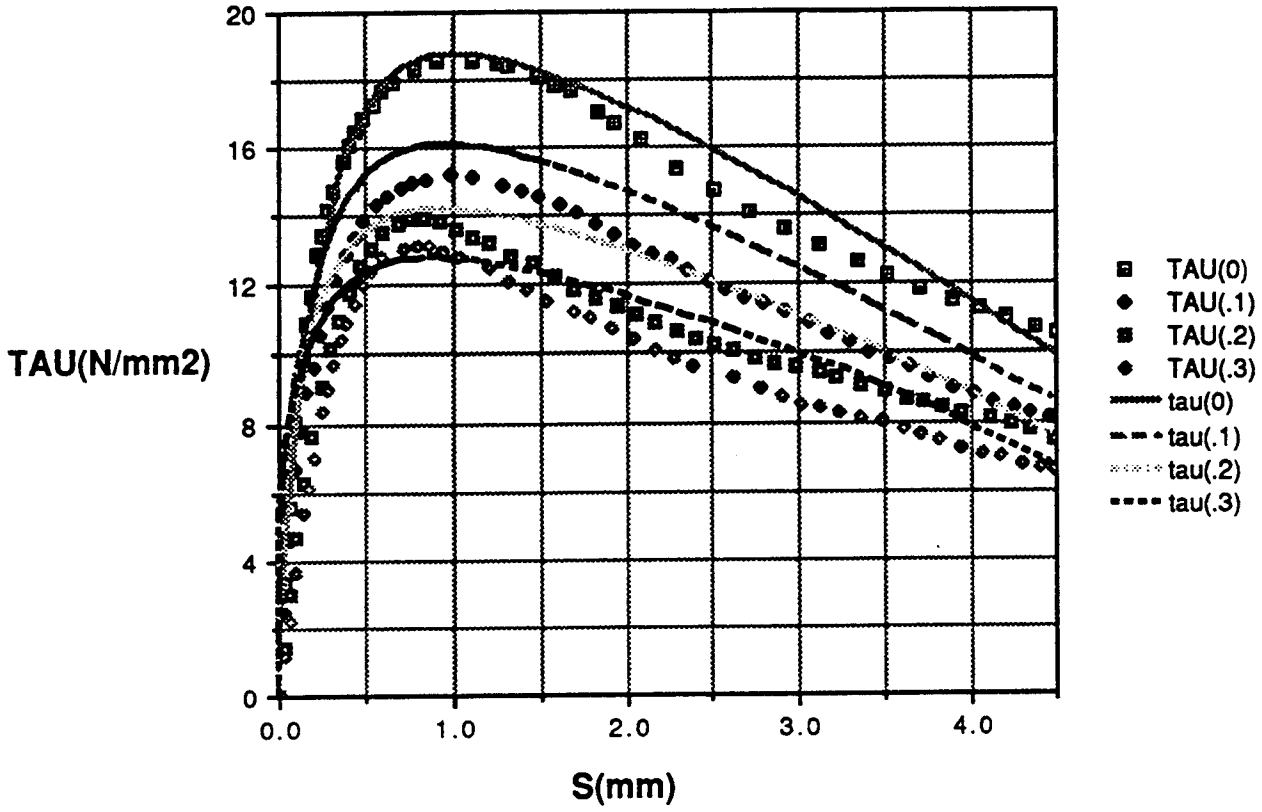

Figure 29. Model Predictions for Shear Bond Stress vs. Slip - Gambarova's Test

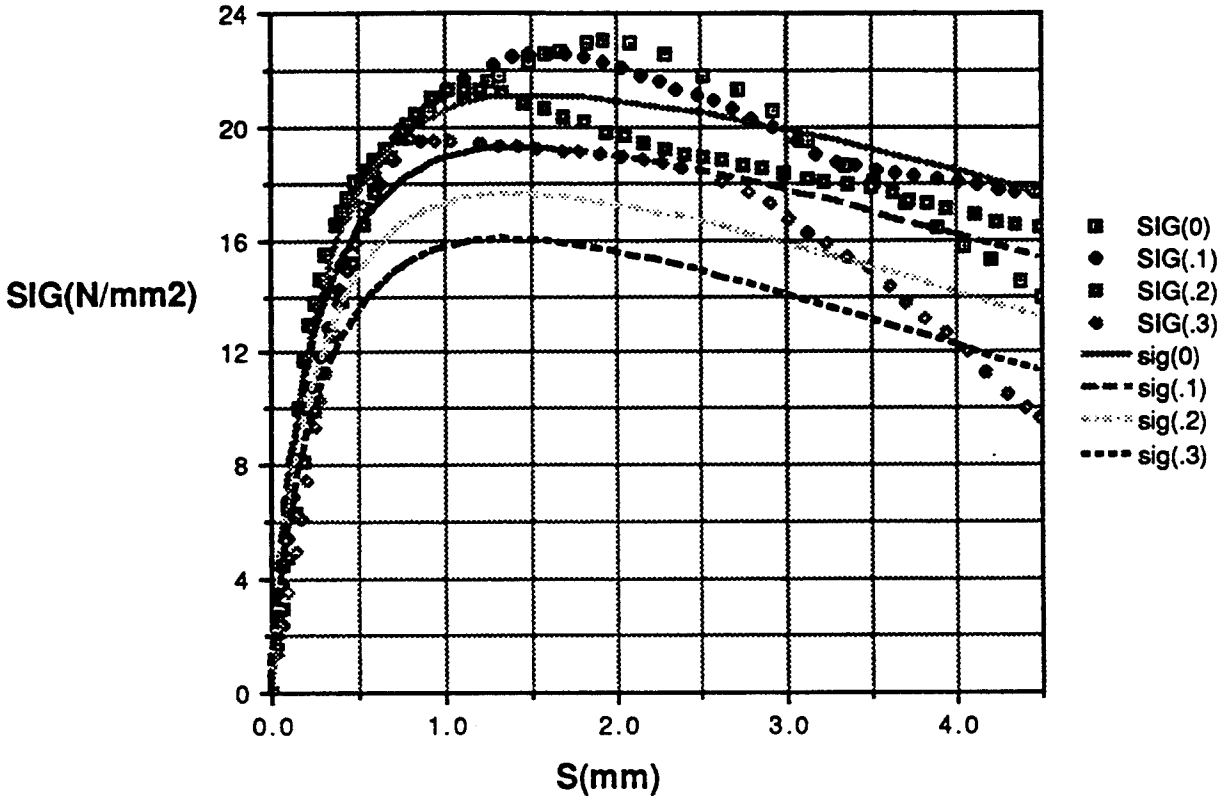

Figure 30. Model Predictions for the Normal Bond Stress vs. Slip - Gambarova's Tests

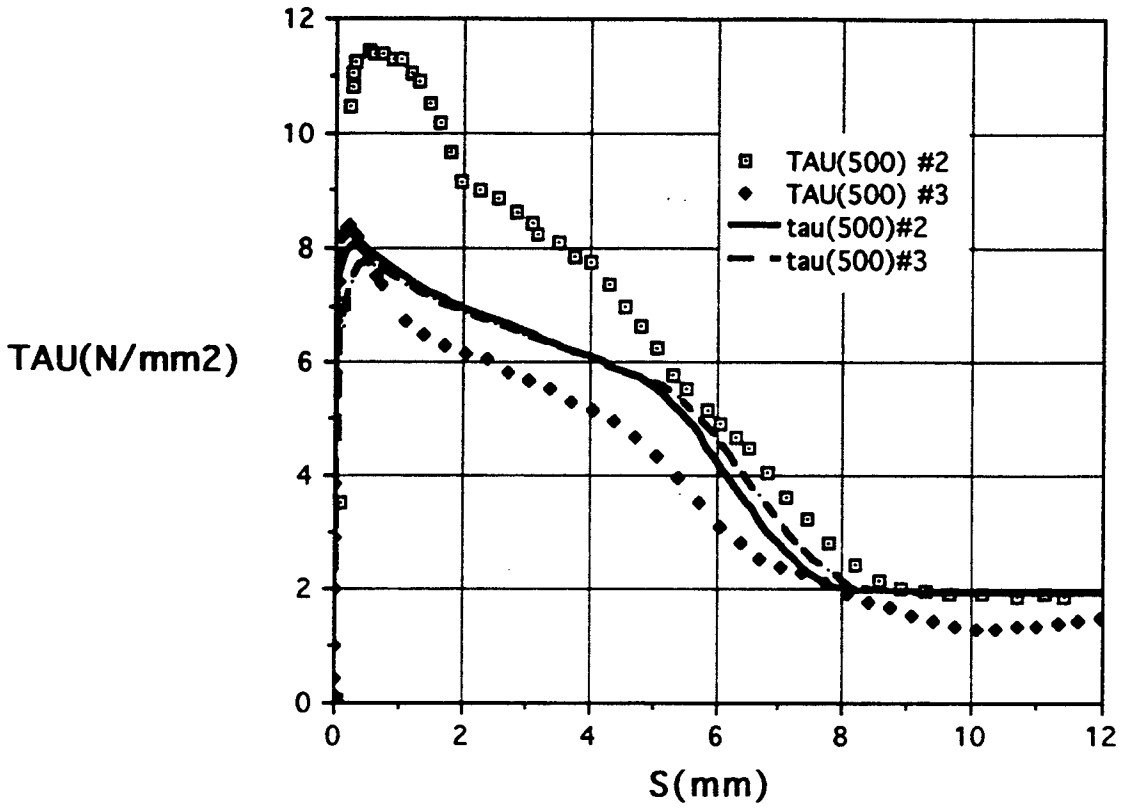

Figure 31. Model Predictions of Bond Stress vs. Slip - Malvar's Test 500 psi Level

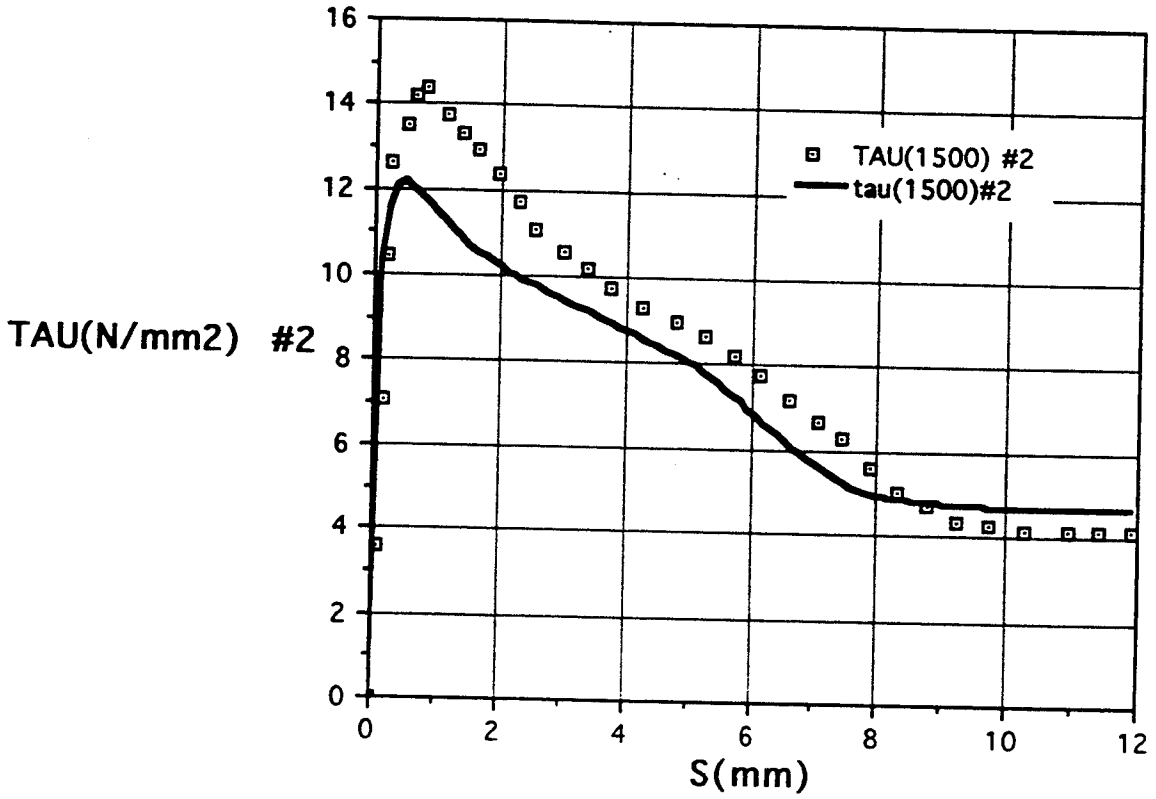

Figure 32. Model Predictions of Bond Stress vs. Slip - Malvar's Test 1500 psi Level

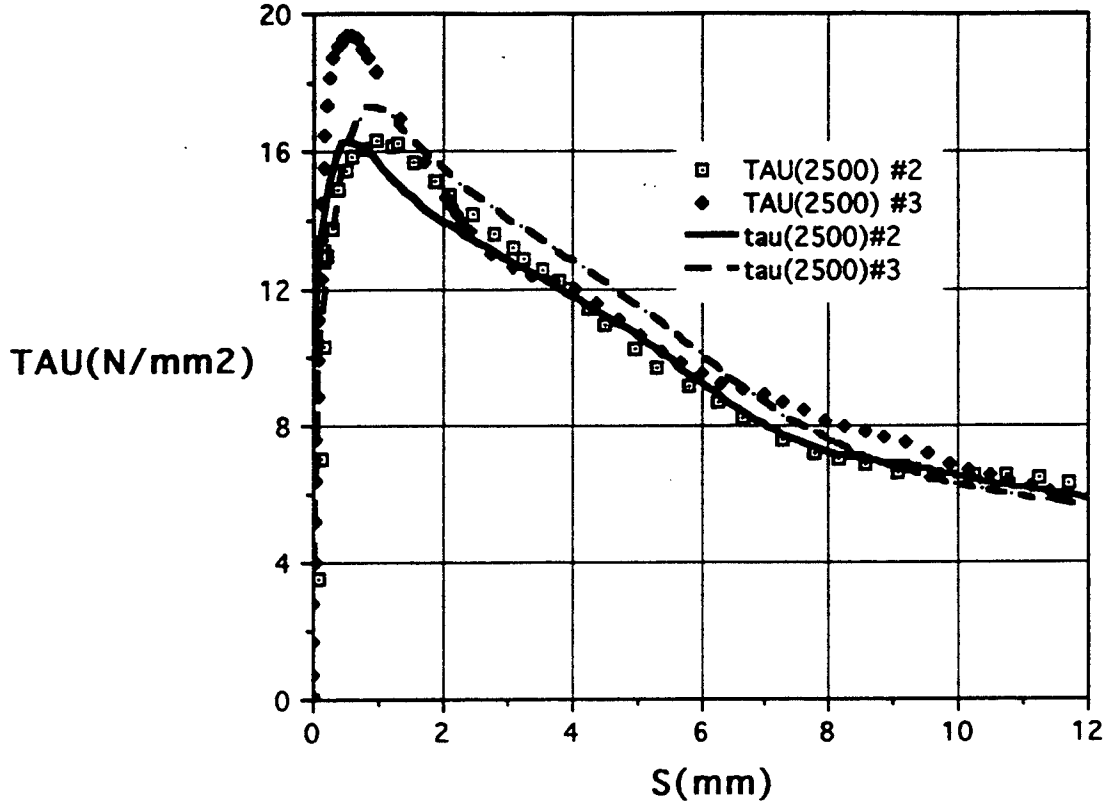

Figure 33. Model Predictions of Bond Stress vs. Slip - Malvar's Test 2500 psi Level

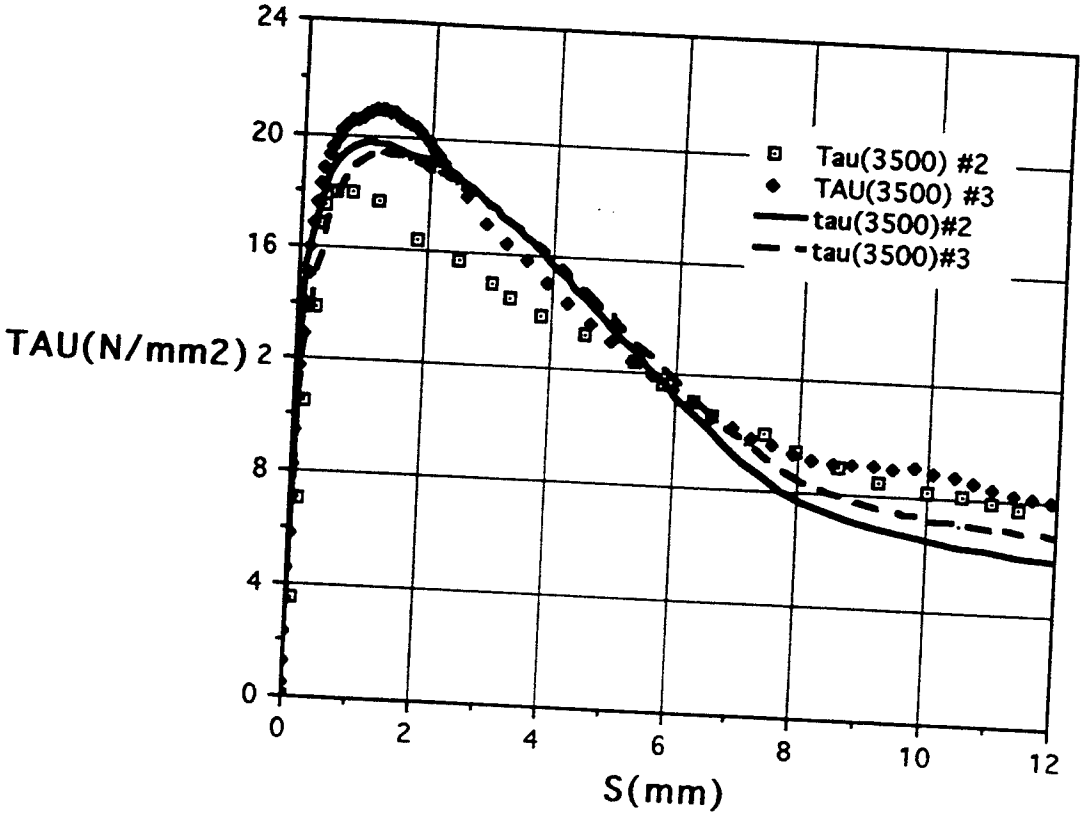

Figure 34. Model Predictions of Bond Stress vs. Slip - Malvar's Test 3500 psi Level

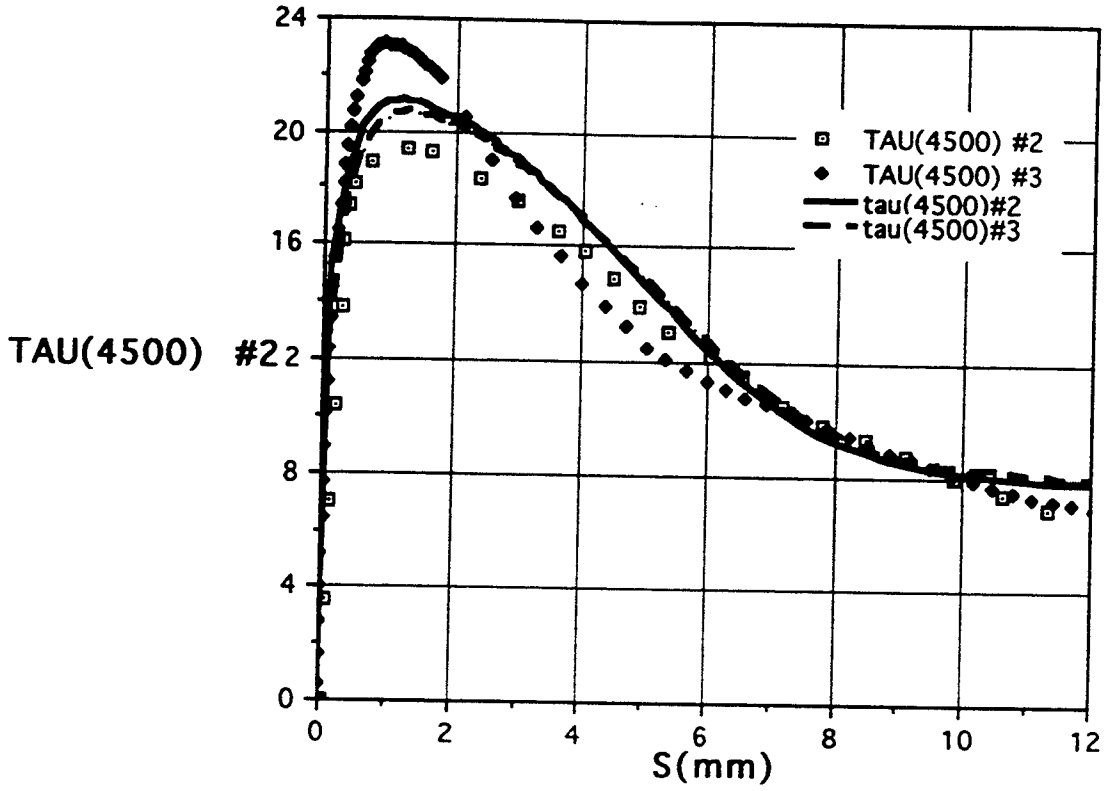

Figure 35. Model Predictions of Bond Stress vs. Slip - Malvar's Test 4500 psi Level

very sensitive to the variations in the test series. The experimental data indicates the bars used in series #3 typically reach higher bond stresses (the exception being the 500 psi test where scatter is typically greater with the more brittle response). Since no measure of experimental scatter is available for this data (i.e., using the same lug configurations) no attempt was made adjust the model for this trend. The agreement between the model predictions and the experimental results is quite acceptable. The model results typically fall between the results of the two test series (at their peaks) and are likely to fall within the range of experimental scatter of each series of tests.

In additional to bond stress, Malvar reports the average radial growth of the outside of the cylinder. He stated that due to experimental problems the validity of the recorded values for the series #2 tests at the 500 and 1500 psi levels is questionable. From the model analysis the radial dilation, q_2, of the bond zone is determined. This quantity is obviously related to the external growth of the cylinder. When the cracks are open it differs only by the radial compression of the concrete between the bond zone and the external surface of the concrete cylinder, however, when the cracks are closed or partially closed the relationship is not simple. Instead of attempting to predict the total growth of the external surface of the cylinder only the bond zone dilation is reported here.

The dilation (in mm) given by Malvar's experimental data and the model predictions are compared in Figs. 36-40. Because the splitting cracks may have been partially closed during the reloading process and this condition is difficult to model accurately, only predictions of dilation are given once the reloading is complete. Although the response varies significantly between the two test series, it appears the model yields good qualitative agreement and reasonable quantitative agreement with the experimental results. In comparing the results consider that the magnitude of radial dilations is very small (~0.03 to 0.5 mm) and thus are the most difficult quantity to measure in these experiments. In addition there has been no measure of experimental scatter.

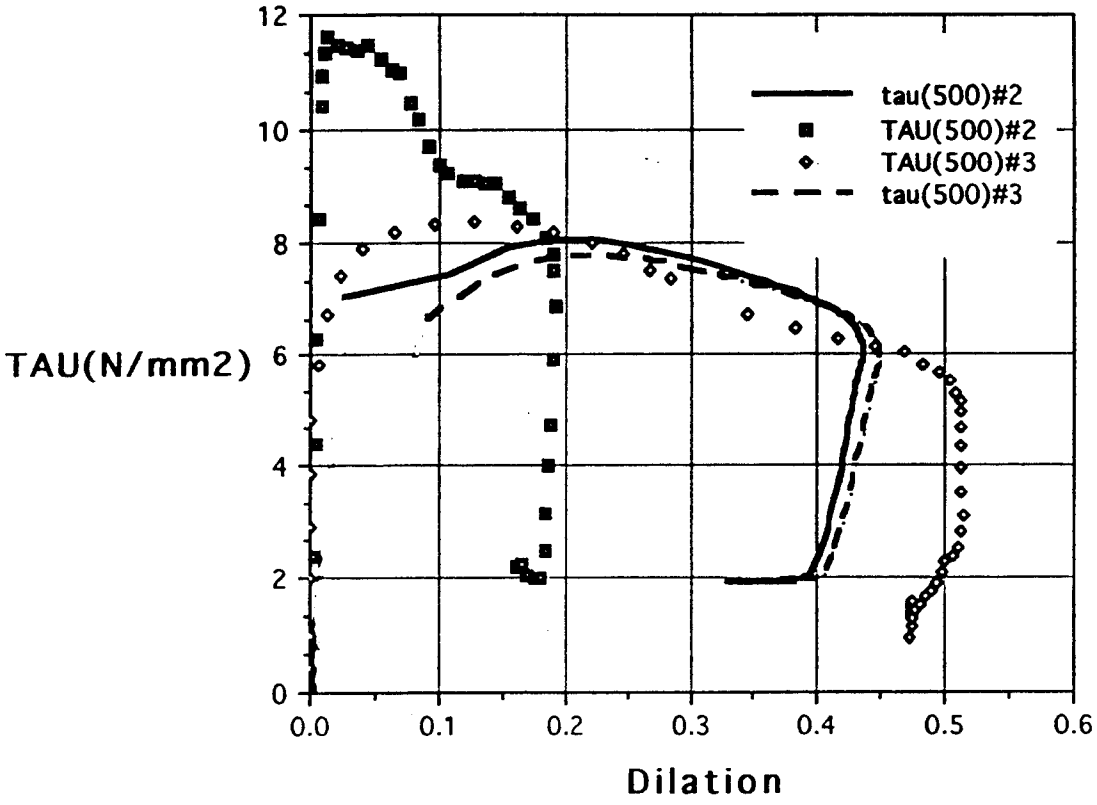

Figure 36. Model Predictions of Bond Stress vs. Dilation - Malvar's Test 500 psi Level

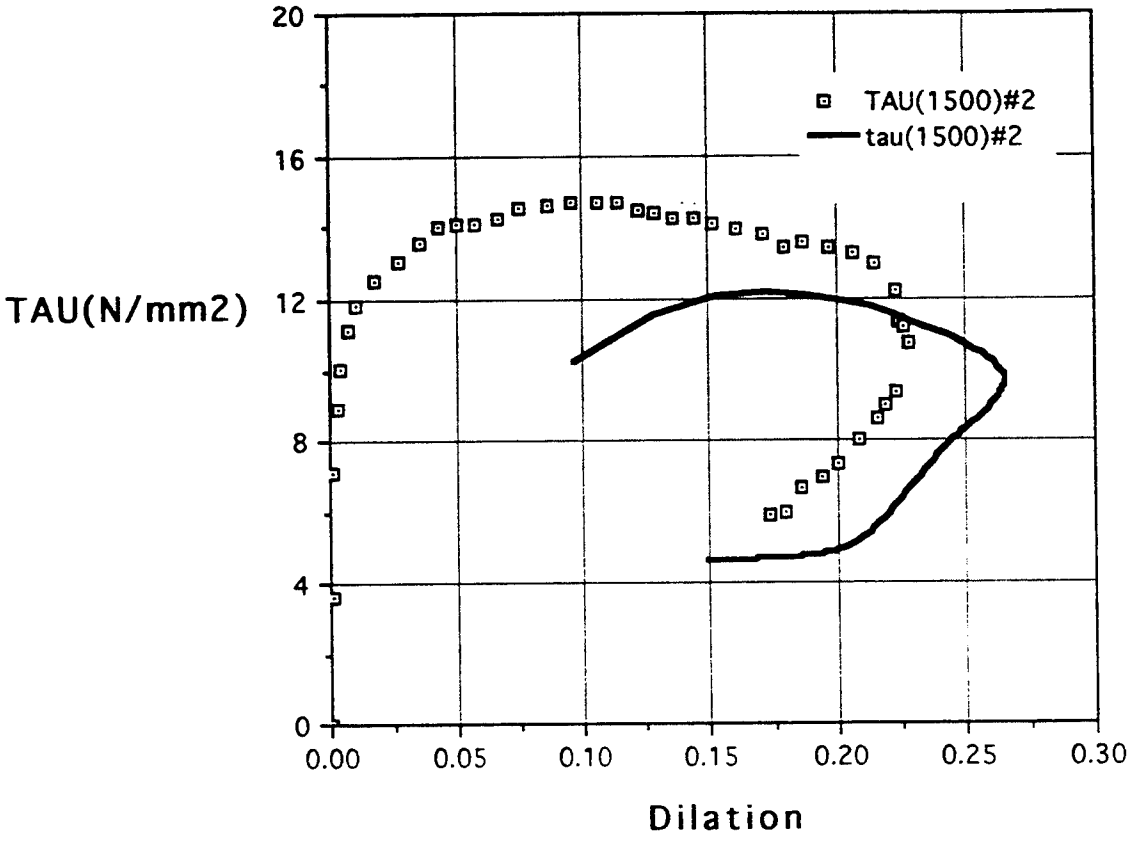

Figure 37. Model Predictions of Bond Stress vs. Dilation - Malvar's Test 1500 psi Level

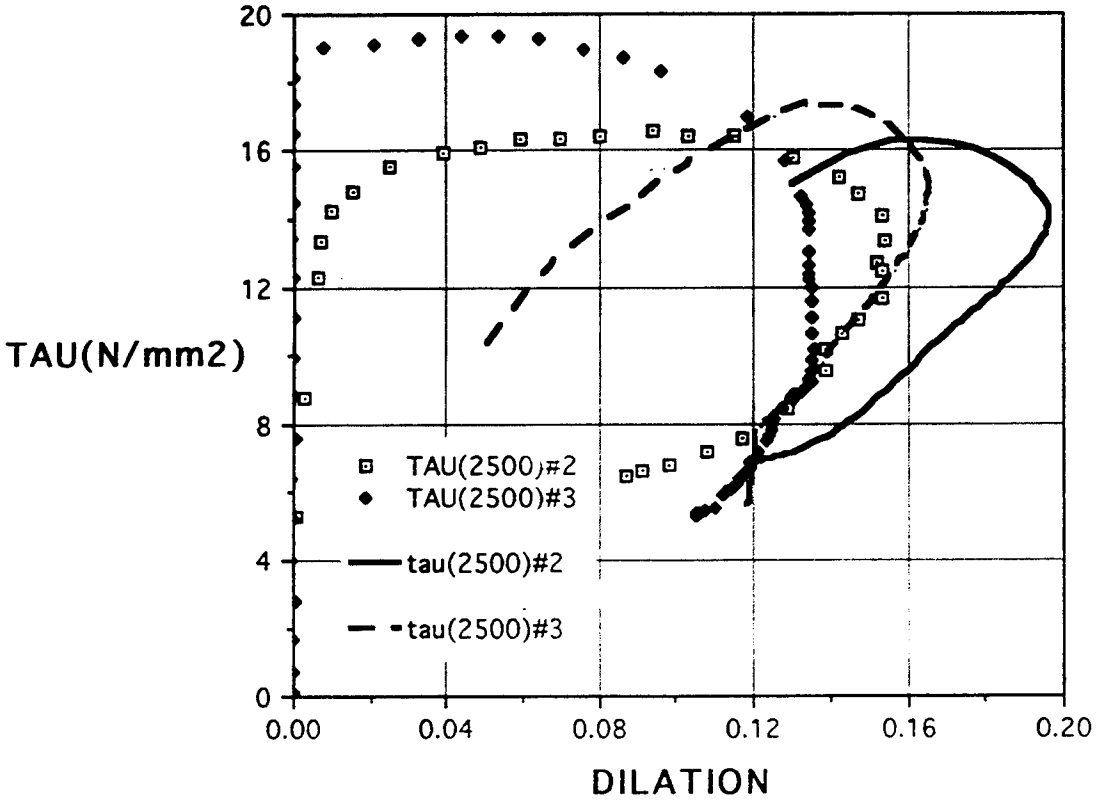

Figure 38. Model Predictions of Bond Stress vs. Dilation - Malvar's Test 2500 psi Level

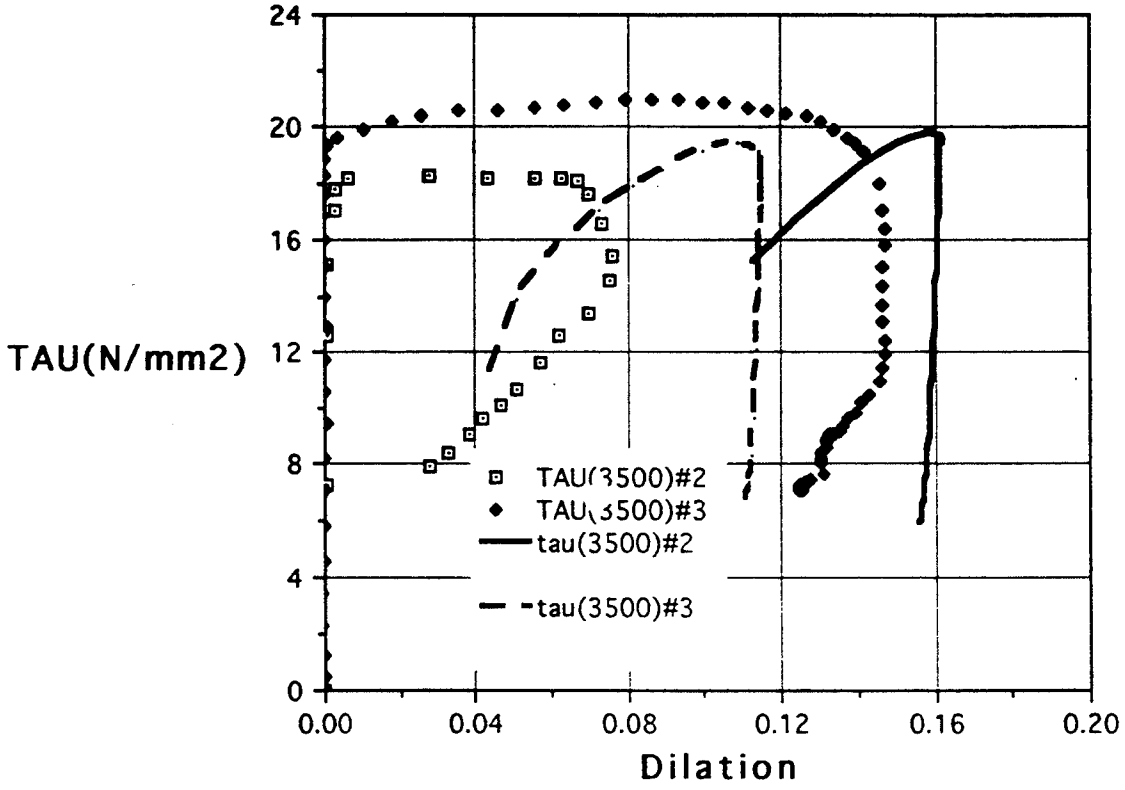

Figure 39. Model Predictions of Bond Stress vs. Dilation - Malvar's Test 3500 psi Level

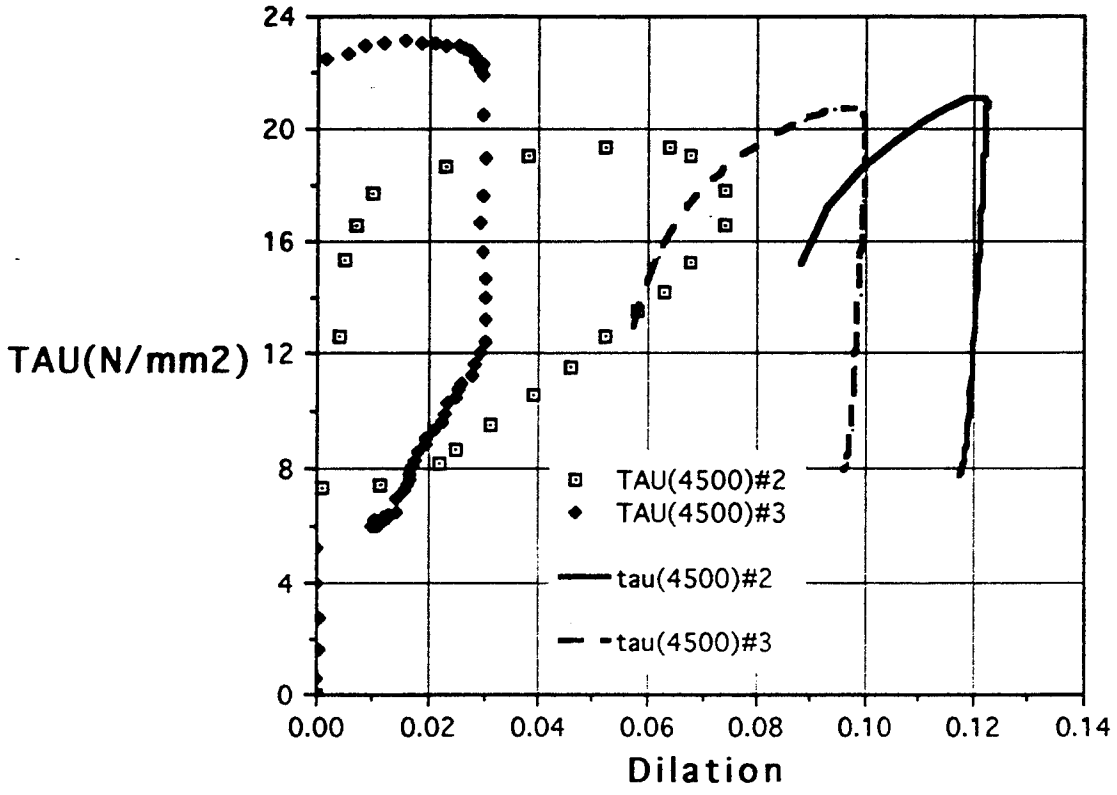

Figure 40. Model Predictions of Bond Stress vs. Dilation - Malvar's Test 4500 psi Level

7.3. Rehm's Data

Figure 41 compares model predictions (analysis of Section 5.4 with $f_c' = 23.5$ kN/mm^2) to experimental results (Rehm 1979). Overall the agreement is quite acceptable. The end of the analytical curve is where the analysis predicted the occurrence of the maximum bond stress. If one assumes the end of the reported experimental data is where the peak stress occurred (the end of a stress controlled test) then the agreement for this phenomenon is quite good.

The smaller initial slope of the predicted response is a result of using elastic moduli for the undamaged bond which are too small and/or using a yield function which passes through the origin, see Cox (1994). The elastic properties for the model were calibrated primarily from unloading-reloading data given in Eligehausen (1983). Another factor which may contribute to this discrepancy is adhesion. Because in field situations the unknown effects of shrinkage and small preloads (including temperature changes) may markedly affect this phenomenon, no attempt has been made to include it in the model.

7.4. Eligehausen's Data

7.4.1. Monotonic tests

Figure 42 gives a comparison of the model predictions (analysis of Section 5.2) to the experimental results of Eligehausen's (1983) Series 2 monotonic tests. The experimental results contain his, lowest, highest and average measurements for the series.

Another way of presenting this comparison is given in Fig. 43. The plastic work done by the bond shear stress is compared for the model predictions and the experimental results. This is a particularly significant format for evaluating the model as one of the primary motivations for attempting to model reinforcement-concrete bond is to be able to properly account for energy dissipation in dynamic analyses of reinforced concrete structures. It would be preferable to compare total plastic work, however, there is not enough experimental information for Eligehausen's tests to permit the calculation of the plastic work due to the normal bond stress.

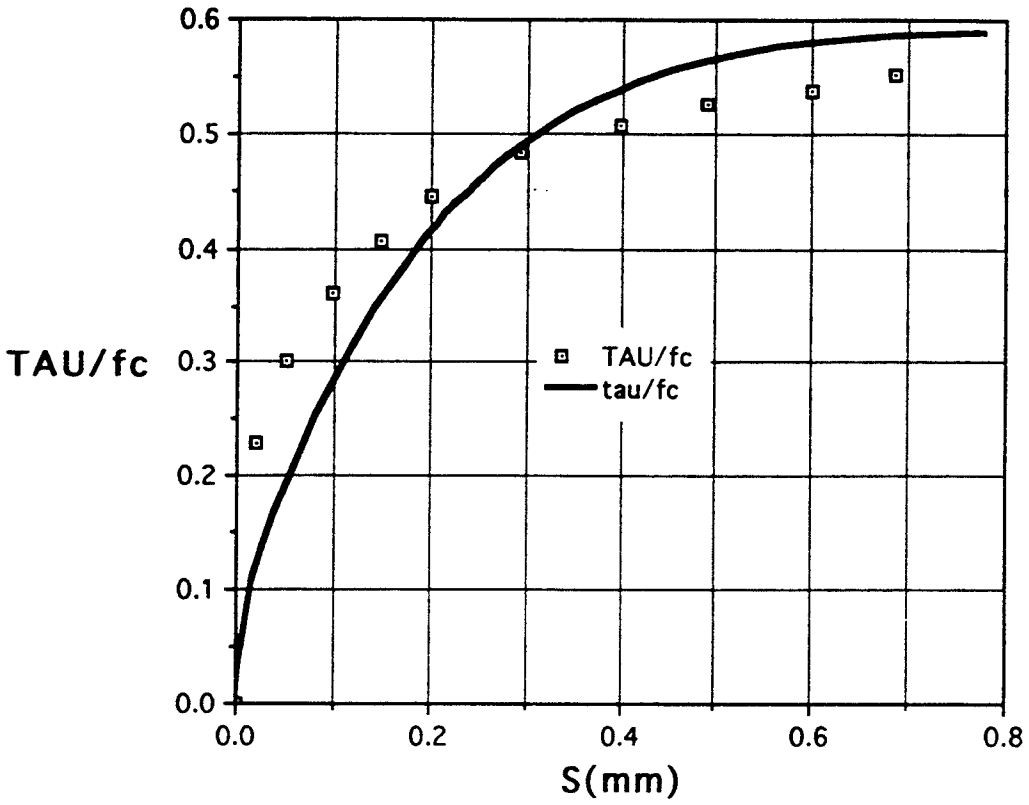

Figure 41. Model Predictions of Bond Stress vs. Slip - Rehm's Test

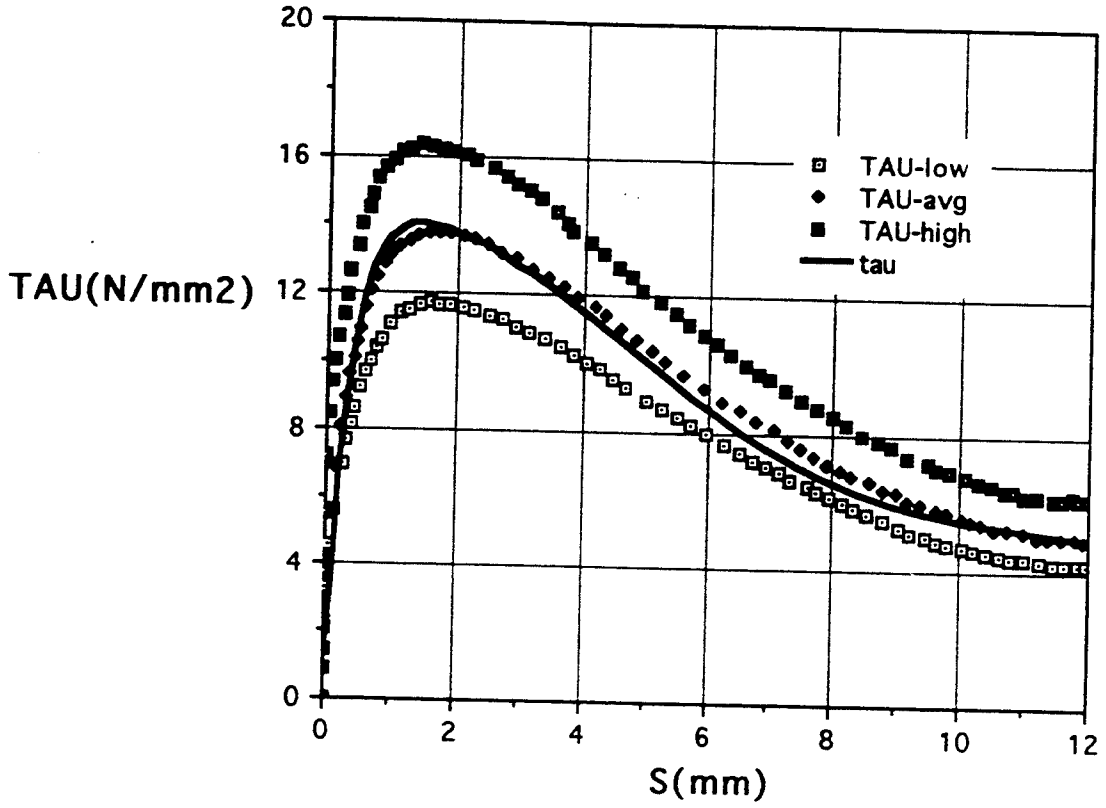

Figure 42. Model Predictions of Bond Stress vs. Slip - Eligehausen's Series #2 Tests

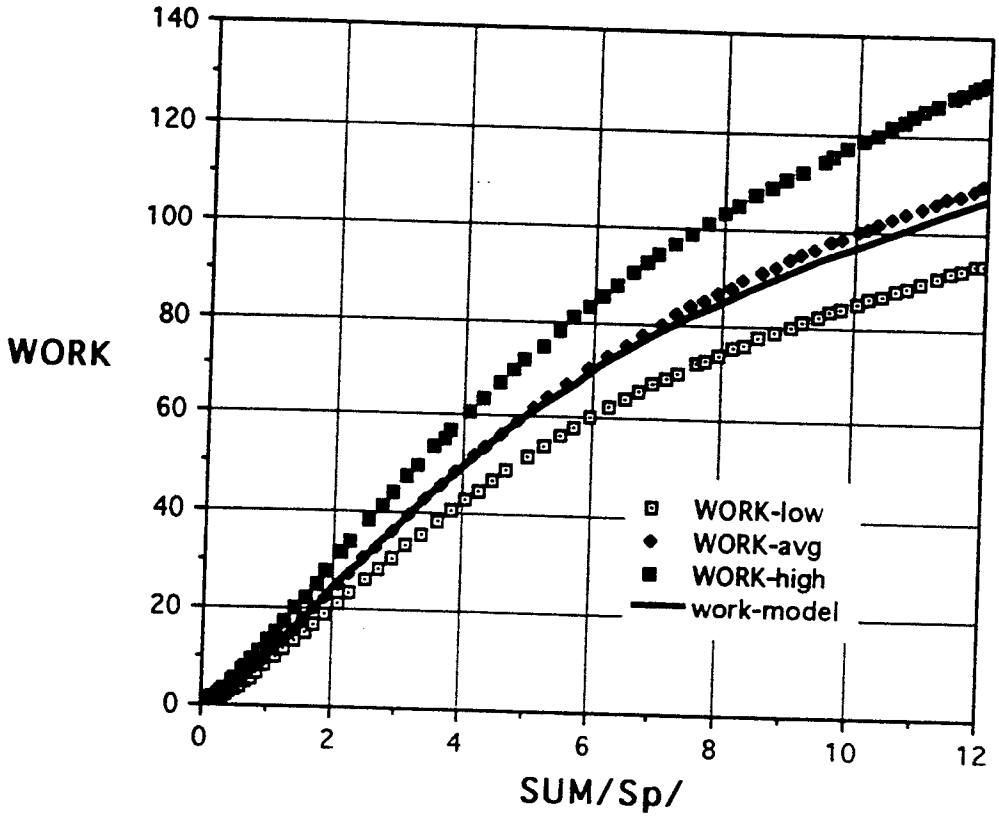

Figure 43. Comparison of Plastic Work (shear) - Eligehausen's Monotonic Test

Figure 44 gives a comparison for a test series (#4) that used a concrete with quite a different strength ($f_c' = 55$ N/mm^2 as compared to 30 N/mm^2 for all the other series).

Little effort was expended in attempting to fine tune the model to produce a perfect fit of Eligehausen's average monotonic results, instead the model was primarily calibrated using the results of Gambarova and Malvar. In this light and considering the major assumptions used in modeling Eligehausen's tests and the experimental scatter, the predictions appear to be very good.

7.4.2. Cyclic tests

Eligehausen (1983) performed a series of cyclic (fixed limits of slip) tests on his pull-out specimen. This series included tests that cycled between zero and a fixed limit of positive slip (see Fig. 45) and tests that cycled between numerically equal values of positive and negative slips (see Figs. 46 and 47). After a prescribed number of cycles, his tests were completed monotonically to the point where only residual frictional resistance remained. The monotonic completion of the test in some cases was carried out after only one cycle and some after ten. Both results are shown on the same graph in Figs. 46 and 47. For the case of the ten cycle tests only the first, second and tenth cycles were reported.

Eligehausen's figures also show the average of the monotonic test results. In the absence of experimental scatter, the cyclic curves would be identical to the monotonic curves prior to the initiation of the first unloading segment. Thus, the differences between the two curves give some indication of the discrepancies between the predicted and experimental results that can be possibly attributed to experimental scatter. (This is the case because the model was to some extent calibrated to give good agreement with Eligehausen's average monotonic results.)

Figure 48 is the prediction for the test data shown in Fig. 45; Fig. 49 corresponds to Fig. 46; and Fig. 50 corresponds to Fig. 47. Attempts to compare the experimental and predicted results on the same graphs were found to be overly confusing.

Qualitatively, the predictions of the model appear to capture all the salient features of the experimental data; the only striking differences are the spikes that occur in the predictions at the beginning of each traverse between the prescribed

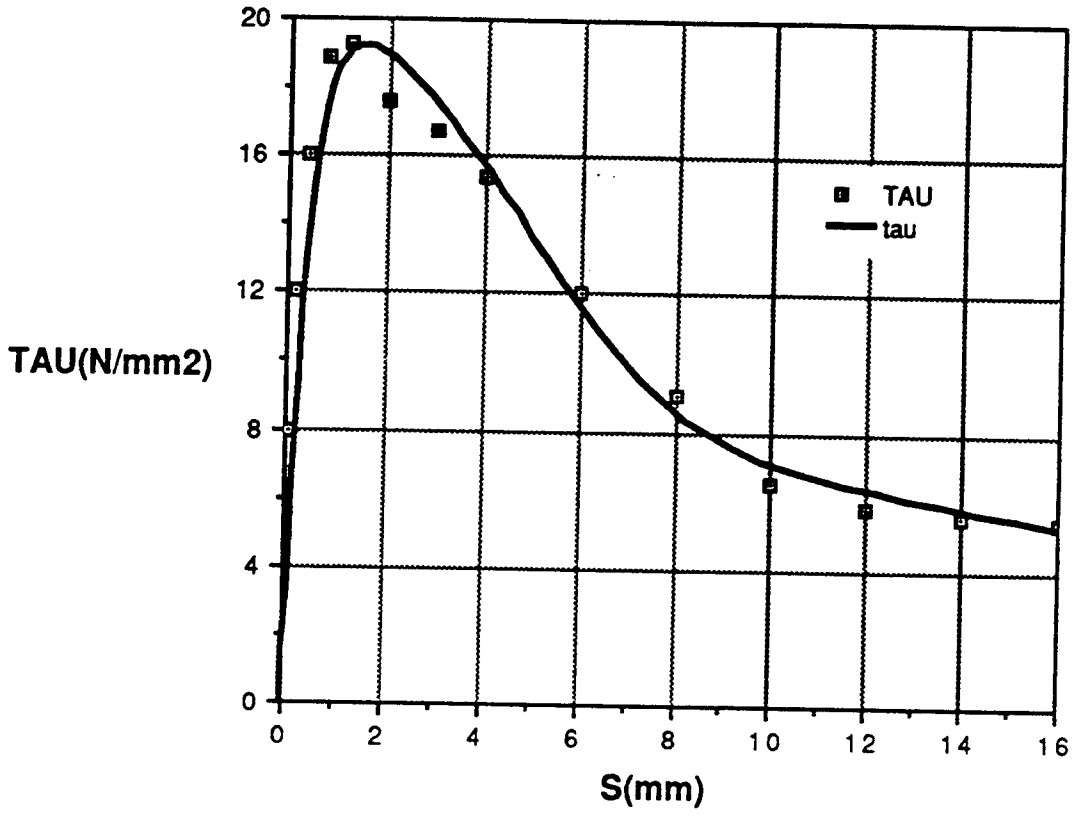

Figure 44. Model Predictions of Bond Stress vs. Slip - Eligehausen's Series 4.1 ($f_c' = 55$)

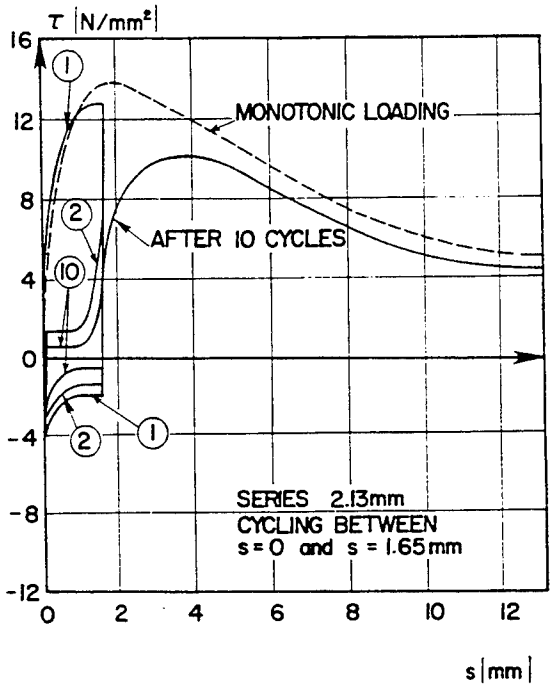

Figure 45. Bond Stress vs. Slip for Cyclic Test - Eligehausen's Fig. 4.34

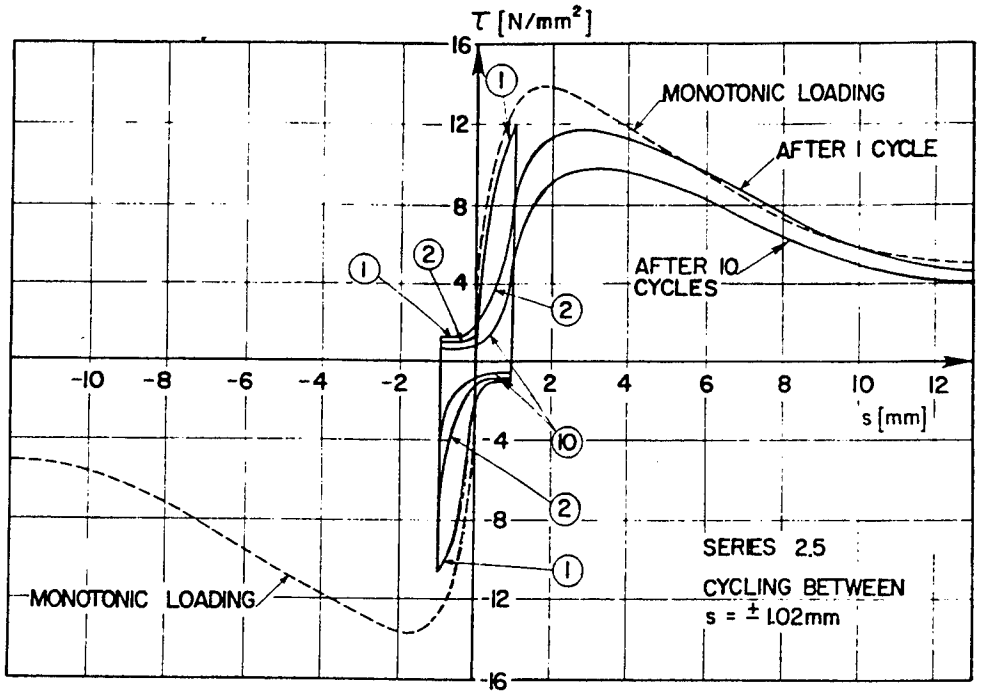

Figure 46. Bond Stress vs. Slip for Cyclic Test - Eligehausen's Fig. 4.26

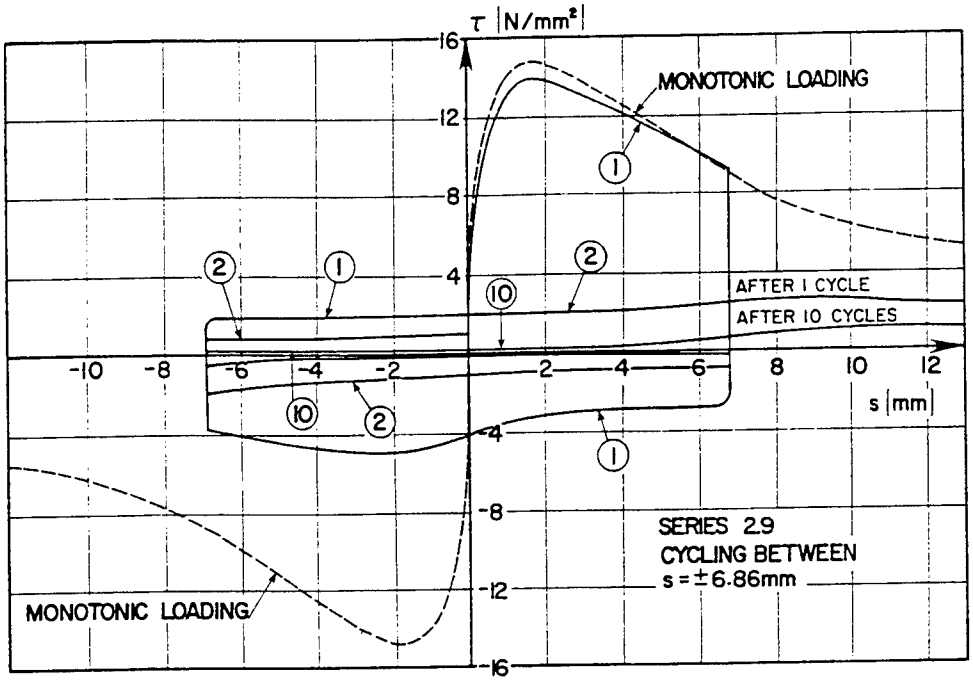

Figure 47. Bond Stress vs. Slip for Cyclic Test - Eligehausen's Fig. 4.30

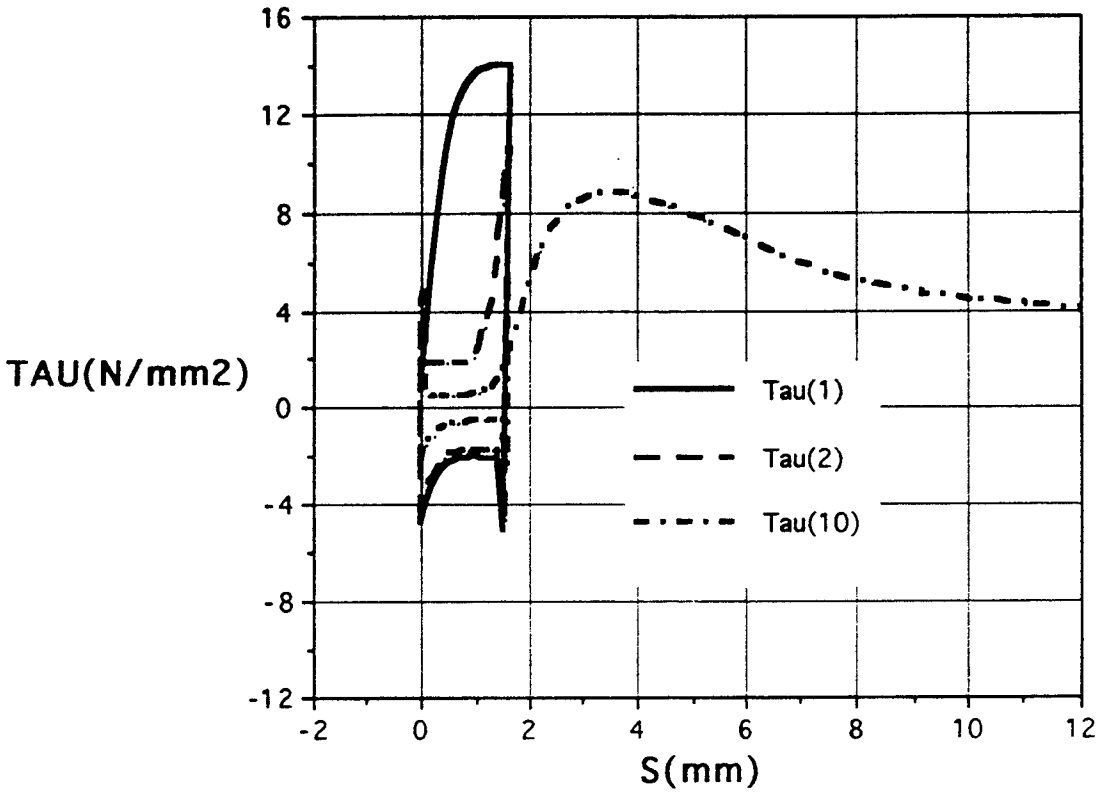

Figure 48. Model Predictions of Bond Stress vs. Slip - Compare to Eligehausen's Fig. 4.34

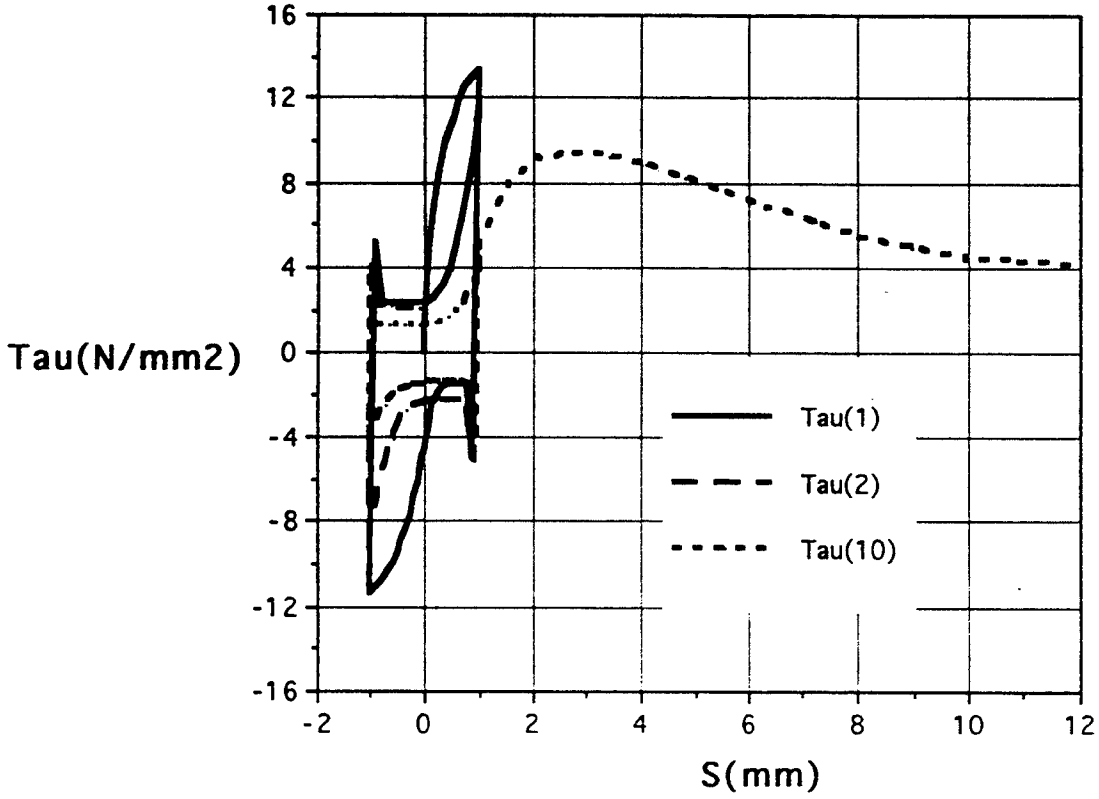

Figure 49. Model Predictions of Bond Stress vs. Slip - Compare to Eligehausen's Fig. 4.26

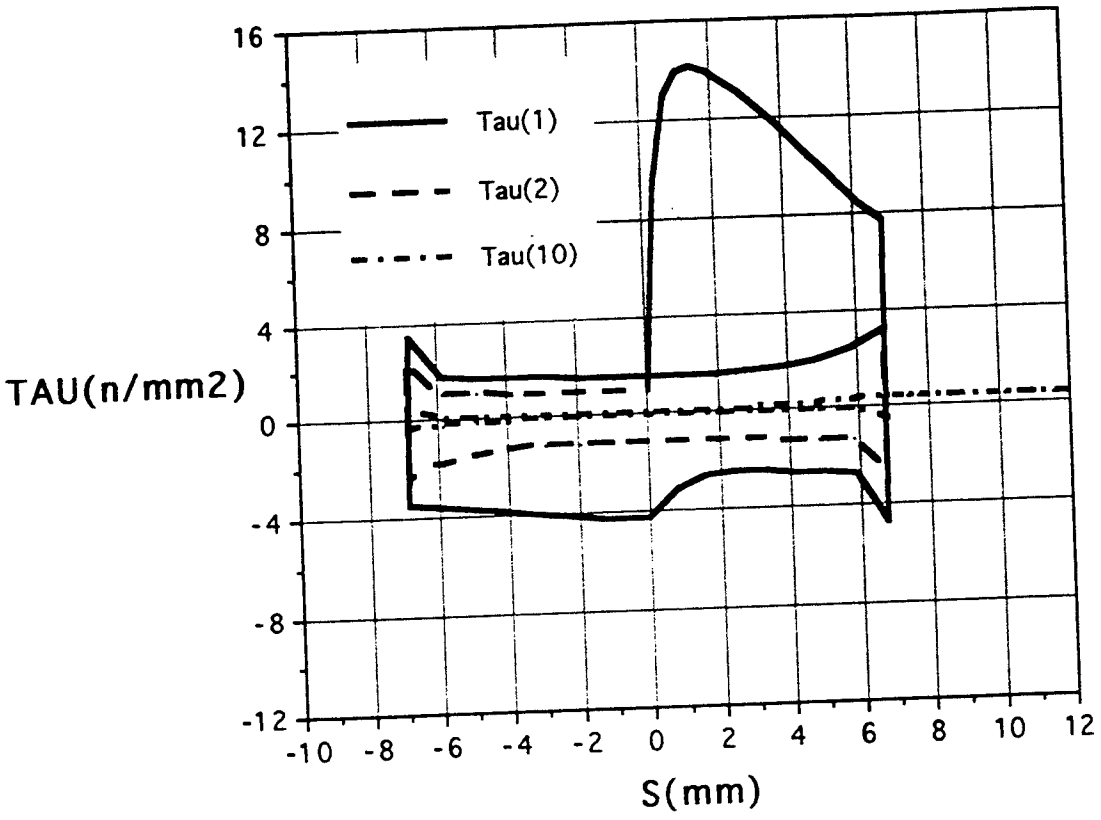

Figure 50. Model Predictions of Bond Stress vs. Slip - Compare to Eligehausen's Fig. 4.30

limits of slip. For the model this occurs because of the abrupt loss of wedging action between the lug and the intact concrete as the lug backs away from it.

In the prediction of this phenomenon the width of the spike is controlled by the size of the solution step. Even though it is felt that this phenomenon occurs nearly instantaneously (essentially a spike of zero width) it is computationally convenient to spread it over one solution step (see Section 6.2.5).

Two possibilities exist to explain the discrepancy between the experimental and analytical results on this point. One is that the phenomenon is real but happens over such a short distance that the experiment could not capture it. The second is that some other physical mechanism is present (and not captured by the model) that smoothes out this abrupt loss of wedging action. Whether or not the spike is in fact a real phenomenon would seem to be of little consequence for applications of the model to real problems (it would, however, be possible to construct hypothetical circumstances for which it would be significant).

In an attempt to more directly compare experimental and predicted results, and to compare one of the most significant consequence of reinforcement-concrete bond behavior, comparisons of dissipated energy by the bond shear stress are shown in Figs. 51 and 52. The comparison in Fig. 51 is for the first cycle and monotonic completion of the test reported in Fig. 46. In Fig. 52 a comparison is given for the first two cycles of the test reported in Fig. 47. The abscissas are the running sums of the absolute values of the incremental slips (total distances traveled) and, thus, are measures of time elapsed. As previously noted Eligehausen did not report results for cycles two through nine and, thus unfortunately, comparisons can not be made for the ten cycle tests; however, the comparisons that can be made are most encouraging.

7.5. Observations

Table 2 gives some of the physical parameters for each of the test series considered in this section. The concrete tensile strengths and elastic moduli were calculated using the correlations given in Appendix C. For all predictions the model parameters of Table 1 were used.

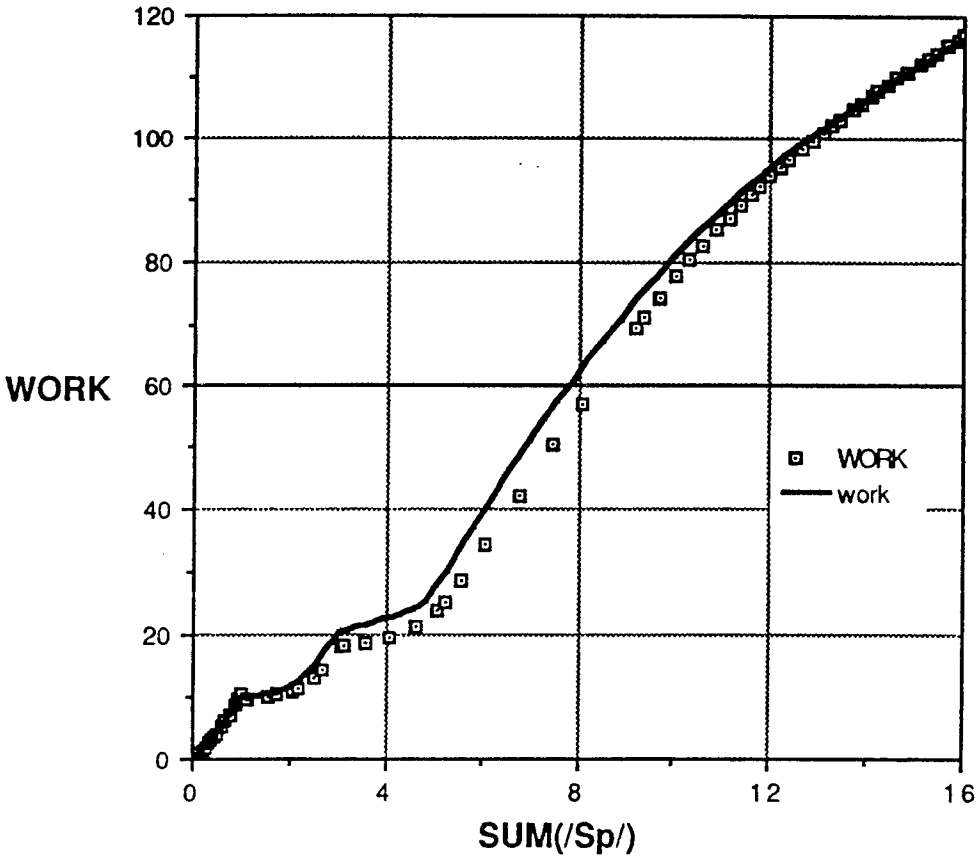

Figure 51. Comparison of Plastic Work (shear) - One Cycle (including monotonic completion) of Eligehausen's Fig. 4.26

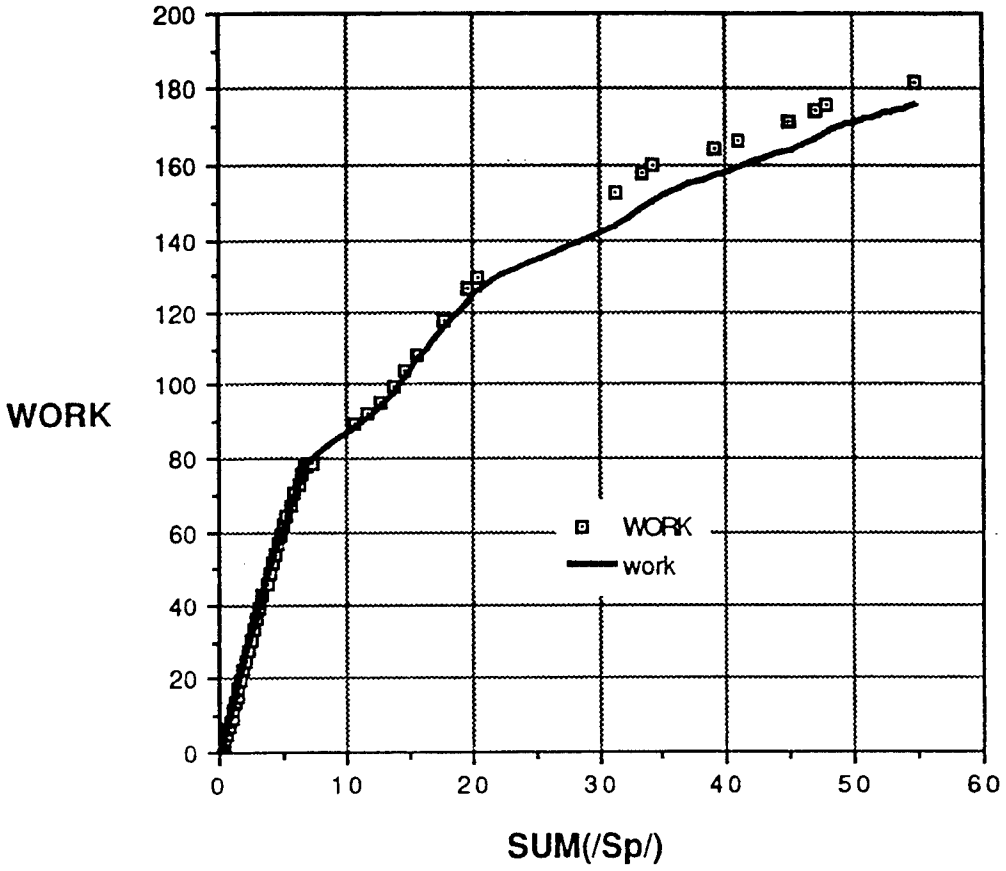

Figure 52. Comparison of Plastic Work (shear) - Two Cycles of Eligehausen's Fig. 4.30

Experimental Study	Test Series	Concrete Strength (N/mm^2)	Lug Spacing (mm)	Lug Angle (degrees)	Bar Diameter (mm)
Eligehausen	#2	30	14	19	25
	#4	55	14	19	25
Gambarova		40	11	38	18
Malvar	#2	40	13	22	19
	#3	39	13	0	19
Rehm		23	8.4	38	14

Table 2. Physical Parameters Describing the Bond

From Table 2 it is seen that the database includes a fairly wide range of concrete strengths and bar lug angles, and a reasonable range of lug spacings and bar diameters. Additionally, the geometric configurations of the test specimens span a wide spectrum of conditions (see Section 5).

It is felt that the comparisons given in this section clearly demonstrate the ability of the model to describe reinforcement-concrete bond behavior under a variety of conditions for both monotonic and cyclic loadings.

8. CONCLUSIONS AND RECOMMENDATIONS

An elastic-plastic bond model has been developed that has the capability of describing the bond between reinforcement and concrete for a wide variety of conditions. The model has been calibrated for normal strength concrete and standard types of steel reinforcing bars. The model only requires a knowledge of the compressive strength of the concrete (it is assumed that the concrete's tensile strength and initial elastic modulus can be calculated from this value), the bar diameter, the spacing between lugs and the angle the lugs make with the axis of the bar.

By varying only the above mentioned properties and using simplified specimen models, the results of several research studies on monotonic loading were reproduced with acceptable accuracy. Extension of the model to cyclic loading has given encouraging results on one data set both in terms of stress-strain response and plastic work. Validation is inherently never complete, and models are never as general as nature; but the bond plasticity model presented in this report represents a significant improvement over status quo one-dimensional models

There are several aspects of the model that should be refined as additional experimental evidence becomes available. These include the following:

Some of the functions selected to represent various facets of the model, such as the non-associative flow rule and the hardening function, are quite lengthy. Further investigation may lead to simplified expressions without sacrificing accuracy.

While the use of the closest distance between lugs in the definition of damage in Eq. (51) would appear to improve the accuracy of the model, further evidence is needed before this hypothesis is firmly established.

In the current model the lug height does not appear as a physical parameter. This is based on the assumption that for standard bars the ratio of lug height to bar diameter does not vary significantly. Thus, the dependence of bond behavior on lug height is subsumed in the dependence on bar diameter. The validity of this assumption needs to be investigated.

It has been experimentally observed that the casting direction of the concrete relative to the orientation of the bar has an appreciable affect on the bond behavior. This phenomenon may be significant but has not been included in this version of the model.

It appears that making the elastic properties of the model damage dependent would considerably improve the accuracy of predictions for small slip response.

The assumption that the initial value of the hardening function is the same as the completely damaged value was a matter of convenience, however, there does not appear to be any physical justification. The removal of this assumption from the model would most likely improve the accuracy of predictions for small slips.

While the model has been implemented by Cox (1994) in a finite element code and used to analyze simple reinforced-concrete, bond test configurations, much work remains to be done before the model can be used in routine finite element analyses of complicated field configurations. Means must be found for implementing the model so that an excessively fine finite element grid is not required. While the work of McMichael (1993) on the development of a composite finite element model for the bar, the bond and bond layer is promising, much work remains to be done in this area. In particular means must be developed for incorporating the model in "embedded" and "distributed" finite element representations of reinforcement.

9. REFERENCES

Chang, K.-T. (1992), "A one dimensional finite element model of bond behavior in reinforced concrete," M.S. Thesis, Department of Civil Engineering, University of California, Davis.

Cox, J.V. (1993), "Development of a plasticity bond model for reinforced concrete - theory and validation for monotonic applications," Ph.D. dissertation, Civil Engineering Department, University of California, Davis (in publication).

Cowell, A.D., V.V. Bertero, and E.P. Popov (1982), "An investigation of local bond slip under variation of specimen parameters," Earthquake Engineering Research Center, Report No. UCB/EERC 82/23, University of California, Berkeley.

Daniels, B.J., A. Nussbaumer, and M. Crisinel (1989), "Non-linear analysis of composite members in bending and shear," Publication ICOM 223, Institut de Statique et Structures, Départment de Génie Civil, Ecole Polytechnique Federale de Lausanne.

Edwards, A.D. and P.J. Yannopoulos (1978), "Local bond-stress-slip relationship under repeated loading," Magazine of Concrete Research, Vol. 30, No. 103, June.

Eligehausen, R., E.P. Popov, and V.V. Bertero (1983), "Local bond stress-slip relations of deformed bars under generalized excitations," Report UCB/EERC-83/23, University of California, Berkeley, October.

Gambarova, P.G., G.P. Rosati, and B. Zasso (1989), "Steel-to-concrete bond after concrete splitting: test results," Materials and Structures, Vol. 22, No. 127, January, pp. 35-47.

Malvar, L.J. (1991), "Bond of reinforcement under controlled confinement," Technical Note 1833, Naval Civil Engineering Laboratory, Port Hueneme, CA, June (also in: ACI Materials Journal, Vol. 89, No. 6, pp. 593-601, Nov.-Dec., 1992).

McMichael, L. (1993), "A composite finite element model for reinforced concrete," M.S. Thesis, Department of Civil Engineering, University of California, Davis (in publication).

Mehlhorn, G. and M. Keuser (1985), "Isoparametric contact elements for analysis of reinforced concrete structures," Finite Element Analysis of Reinforced Concrete Structures, ASCE, Proceedings of a Seminar sponsored by the Japan Society for the Promotion of Science and the US National Science Foundation, Tokyo, Japan, pp. 329-347.

Menzel, G.A. (1941), "A proposed standard deformed bar for reinforced concrete," presented at the 17th Semi-Annual Meeting, Concrete Reinforcing Steel Institute, Colorado Springs, CO, September.

Mindess, S. and J.F. Young (1981), Concrete, Prentice-Hall, Englewood Cliffs, New Jersey.

Morita, S. and T. Kaku (1979), "Splitting bond failures of large deformed reinforcing bars," ACI Journal Proc., Vol. 76, No. 1, pp. 93-110.

Rehm, G. and R. Eligehausen (1979), "Bond of ribbed bars under high cycle repeat loads," ACI Journal, Vol. 76, No. 2, February, pp. 297-309.

Shima, H., L. Chou and H. Okamura (1987), "Micro and macro models for bond in reinforced concrete," Journal of the Faculty of Engineering, The University of Tokyo (B), Vol. 39, No. 2, pp. 133-194.

Tepfers, R. (1979), "Cracking of concrete cover along anchored deformed reinforcing bars," Magazine of Concrete Research, Vol. 31, No. 106, pp. 3-12.

Timoshenko, S.P. and J.N. Goodier (1987), Theory of Elasticity, 3rd edition, McGraw-Hill, New York, NY.

APPENDIX A - Relationships Between Local Strain Measurements and Bond Behavior

A number of experimental studies (e.g., see Cowell 1982 and Shima 1987) have measured the strain distribution in the reinforcing rod of a "pull-out" or "tension" bond test and have attempted to calculate from these measurements the distribution of bond stress and slip. These calculations are based on the following analysis.

For the reinforcing bar elastic behavior is assumed (modulus of E_r). From the measured axial strain, ε_z, and the assumption that the stresses σ_r and σ_θ in the reinforcing bar can be neglected, the axial force distribution in the rod is found:

$$F(z) \approx \pi D_b^2 E_r \varepsilon_z / 4 \qquad (A\text{-}1)$$

From equilibrium it is seen that changes in the axial force must be balanced by the bond shear stress, i.e.,

$$\pi D_b \tau = \frac{dF}{dz} \qquad (A\text{-}2)$$

thus:

$$\tau \approx \frac{D_b E_r}{4} \frac{d\varepsilon_z}{dz} \qquad (A\text{-}3)$$

Of course taking a derivative of the experimentally determined quantity ε_z greatly magnifies any experimental error. This is especially worrisome in light of the expected local uncertainties in ε_z due to the inhomogeneous character of the concrete, the bar's surface geometry (i.e., the presence of the lugs), and the role that local failure of the concrete plays in determining bond behavior.

In order to calculate a local bond slip "s" either the deformation of the concrete must be: (1) measured or (2) neglected relative to the axial deformation of the reinforcing bar. In the above referenced studies the later is assumed and hence $s = u_z$ (the axial displacement of the bar). Another way of expressing this approximation is to

assume that the concrete is rigid. This assumption depends upon the concrete component of the test specimen being massive relative to the reinforcing bar and the neglecting of any local deformations in the concrete in the vicinity of the bond. The bar displacement is the integral of the axial strain:

$$s \approx u_z = u_0 + \int \varepsilon_z \, dz \qquad \text{(A-4)}$$

The constant of integration u_0 is determined from the boundary conditions of the test. The integration process tends to smooth out experimental errors in ε_z, however, the uncertainties introduced by treating the concrete as rigid remain.

Thus, from a measurement of the axial strain distribution in the reinforcing bar, bond stress vs. bond slip can be approximately determined using Eqs. (A-3) and (A-4).

APPENDIX B - Response of an Embedded Semi-Infinite Reinforcing Bar

Consider a semi-infinite reinforcing bar (diameter of D_{b_v}) embedded in a half space of concrete and subjected to a "pull-out" force F_o applied to its free end. Denote the slip of the free end of the reinforcing bar relative to the concrete by s_o. It is desired to find $s_o = s_o(F_o)$.

Of course no data exists for this ideal situation, however, Shima (1987) has tested some rather large specimens that can be used to approximate it. His specimen #6 had an embedded length of 40 bar diameters in a concrete cylinder with a diameter of 20 bar diameters. It will be assume that this data approximates the semi-infinite condition as long as the measured strains in the bar remain near zero in the vicinity of the unloaded end. One can either work directly with the data for specimen #6 given in Fig. 2.16 of Shima (1987) or alternatively use the empirical equation that he developed to fit this data, Eq. 2.13 in the cited reference. Eq. 2.13 was used and the results were checked by comparing predictions to Fig. 2.16.

Shima's empirical Eq. 2.13 relates the bond stress at an arbitrary point along the rod to the corresponding bond slip (where $S = s/D_{b_v}$):

$$\tau = 0.9\ (f_c')^{2/3}\ [1 - e^{-40\ S^{0.6}}] \qquad \text{(B-1)}$$

Using the assumptions of Appendix A, differentiating Eq. (A-4) and substituting into Eq. (A-3) gives (let $Z = z/D_{b_v}$):

$$\tau = \frac{E_r}{4}\ \frac{d^2S}{dZ^2} \qquad \text{(B-2)}$$

Combining Eqs. (B-1) and (B-2) gives:

$$\frac{d^2S}{dZ^2} = \frac{3.6\ (f_c')^{2/3}}{E_r}\ [1 - e^{-40S^{0.6}}] \qquad \text{(B-3)}$$

For a semi-infinite bar the boundary conditions are a specified slip s_o at the end of the bar and zero slip at infinity. With these boundary conditions the governing nonlinear differential Eq. (B-3) was solved for a range of values of s_o/D_{b_v} using a packaged finite difference scheme (a concrete strength of 30 N/mm^2 - used in the majority of Eligehausen's tests - along with the value of E_r for steel were assumed). For a given value of s_o/D_{b_v} the value of strain ε_{z_o} at the end of the bar was determined from the solution for S(Z) and Eq. (A-4). In Fig. B-1 the resulting plot of s_o/D_{b_v} vs. ε_{z_o} is given. Curve fitting yielded the following equation:

$$s_o/D_{b_v} = 365\ (\varepsilon_{z_o})^{1.62} \qquad \text{(B-4)}$$

The strain in the bar is simply related to the force (assuming a uniaxial stress state in the bar), thus, giving the desired relationship (where the value of η is 365):

$$s_o/D_{b_v} = \eta\ \{4F_o/[\pi(D_{b_v})^2 E_r]\}^{1.62} \qquad \text{(B-5)}$$

If a different strength concrete is used it can be shown that in Eq. (B-5) the $\eta = 365$ is replaced by:

$$\eta = 365\ (30/f_c')^{(1.6/3)} \qquad \text{(B-6)}$$

The above development assumes continuous loading of the rod (i.e., F_o increases monotonically). For unloading-reloading conditions linear elastic behavior is assumed, see Eligehausen (1983). The unloading-reloading modulus, E_{un}, is estimated from the following argument.

For elastic unloading-reloading behavior the rod is treated as a one dimensional axial member supported by an elastic foundation (see Fig. B-2). The concrete is treated as rigid (see Appendix A) and, thus, the foundation reaction τ is just the foundation modulus times the displacement of the rod Δs (the slip). The foundation modulus is assumed to be equal to the reciprocal of A_{11} from Eq. (1), thus (see Eq. 46):

$$\Delta\tau = (E_c/a_{11})\ \Delta s/D_{b_v} \qquad \text{(B-7)}$$

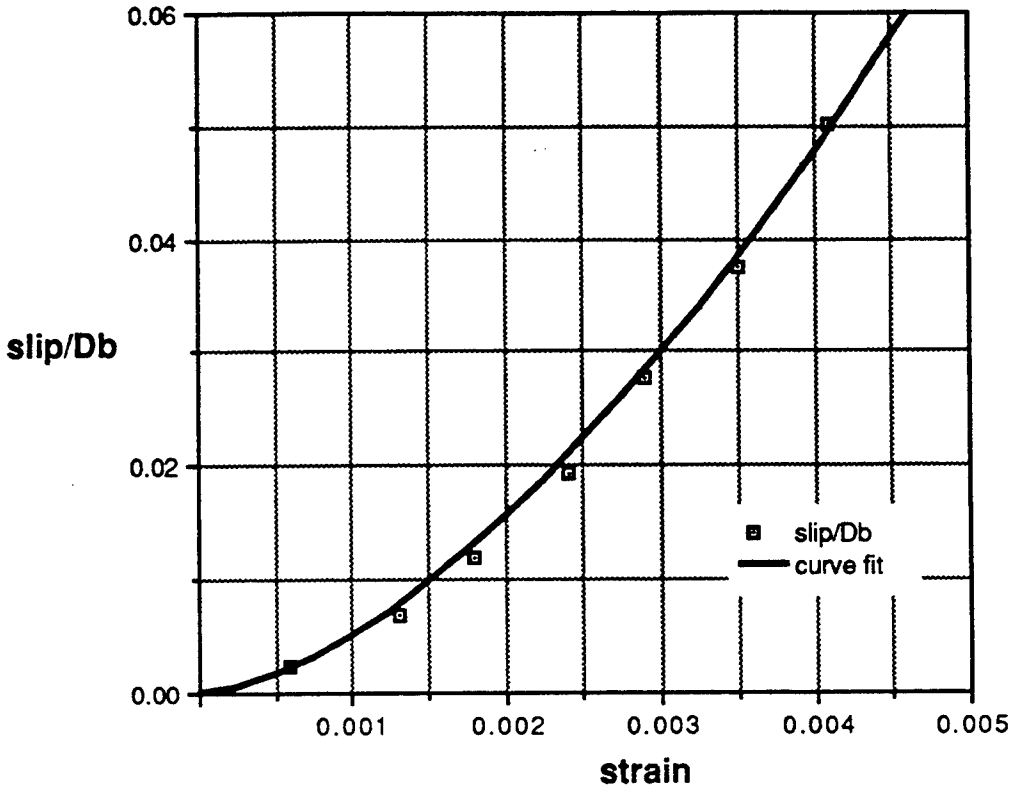

Figure B-1. Response of a Semi-infinite Rod

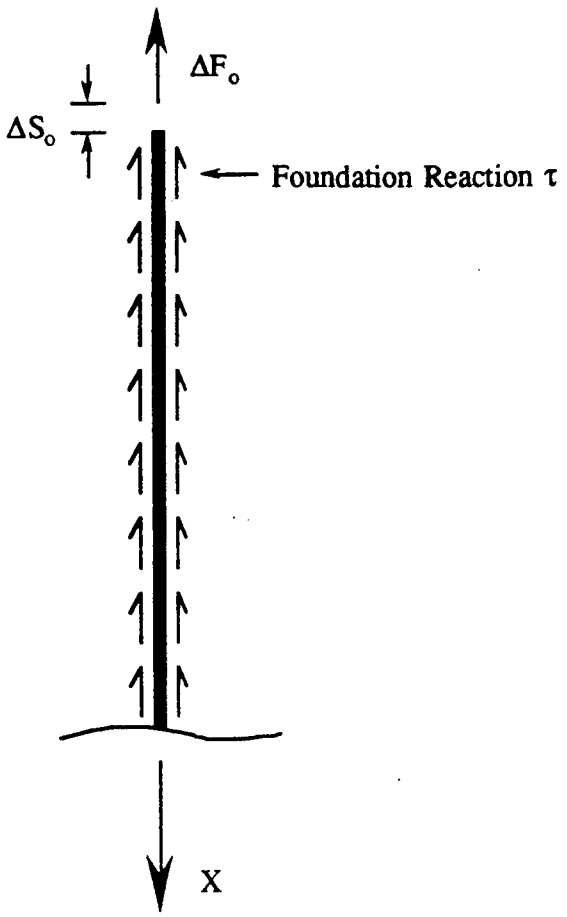

Figure B-2. Rod Supported by an Elastic Foundation

Equilibrium of an element of the rod gives the equation:

$$\frac{d\Delta F}{dx} = \pi D_{b_v} \Delta\tau \qquad \text{(B-8)}$$

Expressing the force in the rod in terms of the strain gives:

$$\Delta F = \frac{\pi}{4} D_{b_v}^2 E_r \frac{d\Delta s}{dx} \qquad \text{(B-9)}$$

Combining the above three equations gives the following differential equation for Δs:

$$\frac{d^2\Delta s}{dx^2} - \frac{4 E_c}{D_{b_v}^2 E_r a_{11}} \Delta s = 0 \qquad \text{(B-10)}$$

Solving the simple differential equation and applying the boundary conditions of a specified displacement at the free end and no displacement at infinity yields:

$$\Delta s = -\Delta s_o \exp\left(-\frac{2}{D_{b_v}} \sqrt{\frac{E_c}{a_{11} E_r}}\, x\right) \qquad \text{(B-11)}$$

Eq. (B-9) gives:

$$\Delta F_o = \frac{\pi D_{b_v}^2}{2} \sqrt{\frac{E_r E_c}{a_{22}}} \frac{\Delta s_o}{D_{b_v}} \qquad \text{(B-12)}$$

Thus, the desired unloading-reloading modulus is:

$$E_{un} = \frac{\pi D_{b_v}^2}{2} \sqrt{\frac{E_r E_c}{a_{11}}} \qquad \text{(B-13)}$$

In Fig. B-3 non-dimensional ($x = \sigma/E_r$ and $y = s_o/D_{b_v}$) plots of the inverses of Eq. (B-5) and Eq. (B-12) are given. It is seen that for a small range of values of strain that the proposed unloading curve falls below the loading curve. Thus, if unloading should be initiated from a value of strain smaller than the value at which the curves

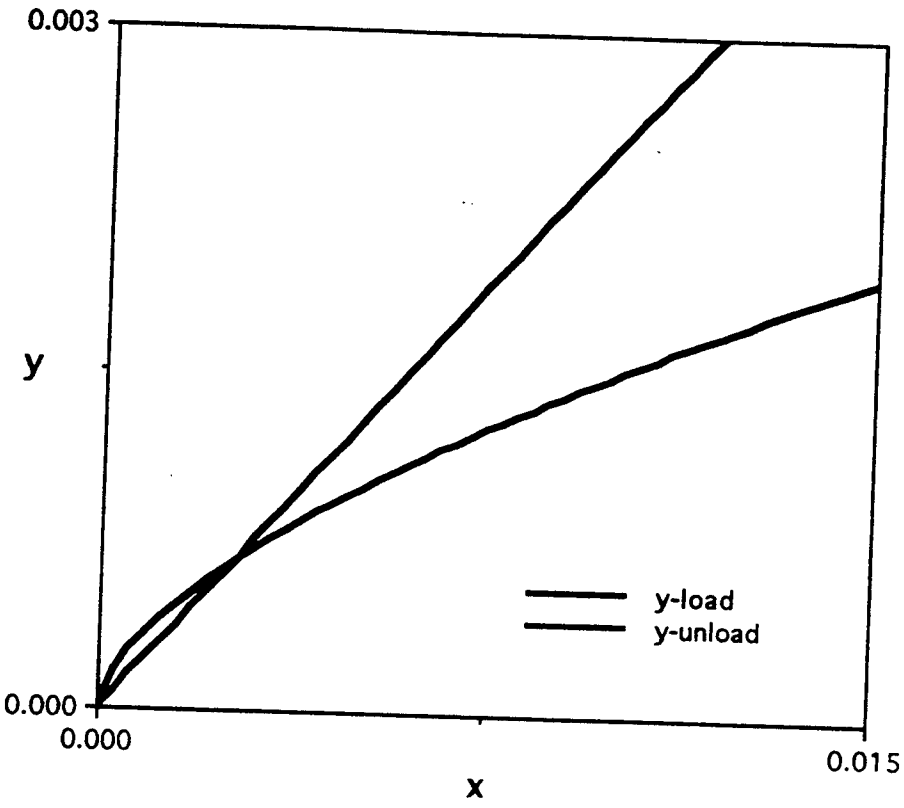

Figure B-3. Loading and Unloading Curves

intersect, the unacceptable situation shown in Fig. B-4a results. This inconsistency is obviously the fault of one or more of the approximations embedded in the two expressions. To avoid this problem, for strains smaller than the value at the intersection, an unloading modulus given by the expression shown below is used ($F_{o_{un}}$ denotes the value of F_o when unloading is initiated).

$$E_{un} = \frac{F_{o_{un}}}{\eta\{4F_{o_{un}}/[\pi(D_{b_v})^2 E_r]\}^{1.62}} \qquad \text{(B-14)}$$

With this expression the behavior shown in Fig. B-4b is obtained.

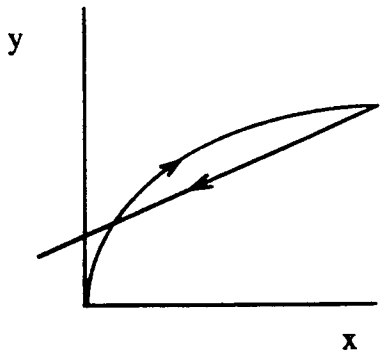

a) Unacceptable Prediction of Unloading

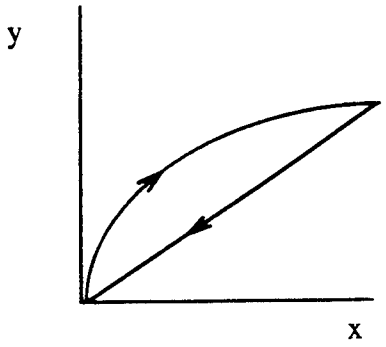

b) Acceptable Prediction of Loading

Figure B-4. Consideration of Unloading for Small Slips

APPENDIX C - Correlation of E_c and f_t with f_c'

It is common practice to use empirical correlations for the calculation of the concrete modulus E_c and the concrete tensile strength f_t from a knowledge of its compressive strength f_c'. A number of such formulas are available in the literature, e.g., see Mindress (1981). For the bond model the initial tangent modulus is the desired concrete modulus. A correlation is found from the experimental results presented by Daniels (1989). Values taken from Fig. 8 of the cited references are plotted in Fig. C-1. An acceptable fit of the data is given by the expression (the units are N/mm^2):

$$E_c = 41000\ (1 - e^{-.075 f_c'}) \qquad \text{(C-1)}$$

Many researchers have suggested that the tensile strength of concrete f_t is correlated to the square root of f_c', while other authors have suggested the two-thirds power of f_c'. The data in table 3.3 of Eligehausen (1983) suggests:

$$f_t = 0.3\ f_c'^{2/3} \qquad \text{(C-2)}$$

The authors have compared this formula with experimental measurements from a number of other sources and have found excellent agreement.

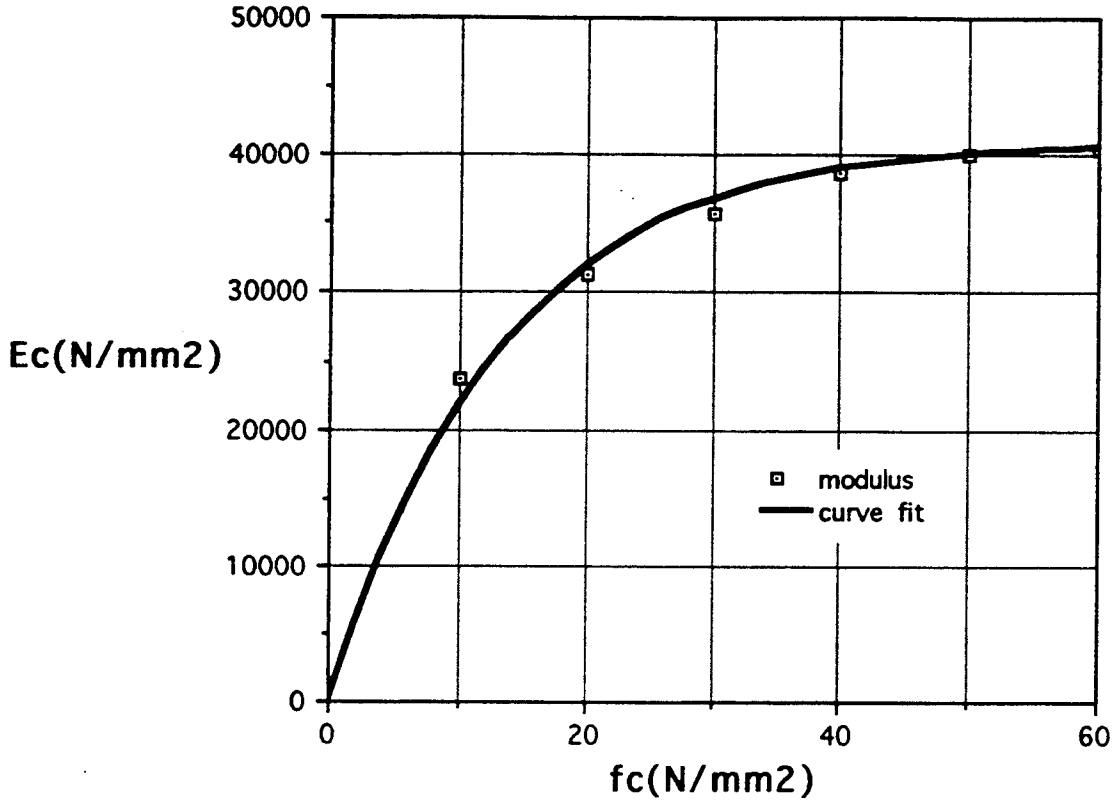

Figure C-1. Relationship between Concrete Modulus and Compressive Strength

APPENDIX D - Theoretical Arguments Concerning the Elastic Properties

In this appendix a very simple theoretical argument will be presented to examine the relative magnitudes of the elastic moduli.

Consider the conditions when (a) splitting cracks have formed in the concrete surrounding the reinforcing bar, (b) the interface has deformed so as to slightly open the splitting cracks (thus no appreciable hoop stress can exist in the bond layer), and (c) the concrete is not in contact with the bar between the lugs.

Figure D-1 shows the relative displacements between the face of the rib and the edge of the bond layer with the rib face as the frame of reference. Assume: (a) that the response is so localized near the face of the rib, that the average relative displacement values (shown in the figure in the local-rib coordinate system) accurately represent the unit cell; (b) no sliding occurs along the rib face; (c) the tractions on the face of the rib are statically equivalent to the negative of the shown resultant forces; and (4) the incremental compliance relationship between the resultants and the relative displacements is uncoupled in the local-rib coordinate system.

The increments in the bond stresses defined in this study are given in terms of the resultants as

$$\begin{Bmatrix} \Delta Q_1 \\ \Delta Q_2 \end{Bmatrix} = \frac{1}{s_L} [R] \begin{Bmatrix} \Delta T \\ \Delta N \end{Bmatrix} \tag{D-1}$$

where

$$[R] = \begin{bmatrix} \cos\beta & -\sin\beta \\ \sin\beta & \cos\beta \end{bmatrix}. \tag{D-2}$$

Similarly, the increments in generalized strains in terms of the relative displacements are given as

$$\begin{Bmatrix} \Delta q_1 \\ \Delta q_2 \end{Bmatrix} = \frac{1}{D_b} [R] \begin{Bmatrix} \Delta t \\ \Delta n \end{Bmatrix}. \tag{D-3}$$

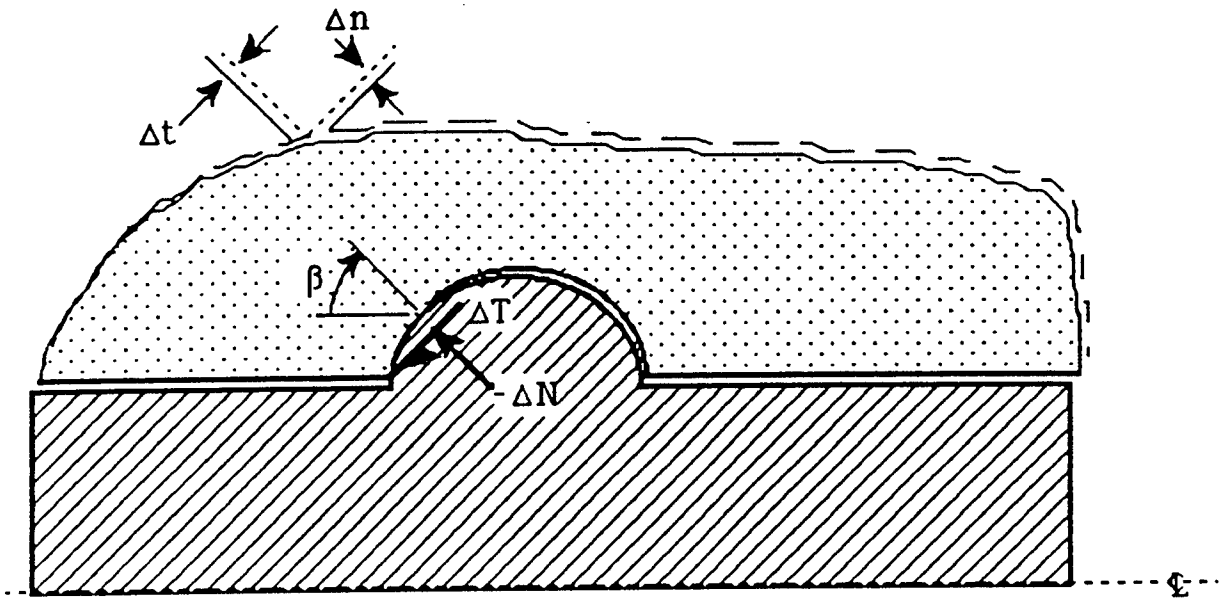

Figure D-1. Schematic of Simple Elastic Bond Layer Model. (Arrows denoted resultant forces on the concrete)

With the assumption that the resultant forces are uncoupled from the relative displacements in the local-rib coordinate system (i.e., these are the axes of orthotropy) the incremental constitutive relationship, in compliance form, is given by

$$\begin{Bmatrix} \Delta t \\ \Delta n \end{Bmatrix} = \begin{bmatrix} \frac{1}{k_t} & 0 \\ 0 & \frac{1}{k_n} \end{bmatrix} \begin{Bmatrix} \Delta T \\ \Delta N \end{Bmatrix}. \qquad \text{(D-4)}$$

Combining the above three relationships gives the incremental compliance relationship for the generalized stresses and strains as

$$\begin{Bmatrix} \Delta q_1 \\ \Delta q_2 \end{Bmatrix} = \frac{s_L}{D_b} [R] \begin{bmatrix} \frac{1}{k_t} & 0 \\ 0 & \frac{1}{k_n} \end{bmatrix} [R]^T \begin{Bmatrix} \Delta Q_1 \\ \Delta Q_2 \end{Bmatrix} \qquad \text{(D-5)}$$

where the orthogonality of [R] has been exploited. Expanding the above relationship gives

$$\begin{Bmatrix} \Delta q_1 \\ \Delta q_2 \end{Bmatrix} = \frac{s_L}{D_b} \begin{bmatrix} \frac{\cos^2\beta}{k_t} + \frac{\sin^2\beta}{k_n} & \frac{\sin 2\beta}{2} \left(\frac{1}{k_t} - \frac{1}{k_n}\right) \\ \frac{\sin 2\beta}{2} \left(\frac{1}{k_t} - \frac{1}{k_n}\right) & \frac{\sin^2\beta}{k_t} + \frac{\cos^2\beta}{k_n} \end{bmatrix} \begin{Bmatrix} \Delta Q_1 \\ \Delta Q_2 \end{Bmatrix}. \qquad \text{(D-6)}$$

The above relationship suggests that the compliance matrix is symmetric. Because the average β is often near forty-five degrees, it is expected that the diagonal terms will be of the same order of magnitude.

DISTRIBUTION LIST

ADINA ENGRG, INC / WALCZAK, WATERTOWN, MA
AFOSR / NA (WU), WASHINGTON, DC
ANATEC APPLICATIONS CORP / CASTRO, SAN DIEGO, CA
ANATEC RESEARCH CORP / RASHID, LA JOLLA, CA
APPLIED RSCH ASSOC, INC / HIGGINS, ALBUQUERQUE, NM
APTEK / SCHWER, SAN JOSE, CA
ARMY EWES / FRANKLIN, VICKSBURG, MI
ARMY EWES / WES (NORMAN), VICKSBURG, MS
ARMY EWES / WES (PETERS), VICKSBURG, MS
ARMY EWES / WESIM-C (N. RADHAKRISHNAN), VICKSBURG, MS
BUREAU OF RECLAMATION / MCLEAN, DENVER, CO
CATHOLIC UNIV / CE DEPT (KIM) WASHINGTON, DC
CENTRIC ENGINEERING SYSTEMS INC / TAYLOR, PALO ALTO, CA
DEPT OF CIVIL ENGRG / KIGER, MORGANTOWN, WV
DOT / TRANSP SYS CEN (TONG), CAMBRIDGE, MA
DTIC / ALEXANDRIA, VA
DTRCEN / (CODE 1720), BETHESDA, MD
EARTH TECH / MURALEETHARAN, IRVINE, CA
GEORGIA TECH / CHAMEAU, ATLANTA, GA
HKS (WEST) INC / REBELO, NEWARK, CA
HKS INC / JOOP NAGTEGAAL, PROVIDENCE, RI
HQ AFESC / RDC (DR. M. KATONA), TYNDALL AFB, FL
KARGOZIAN AND CASE / CRAWFORD, GLENDALE, CA
LAWRENCE LIVERMORE NATIONAL LAB / WHIRLEY, LIVERMORE, CA
LOCKHEED / RSCH LAB (P UNDERWOOD), PALO ALTO, CA
MARC ANALYSIS RSCH CORP / HSU, PALO ALTO, CA
NAVFACENGCOM / CODE 04B2 (J. CECILIO), ALEXANDRIA, VA
NAVFACENGCOM / CODE 04BE (WU), ALEXANDRIA, VA
NORTH CAROLINA STATE UNIV / CE DEPT (GUPTA), RALEIGH, NC
NORTH CAROLINA STATE UNIV / CE DEPT (TUNG), RALEIGH, NC
NORTHWESTERN UNIVERSITY / BAZANT, EVANSTON, IL
NORTHWESTERN UNIVERSITY / CE DEPT (BELYTSCHKO), EVANSTON, IL
NRL / CODE 4430, WASHINGTON, DC
NSF / STRUC & BLDG SYSTEMS (KP CHONG), WASHINGTON, DC
NUSC DET / CODE 44 (CARLSEN), NEW LONDON, CT
OCNR / CODE 1121 (EA SILVA), ARLINGTON, VA
OHIO STATE UNIVERSITY / CE DEPT (SIERAKOWSKI), COLUMBUS, OH
ONR / CODE 1131S, ARLINGTON, VA
ONR / CODE 1132SM, ARLINGTON, VA
OREGON STATE UNIV / CE DEPT (LEONARD), STORRS, CT
OREGON STATE UNIV / CE DEPT (YIM), CORVALLIS, OR
PENN ST UNIV / KROUTHAMMER, UNIVERSITY PARK, PA
PORT OF LA / WITTKOP, SAN PEDRO, CA
SCOPUS TECHNOLOGY INC / (B NOUR-OMID), EMERYVILLE, CA
SRI INTL / ENGRG MECH DEPT (GRANT), MENLO PARK, CA
SRI INTL / ENGRG MECH DEPT (SIMONS), MENLO PARK, CA
STANFORD UNIV / APP MECH DIV (HUGHES), STANFORD, CA
STANFORD UNIV / CE DEPT (PENSKY), STANFORD, CA

STANFORD UNIV / DIV OF APP MECH (SIMO), STANFORD, CA
UNIV OF CALIFORNIA / CE DEPT (HERRMANN), DAVIS, CA
UNIV OF CALIFORNIA / CE DEPT (ROMSTAD), DAVIS, CA
UNIV OF CALIFORNIA / MECH ENGRG DEPT (BAYO), SANTA BARBARA, CA
UNIV OF CALIFORNIA / MECH ENGRG DEPT (LECKIE), SANTA BARBARA, CA
UNIV OF CALIFORNIA / MECH ENGRG DEPT (MCMEEKING), SANTA BARBARA, CA
UNIV OF CALIFORNIA / SELMA, LOS ANGELES, CA
UNIV OF CALIFORNIA / WILSON, BERKELEY, CA
UNIV OF COLORADO / MECH ENGRG DEPT (FELLIPA), BOULDER, CO
UNIV OF COLORADO / MECH ENGRG DEPT (PARK), BOULDER, CO
UNIV OF ILLINOIS / CE LAB (ABRAMS), URBANA, IL
UNIV OF ILLINOIS / CE LAB (PECKNOLD), URBANA, IL
UNIV OF KANSAS / CE DEPT (DARWIN), LAWRENCE, KS
UNIV OF NEVADA / SIDDHARTAN, RENO, NV
UNIV OF TEXAS / CE DEPT (STOKOE), AUSTIN, TX
UNIV OF WYOMING / CIVIL ENGRG DEPT, LARAMIE, WY
WEIDLINGER ASSOC / F.S. WONG, LOS ALTOS, CA
WOODWARD CLYDE CONSULTANTS / MORIWAKI, SANTA ANA, CA